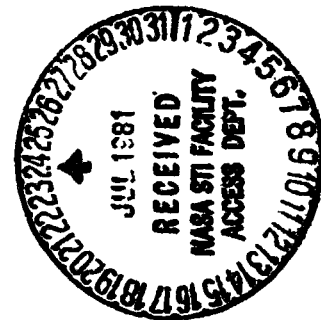# NASA

National Aeronautics and
Space Administration

TURBINE BLADE TIP DURABILITY ANALYSIS

by

R.L. McKnight, J.H. Laflen, and G.T. Spamer

GENERAL ELECTRIC COMPANY

Prepared For

National Aeronautics and Space Administration

NASA Lewis Research Center

1. Report No. NASA CR-165268	2. Government Accession No.	3. Recipient's Catalog No
4. Title and Subtitle Turbine Blade Tip Durability Analysis		5. Report Date February 1981
		6. Performing Organization Code
7. Author(s) R.L. McKnight, J.H. Laflen, and G.T. Spamer		8. Performing Organization Report No. R81AEG372
		10. Work Unit No.
9. Performing Organization Name and Address General Electric Company Aircraft Engine Business Group Cincinnati, Ohio 45215		11. Contract or Grant No. NAS3-22020
		13. Type of Report and Period Covered
12. Sponsoring Agency Name and Address National Aeronautics and Space Administration Lewis Research Center Cleveland, Ohio 44135		14. Sponsoring Agency Code

15. Supplementary Notes

16. Abstract

An air-cooled turbine blade from an aircraft gas turbine engine was chosen for its well documented history of cracking and subjected to advanced analytical and life-prediction techniques. The objective of the research was to verify the utility of advanced structural analysis techniques and advanced life-prediction techniques in the life assessment of hot-section components. In the approach that was used, three-dimensional heat-transfer and stress analyses were applied to the turbine blade mission cycle and the results were input into advanced life-prediction theories. The knowledge gained was used to develop shortcut techniques and to evaluate the proposed life-prediction theories.

17. Key Words (Suggested by Author(s)) Strain Range Partitioning Life Prediction Nonlinear Stress Analysis Aircraft Gas Turbine Engine Turbine Blades	18. Distribution Statement Unclassified - Unlimited		
19. Security Classif. (of this report) Unclassified	20. Security Classif. (of this page) Unclassified	21. No. of Pages	22. Price*

NASA-C-168 (Rev. 6-71)

TABLE OF CONTENTS

LIST OF ILLUSTRATIONS

LIST OF ILLUSTRATIONS (Continued)

LIST OF ILLUSTRATIONS (Continued)

LIST OF ILLUSTRATIONS (Concluded)

LIST OF TABLES

1.0 SUMMARY

The objective of this program was to evaluate the utility of advanced structural-analysis techniques and advanced life-prediction techniques in the life assessment of hot-section components. A particular goal was to assess the extent to which three-dimensional transient heat-transfer analysis and three-dimensional cyclic isoparametric finite-element analysis of a hot-section component would bear upon the accuracy of component life predictions. At the same time, new high-temperature life-prediction theories such as Strain Range Partitioning and the Frequency Modified approaches were to be applied and their efficiency judged along with the older Linear Damage approach. A final objective to this research was to seek shortcut approaches to the problem.

A commercial air-cooled turbine blade with a well-documented history of cracking in the squealer tip region was selected as the vehicle for accomplishing the above objectives. Three-dimensional transient heat-transfer analysis was performed on this turbine blade for a factory test cycle using an in-house finite-difference heat-transfer program, THTD. To perform the stress analysis of this turbine blade, a detailed three-dimensional model of the blade tip region was constructed which consisted of eight-noded isoparametric finite-elements (580 elements and 1119 nodes). As a first step, the transient temperature distributions and mechanical loads were applied to this model and elastic-only runs made on an in-house computer program - MASS. The strain ranges in the critical regions, determined this way, were used to program a thermomechanical test specimen. This was one of the shortcut approaches evaluated.

To perform the cyclic nonlinear analysis, a commercially available program, ANSYS, was chosen. For this analysis, previously determined temperature-dependent cyclic stress-strain curves and creep data were used. The kinematic hardening option was selected for the plasticity analysis, and the creep analysis was performed with the time-hardening rule. Seven complete cycles were run, at which time shakedown was determined to have occurred. As a possible shortcut method, boundary conditions were taken from the three-dimensional elastic and nonlinear runs and applied to simpler models on an in-house cyclic nonlinear program, CYANIDE.

The results of these analyses and the thermomechanical tests were used to make life predictions by the Strain Range Partitioning, Frequency Modified, and Linear Damage theories. Also, crack propagation studies were performed. The results of these predictions were then evaluated against the cracking history, and conclusions and recommendations were made.

2.0 INTRODUCTION

The most critical structural requirements that aircraft gas turbine engines must meet result from the diversity of extreme environmental conditions in the turbine-section components. Accurate life assessment of the components under these conditions requires sound analytical tools and techniques, an understanding of the component operating environment, and comprehensive data on component materials. Inadequate understanding of any or all of these areas may result in either a conservative life prediction or component failure.

Much activity has occurred in recent years, both through Government sponsorship and through in-house programs, to provide the designer with the tools for conducting more accurate design analysis and component life prediction. These efforts encompass advances in analytical stress and life prediction techniques, instrumentation capabilities, and cost-effective, accelerated verification testing.

Advanced structural analysis techniques are available to permit more reliable life prediction in the life-limiting turbine components. However, verification of these methods through application to well-documented failure case histories is lacking.

Although nonlinear stress analysis computer programs are available, they have not been used routinely in hot-section component design because of the extensive computation time required for such applications. Furthermore, poorly defined material constitutive equations have hampered more general use of such computer programs.

In addition, several high-temperature, low-cycle fatigue (LCF) life prediction approaches have been proposed in recent years. These approaches have not yet been applied extensively to hot-section components primarily because critical evaluation through application to well-documented failure case histories is needed.

The Turbine Blade Tip Durability program is intended to apply advanced nonlinear stress analysis and life prediction techniques to a well-documented case history. Using the resultant detailed analysis as a standard, shortcut techniques will be developed in the interest of reduced complexity.

3.0 HOT SECTION COMPONENT DOCUMENTATION

3.1 COMPONENT SELECTION

The Stage 1 high pressure turbine blade was chosen as the hot-section
component to be analyzed because of its significant creep-fatigue problems.
These blades are hollow, air cooled, and paired together on a   three-
tang dovetail as shown in Figure 3.1-1. The material is cast ene b
chosen for its excellent high-temperature creep resistance.

The failure mode for this component is well defined. The blade has a
tip cap just below the actual tip of the blade, this configuration being
designated a "squealer tip." Radial cracks occur in the squealer tip region
as shown in Figures 3.1-2 through 3.1-4. These cracks are a problem on all
such blades; thus, we are addressing a problem which are common to all engine
manufacturers.

3.2 DATA BASE

Because of the quantity of stress and life data, heat transfer data, and
material data ava. able for this part, the selected Stage 1 HPT rotor blade
is an excellent component selection for this program. Available heat trans-
fer and tip cracking data were reviewed. On the basis of these data, it was
decided to utilize a factory test "C" cycle in the analysis, since a transient
analysis of engine parameters and adequate tip cracking data are available for
this cycle. The status of the previous heat transfer and 3-D stress analysis
models was investigated, and it was determined that both of these could be
readily reconstructed.
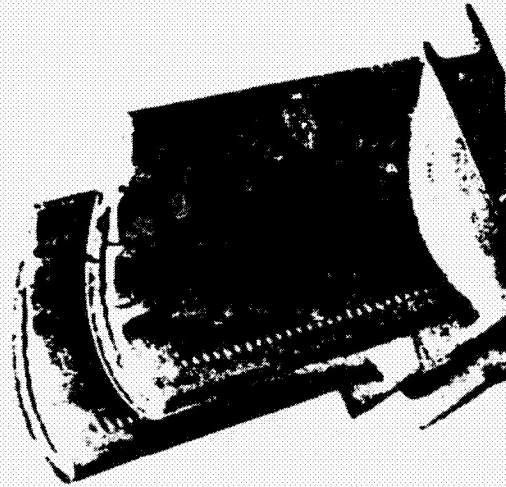
Figure 3.1-1. HPT Stage 1 Blades.
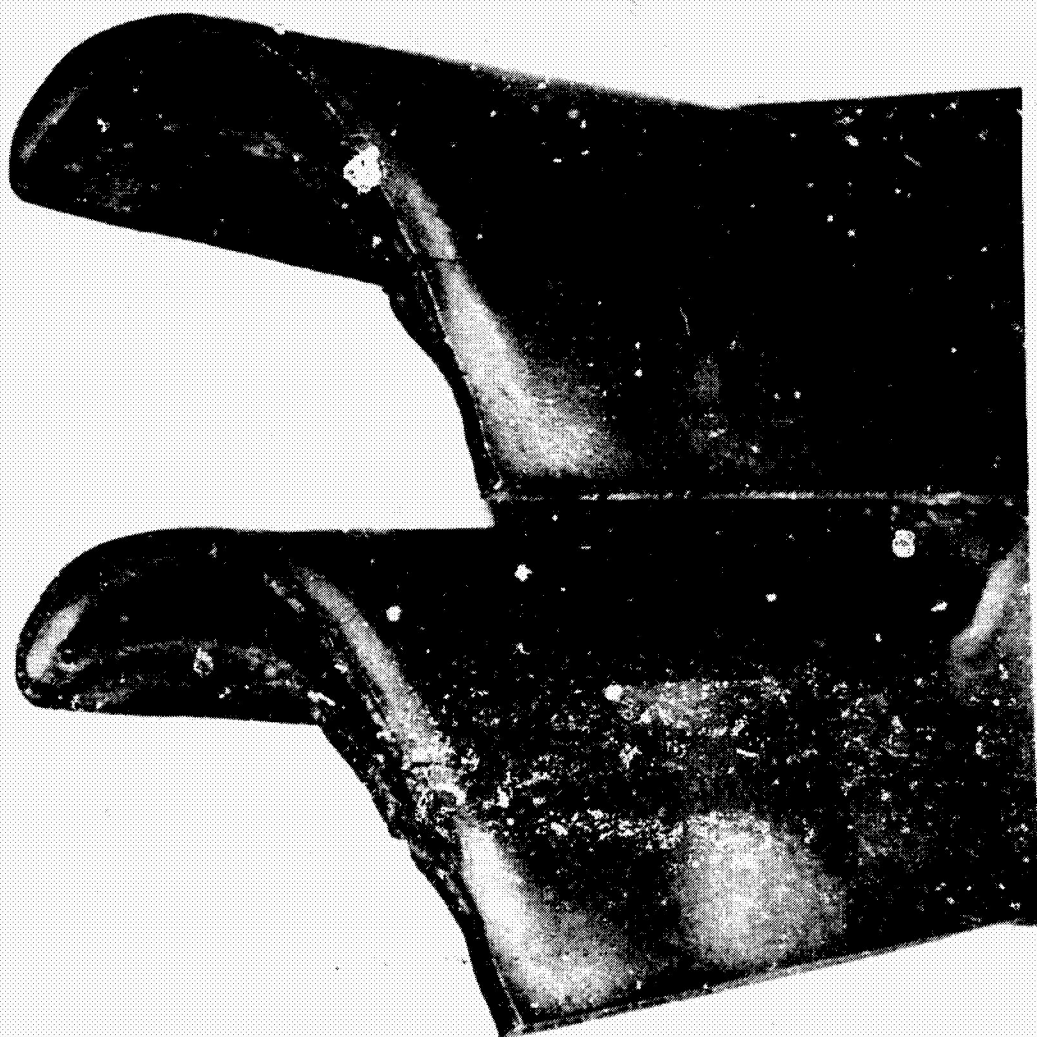
4

Figure 3.1-2. Typical Turbine Blade Tip Cracking - Example 1.

Figure 3.1-3. Typical Turbine Blade Tip Cracking - Example 2.
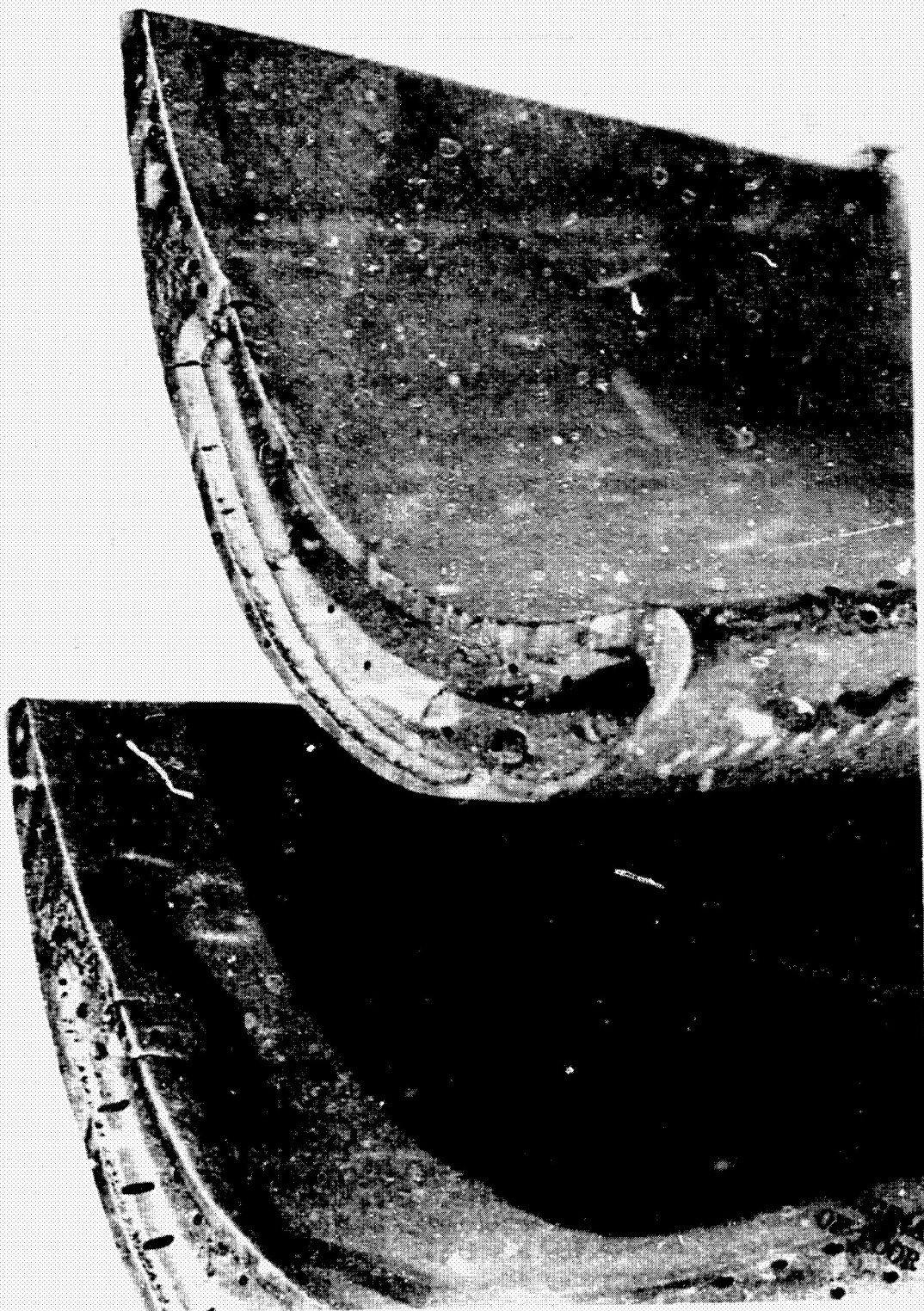
6

Figure 3.1-4 Typical Turbine Blade Tip Cracking - Example 3.

4.0 HEAT TRANSFER AND STRESS-STRAIN ANALYSIS

4.1 HEAT TRANSFER MODEL

The heat-transfer ana /sis was accomplished using a three-dimensional THTD model of the component blade tip region. THTD (Transient Heat Transfer - Version D) is an in-house heat-transfer analysis program capable of computing both transient and steady-state temperatures for large, complex three-dimensional problems. Film coefficients and boundary conditions were obtained from model test data for the tip region and from temperature measurements from factory test engines. Temperatures were calculated at conditions consistent with those of a factory engine test ("CX" cycle) which has well documented conditions of blade tip distress (Reference 1). The thermal transient that was analyzed is typical of field engine transients ("C" cycle). The difference between the test and analysis cycles exists in the two additional chop-and-burst portions between the ground idle and takeoff settings found in the test (CX) cycle (Figure 4.1-1). This was done to decrease test time and will be accounted for in all life predictions. The mission transient cycle is presented in Figures 4.1-2 and 4.1-3 in terms of turbine inlet (T_4) and compressor discharge (T_3) temperatures, and core engine speed, respectively.

4.2 FINITE-ELEMENT MODEL

An existing three-dimensional finite-element model of the component blade tip above the 75% span was retrieved from tape storage. The idealization which consists of 580 eight-noded isoparametric brick elements and 1119 nodes is presented in Figure 4.2-1. A more detailed, exploded view, depicting the squealer tip, tip cap, webs, and span as discrete three-dimensional components is shown in Figure 4.2-2. The spanwise length of the model was sufficient to preclude interference between the applied bottom boundary conditions and the squealer tip region, which is the region of interest.

The isoparametric element was chosen because of its capability to model almost any three-dimensional geometry and temperature distribution very accurately. The eight-noded brick was used exclusively because the 16- and 20-noded bricks in the ANSYS element library lacked creep capabilities. Specifically, the eight-noded brick element is an isoparametric hexahedral box element with eight nodal points and 33 degrees of freedom (three displacement components at each of the eight nodal points and nine internal degrees of freedom). The displacement field at any point within the element is assumed to be quadratic, giving rise to strain components which vary linearly across the element. For this reason, structures in which bending effects are significant can be modeled using relatively few elements. Thus, it was possible to model the blade tip region using only one element in the thickness direction.

8

CX CYCLE

Take reading @ 10th minute of cycle

T, T/O N1 rpm must be
between 3475 and
3560 corrected N1

Starter off

5 seconds

Trim to peak
allowable

5 to 10 second
throttle
movement

2800 rpm N₁/√θ
or 2800 physical
whichever is greater

NOT INCLUDED
FOR "C" CYCLE

T/O PLA

20 sec

15-20
seconds

Takeoff

Climb
T/O-80 rpm N1

Approach

Flight Idle

Idle

Motoring
@ 2000 rpm

Zero

Max. Reverse

Time, Minutes

1   2   3   4   5   6   7   8   9   10   11   12   13   14   15   16   17   18   19   20

Figure 4.1-1. Factory Test Cycle Definition.

9
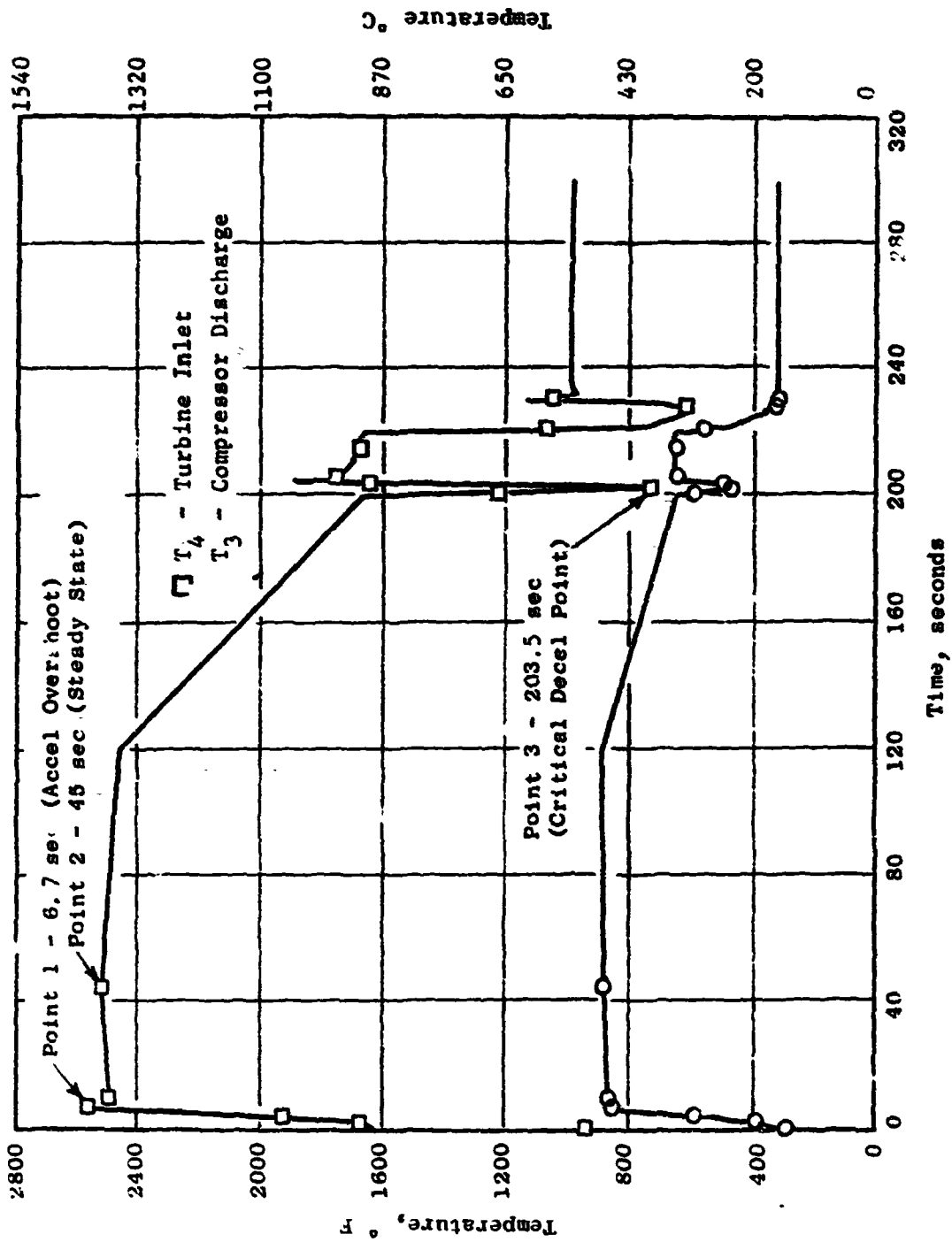
Figure 4.1-2. Mission Cycle Transient - Turbine Inlet and Compressor
Discharge Temperatures.
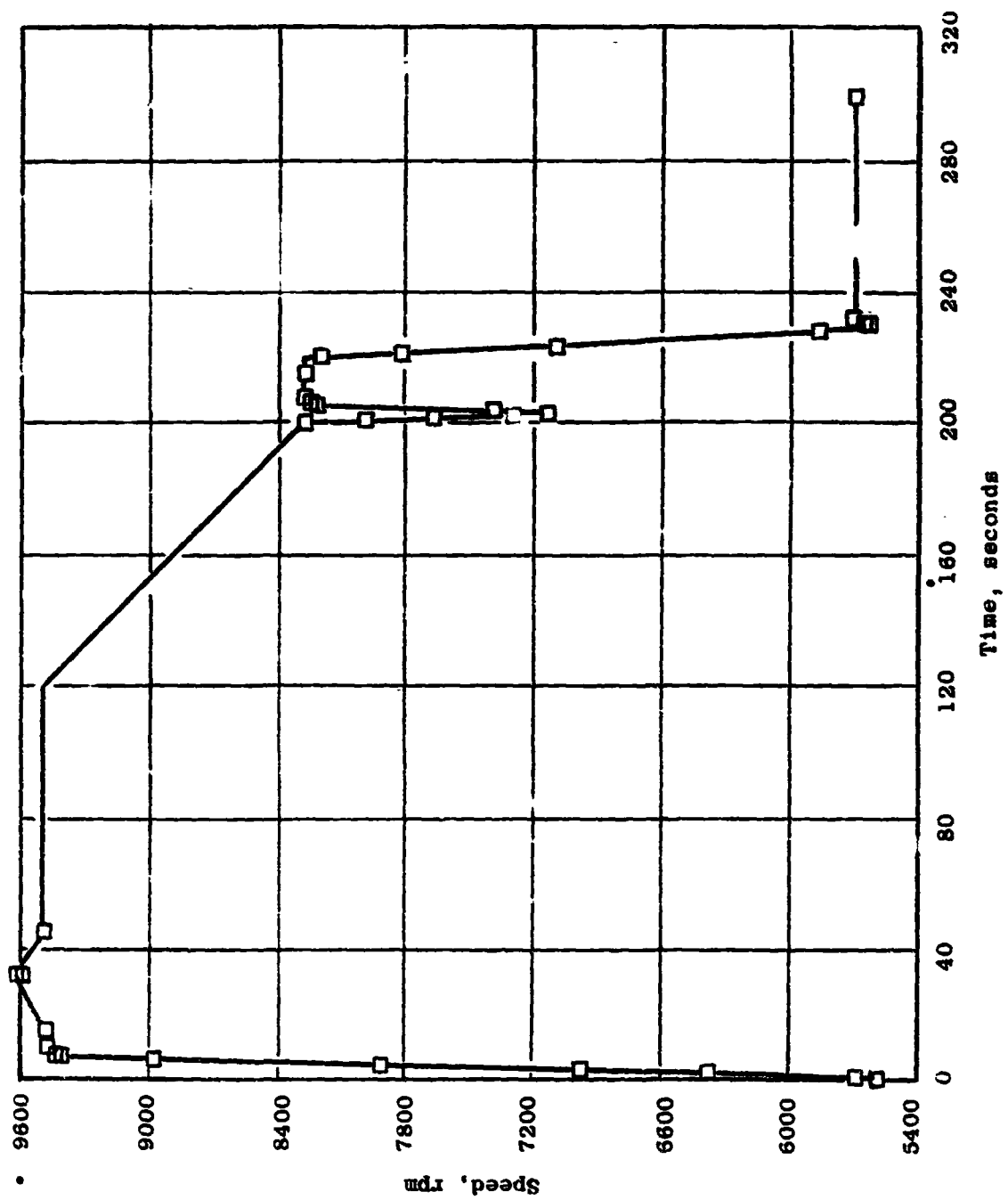
Figure 4.1-3. Mission Cycle Transient - Core Engine Speed.

11
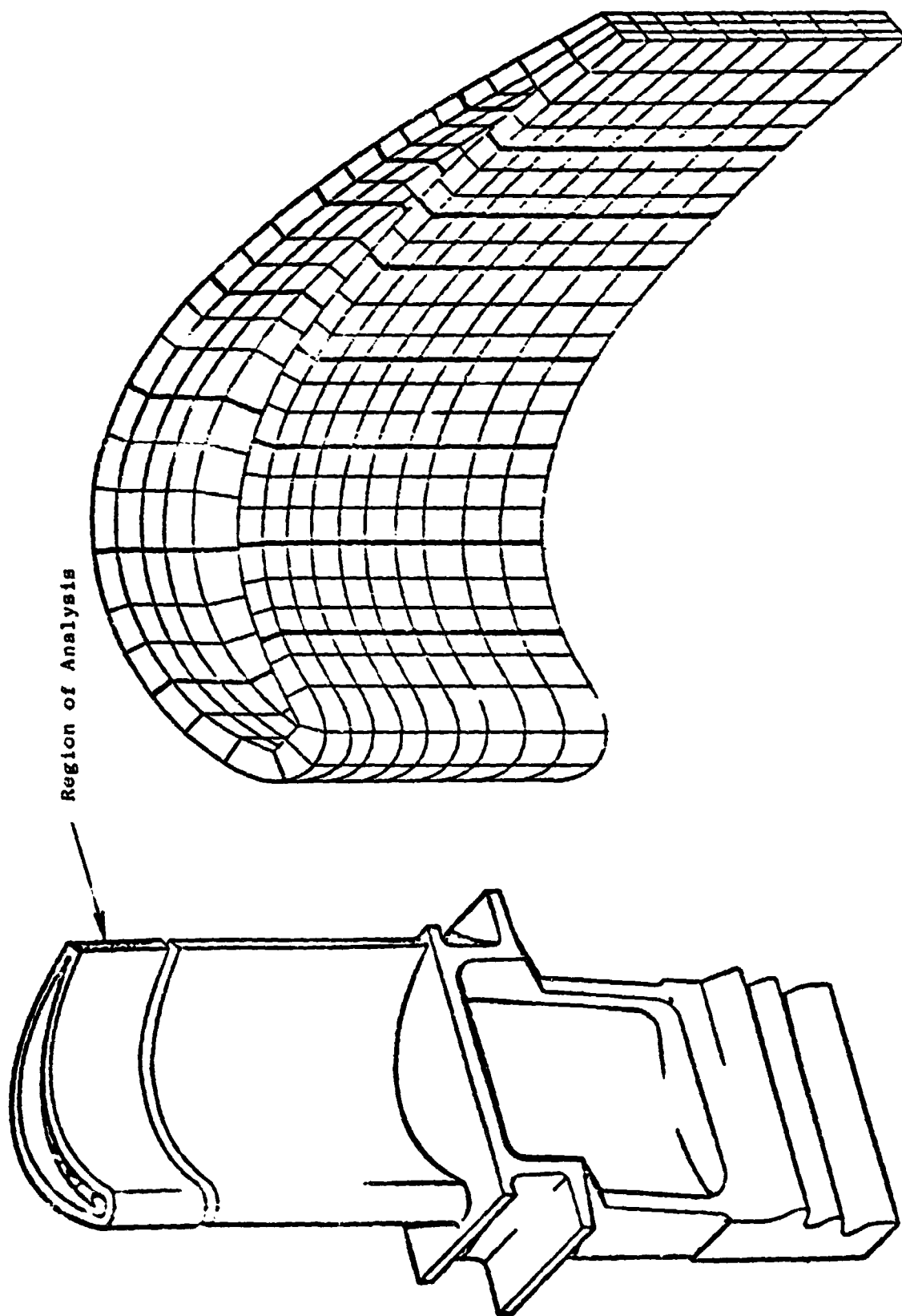
Region of Analysis

Figure 4.2-1. 3-D Model of HPT Blade Tip Region.

12
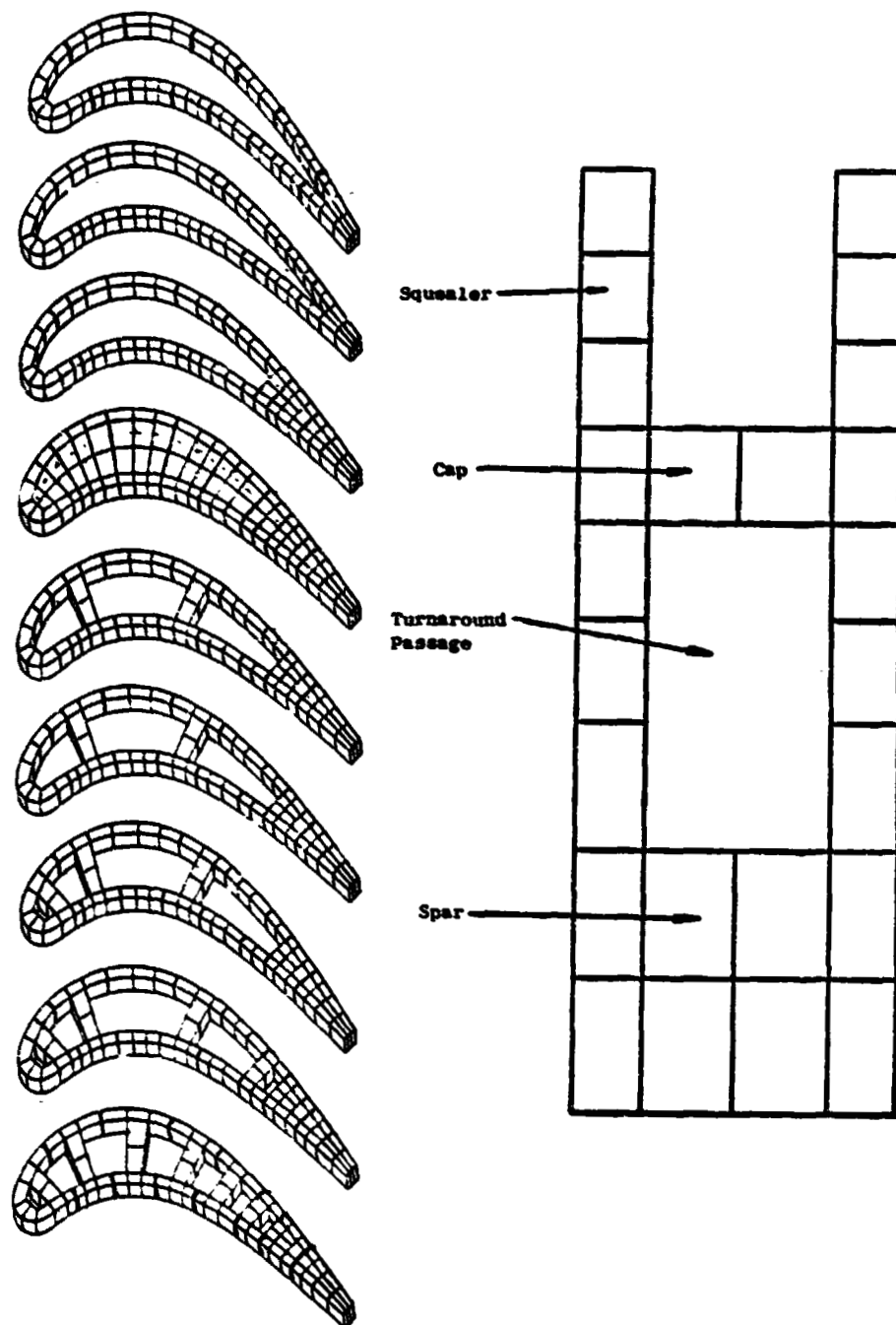
Figure 4.2-2. Details of 3-D Model of HPT Blade Tip.

4.3 MATERIAL PROPERTIES

René 80 is a well characterized material in terms of the stress-strain response and creep properties required for analysis. Material properties data for the temperature range considered – 340° C to 1150° C (650° F – 2100° F) – were for the most part available in the General Electric Materials Properties Handbook. Additionally, a small amount of material testing was conducted on René 80 at 1150° C (2100° F). This was very useful for this program since there are regions of the blade tip in this temperature range. The tests included some stress-strain data, creep data, and one A = -1 strain range and strain-rate-controlled LCF test. Evaluation of these data has generated some significant pieces of information. Primary among these is an appreciably lower Young's modulus than that being used, which was obtained by extrapolating from data ending at 980° C (1800° F). In addition, the cyclic stress-strain curves displayed an anomaly not previously experienced. Above a strain rate of approximately 6%/min. there were dips in the tops and bottoms of the hysteresis loops. These data have been incorporated into our existing data bank.

Plots of René 80 material properties used for analysis include:

- Elastic modulus versus temperature   Figure 4.3-1

- Cyclic stress versus strain   Figure 4.3-2

- Coefficient of thermal expansion   Figure 4.3-3
  versus temperature

- Poisson's ratio versus temperature   Figure 4.3-4

- Creep strain versus time   Figures 4.3-5 –
                                                        4.3-11

Thin-wall [1.1-mm (42-mil) thickness] creep data were used because they most closely represented the actual squealer tip thicknesses.

4.4 ANALYTICAL PROCEDURE

The Turbine Blade Tip Program is intended to apply advanced nonlinear stress analysis and life prediction techniques to a well-documented case history. Additionally, shortcut techniques employing elastic stress analysis were to be investigated in the interest of reduced complexity.

The ANSYS Program was chosen for use in three-dimensional cyclic nonlinear inelastic stress analysis of the turbine blade tip region because of its extensive capabilities and its ability to solve large structural problems. The ANSYS Program uses an initial strain approach for determining plasticity effects. This method computes a reference elastic material stiffness and corresponding elastic strains for each time step. The procedure uses an iterative solution technique with a constant triangularized stiffness matrix
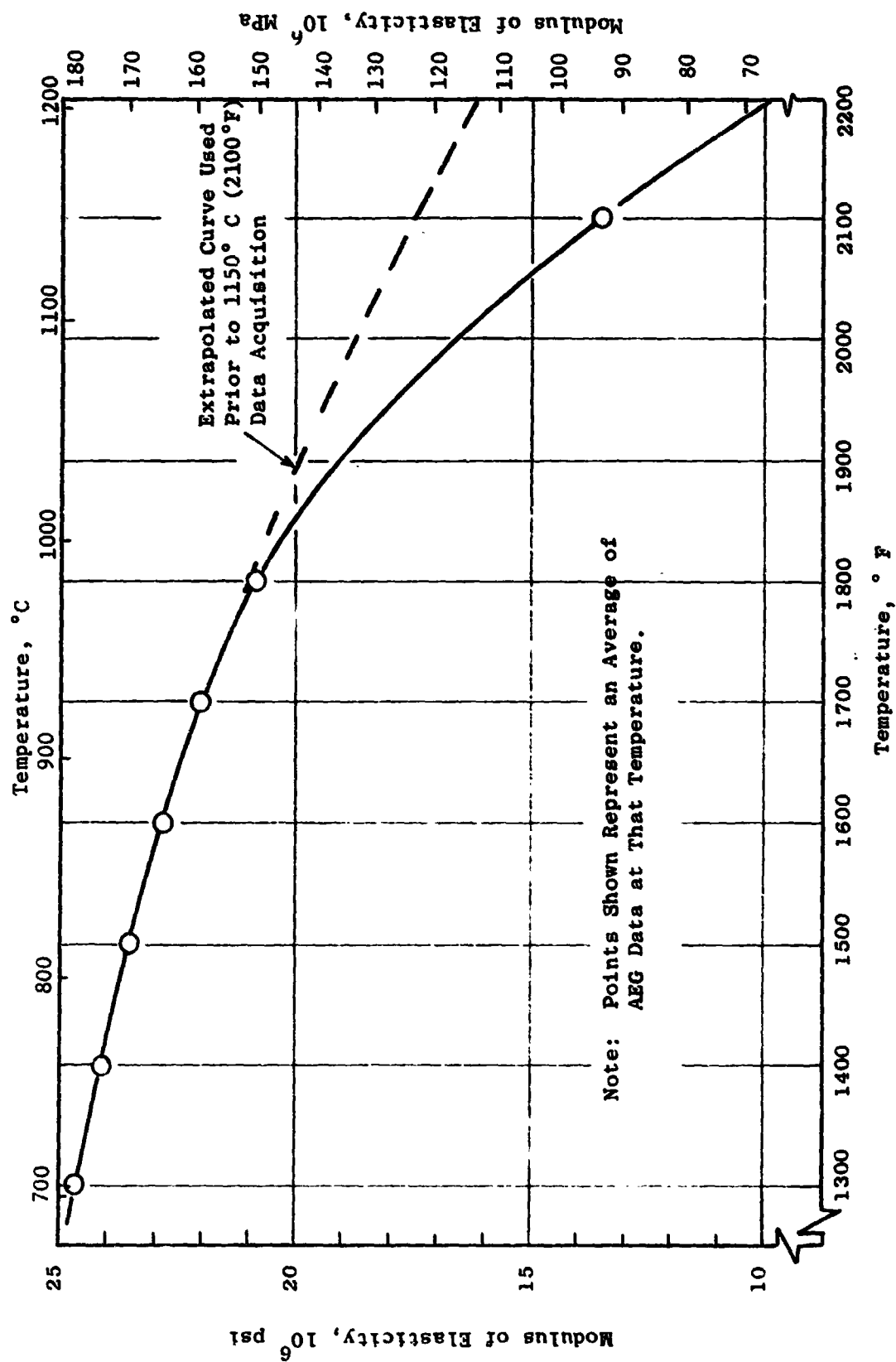
Figure 4.3-1. Elastic Modulus vs. Temperature for René 80.

15

STRESS, MPa

1600
1500
1400
1300
1200
1100
1000
900
800
700
600
500
400
300
200
100

2.0 1.8 1.6 1.4 1.2 1.0 0.8 0.6 0.4 0.2 0

PCT. STRAIN

	20° C (70° F)
	650° C (1200° F)
	870° C (1600° F)
	930° C (1700° F)
	980° C (1800° F)
	1040° C (1900° F)
	1100° C (2000° F)
	1150° C (2100° F)

240 210 180 150 120 90 60 30 0

STRESS, ksi
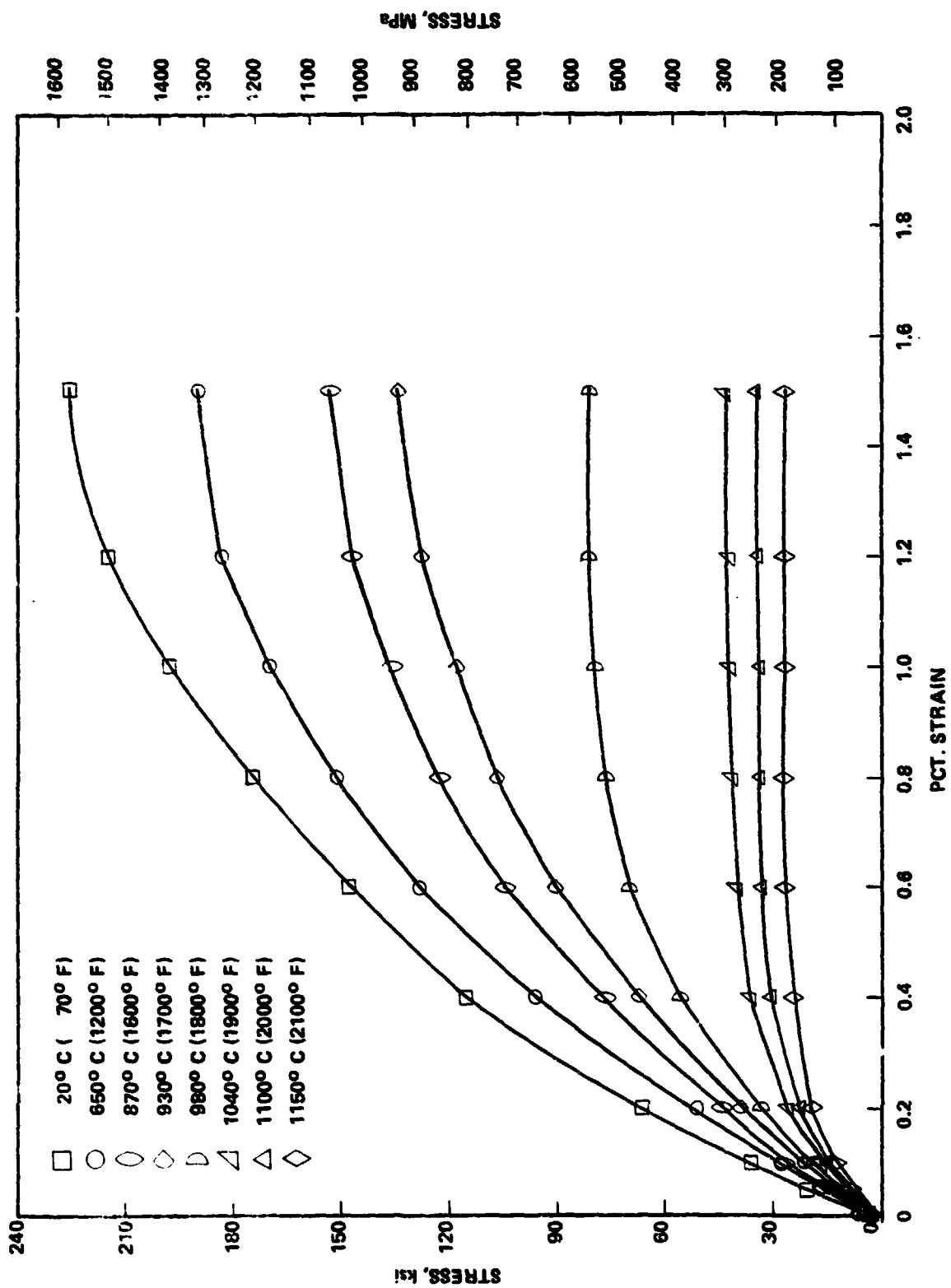
Figure 4.3-2. Cyclic Stress-Strain Curves for René 80.

16
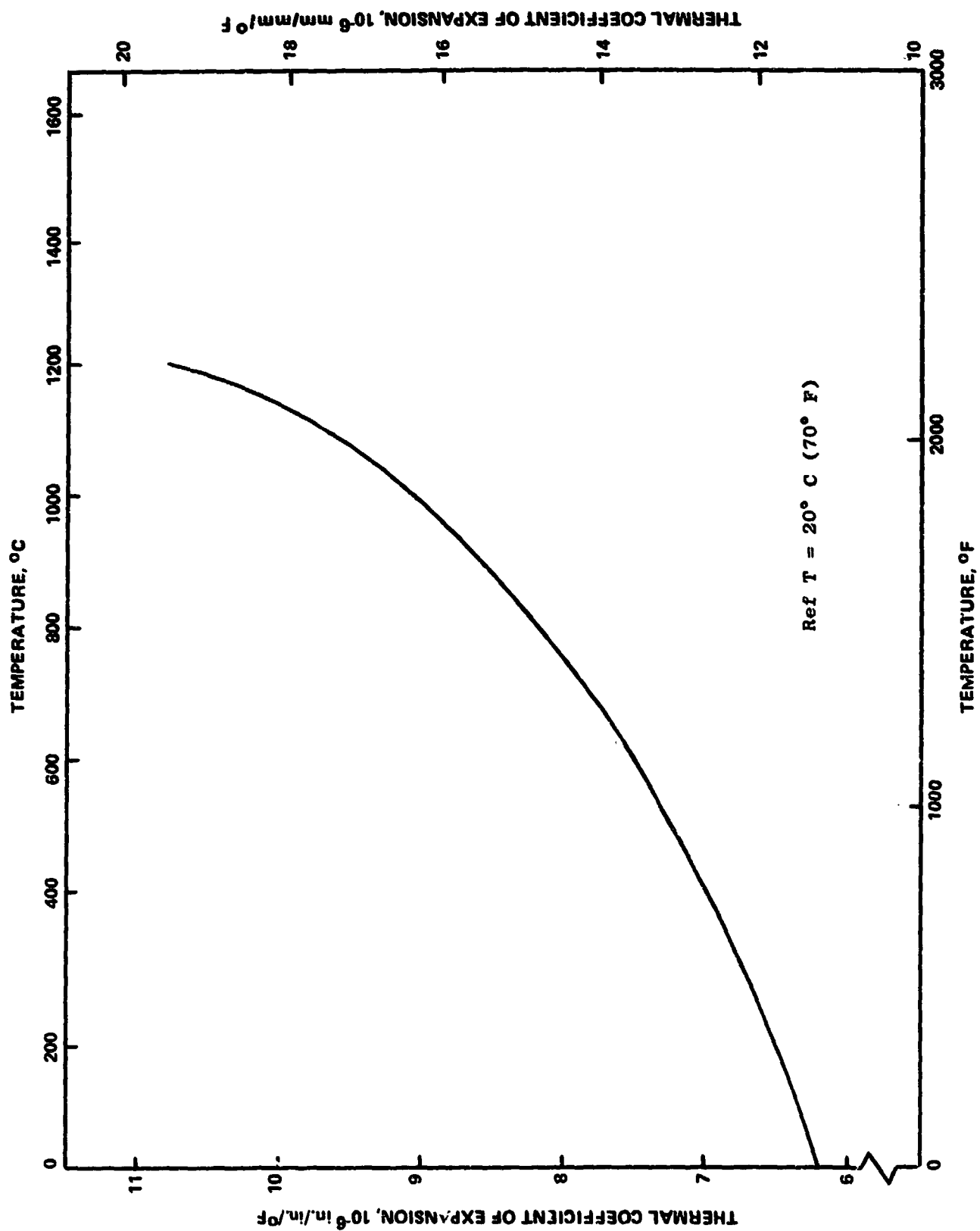
Figure 4.3-3. Coefficient of Thermal Expansion vs. Temperature for René 80.

17
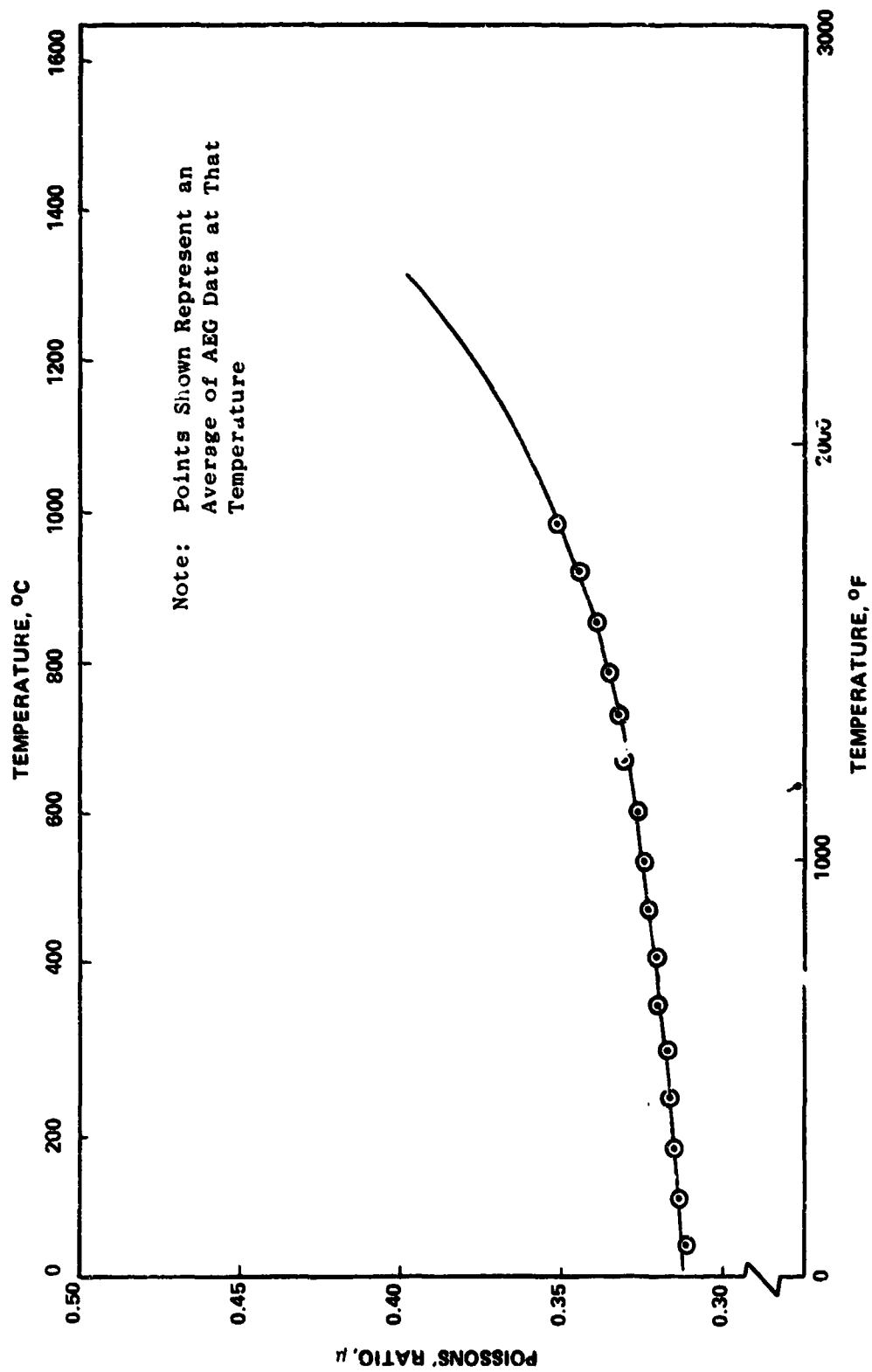
Figure 4.3-4. Poisson's Ratio vs. Temperature for René 80.

18
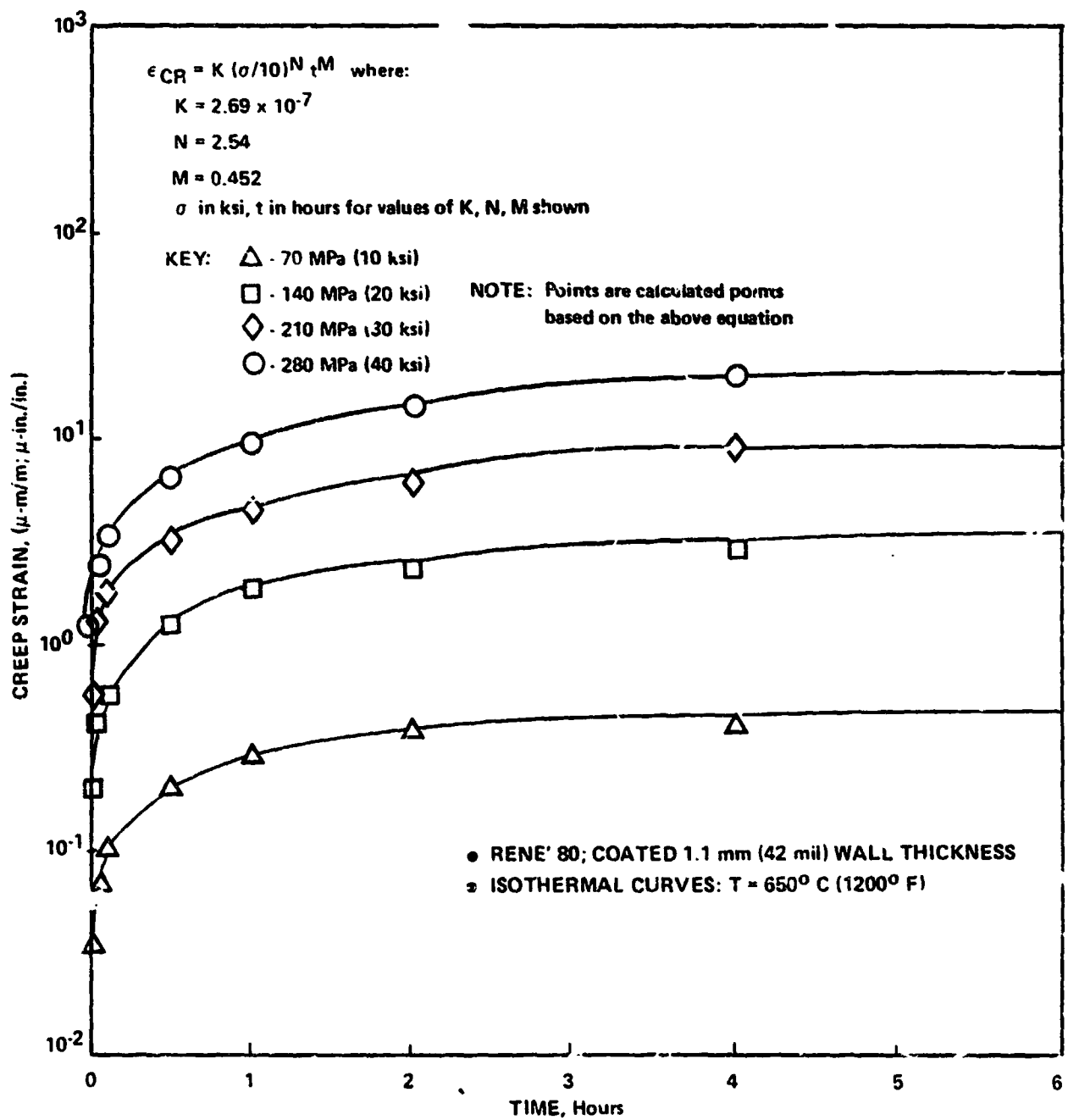
Figure 4.3-5. Creep Strain vs. Time for René 80.

CREEP STRAIN, (μ·m/m; μ·in./in.)

TIME, Hours

$\epsilon_{CR} = K\,(\sigma/10)^N\,t^M$ where:

K = 1.12 × 10⁻⁶

N = 5.19

M = 0.685

σ in ksi, t in hours for values of K, N, M shown

KEY: △ · 70 MPa (10 ksi)
◻ · 140 MPa (20 ksi)
◇ · 210 MPa (30 ksi)
○ · 280 MPa (40 ksi)

NOTE: Points are calculated points based on the above equation

● RENE' 80, COATED 1.1 mm (42 mil) WALL THICKNESS

● ISOTHERMAL CURVES: T = 870° C (1600° F)
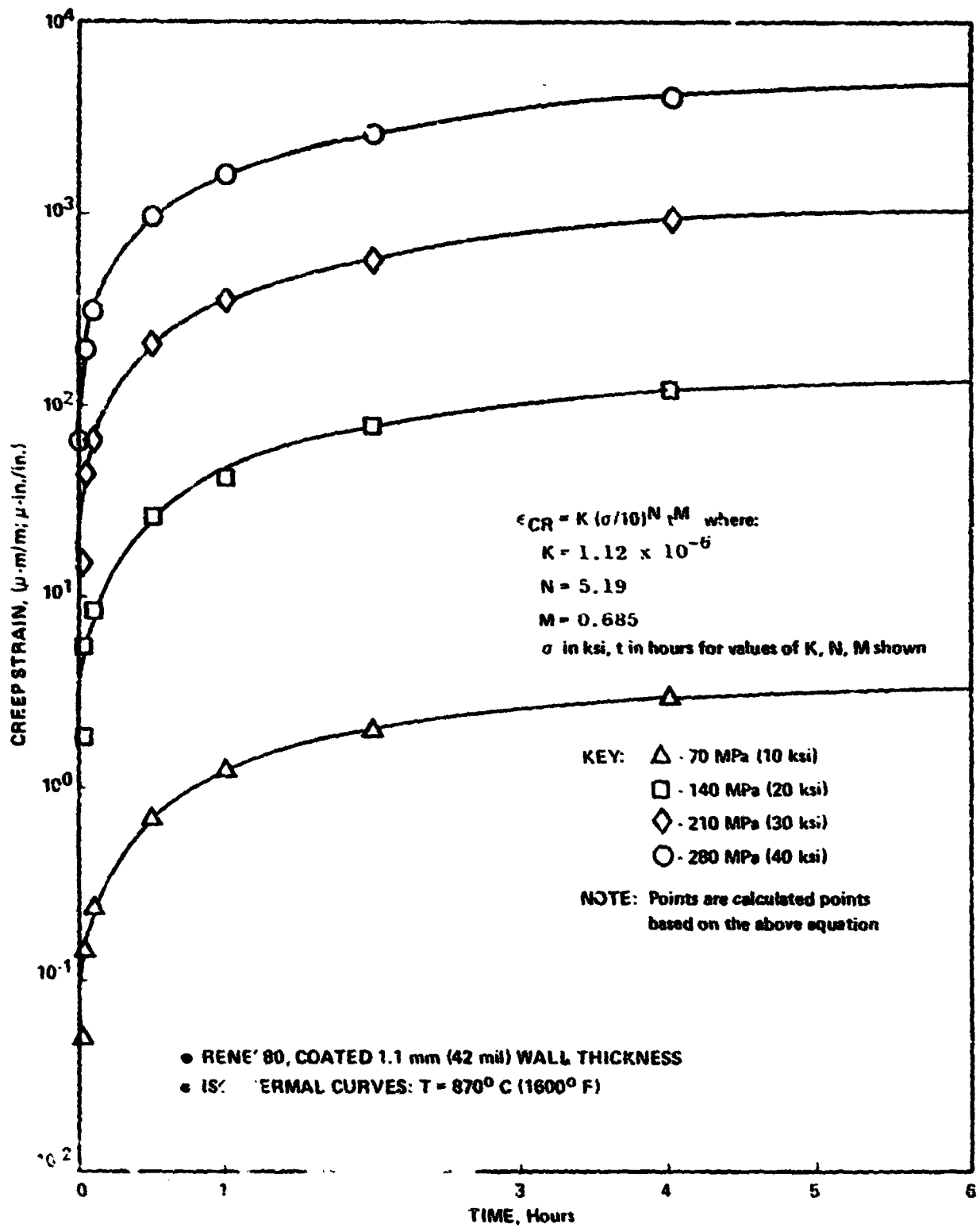
Figure 4.3-6. Creep Strain vs. Time for René 80.

20
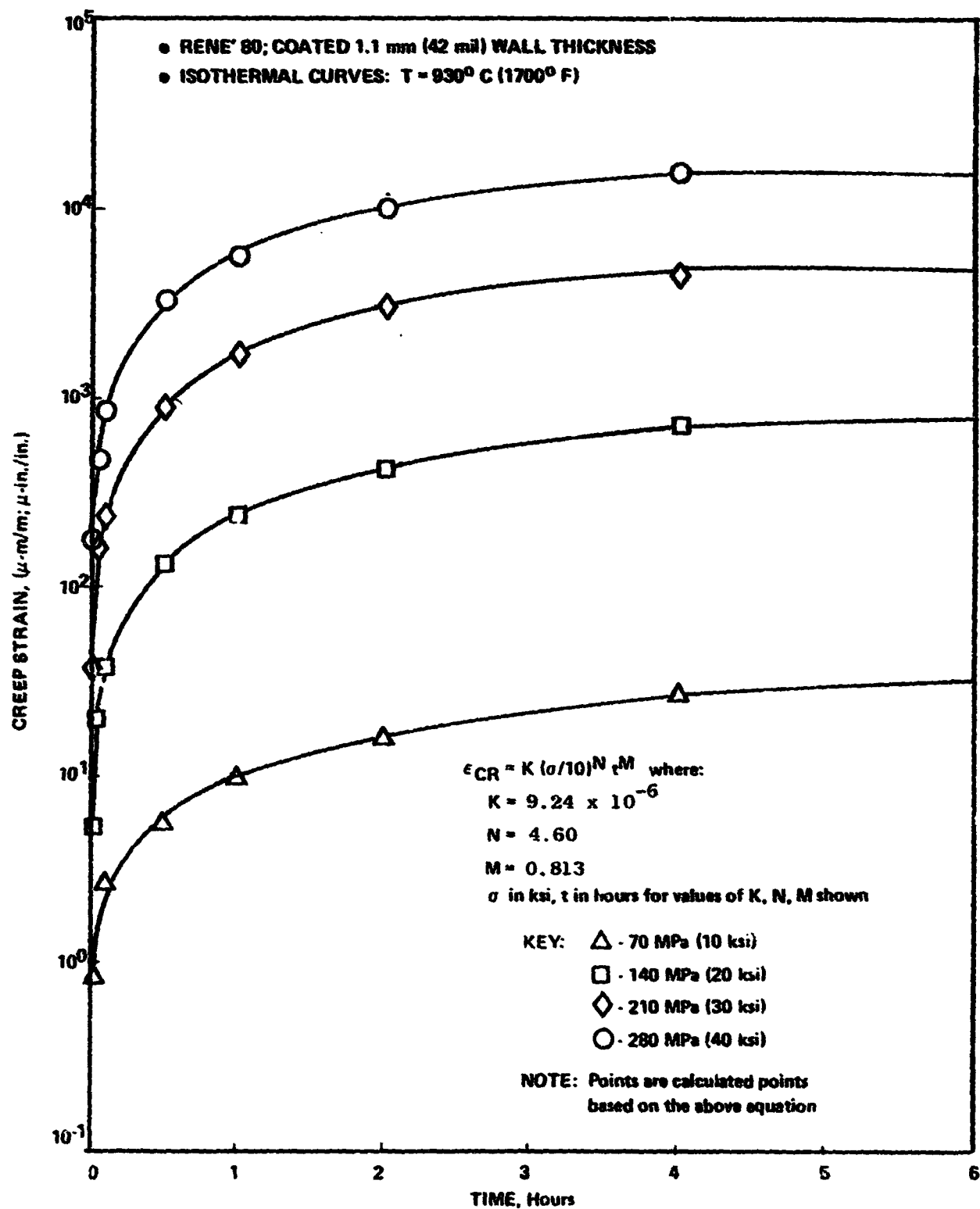
Figure 4.3-7. Creep Strain vs. Time for René 80.
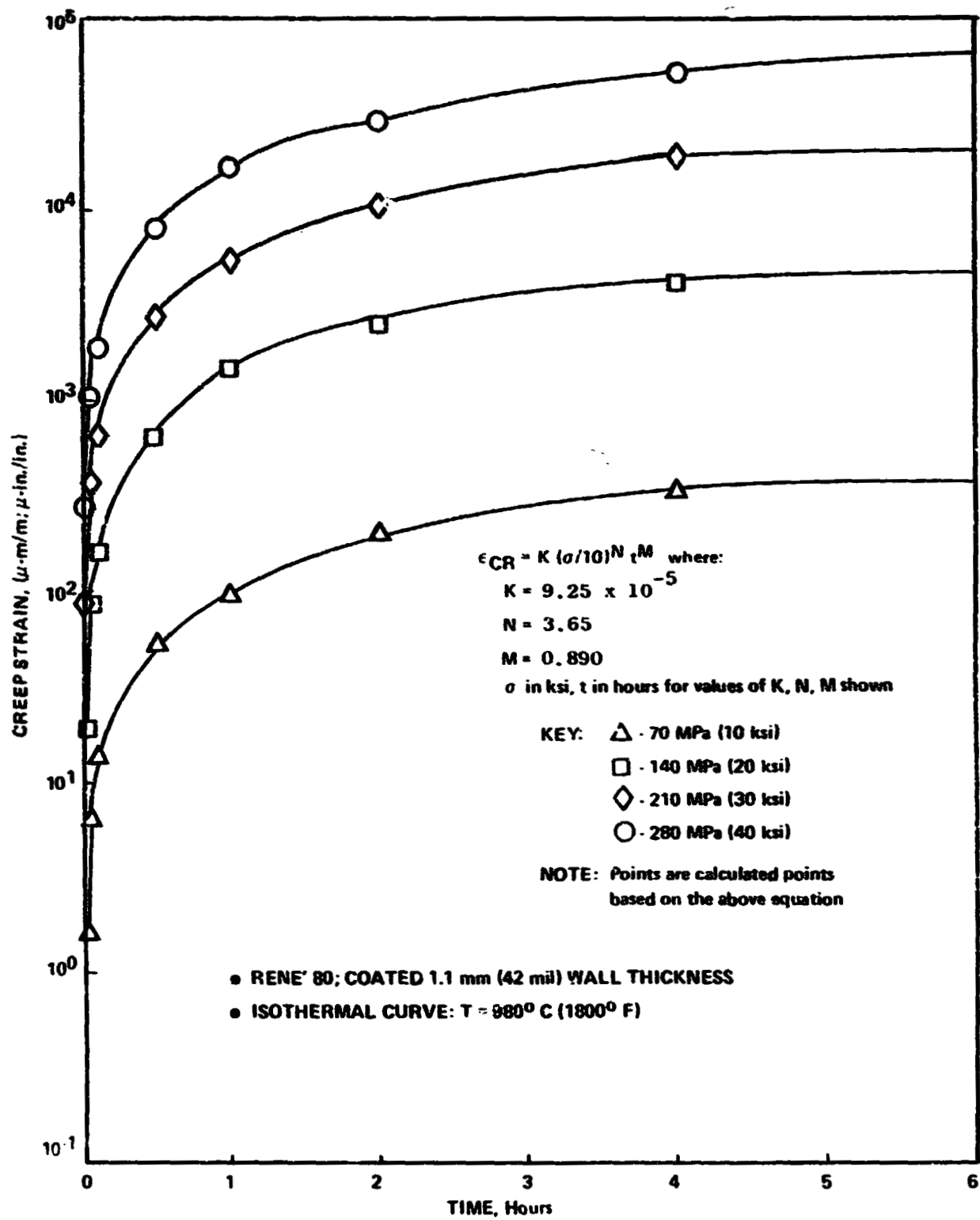
Figure 4.3-8. Creep Strain vs. Time for René 80.
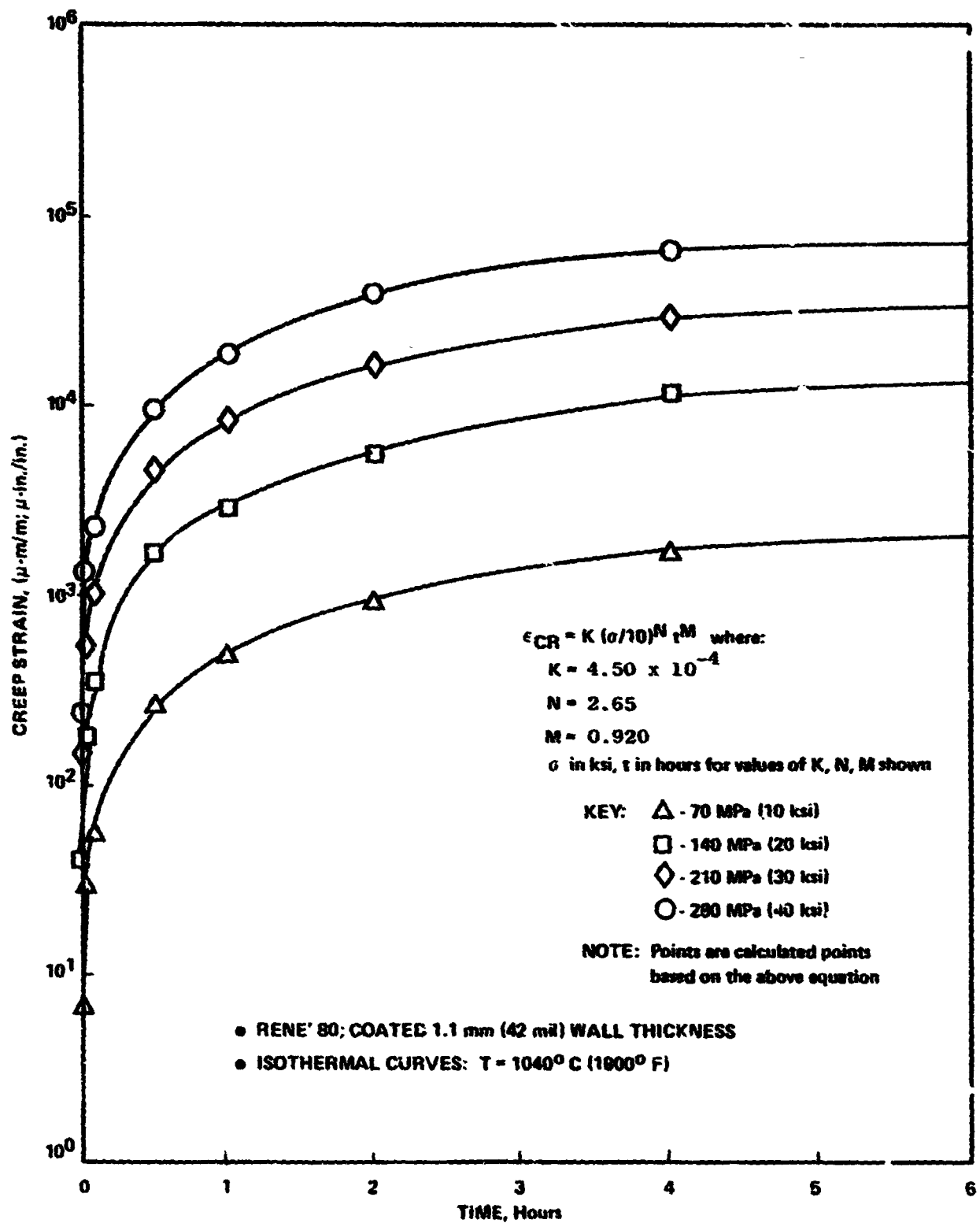
Figure 4.3-9. Creep Strain vs. Time for René 80.
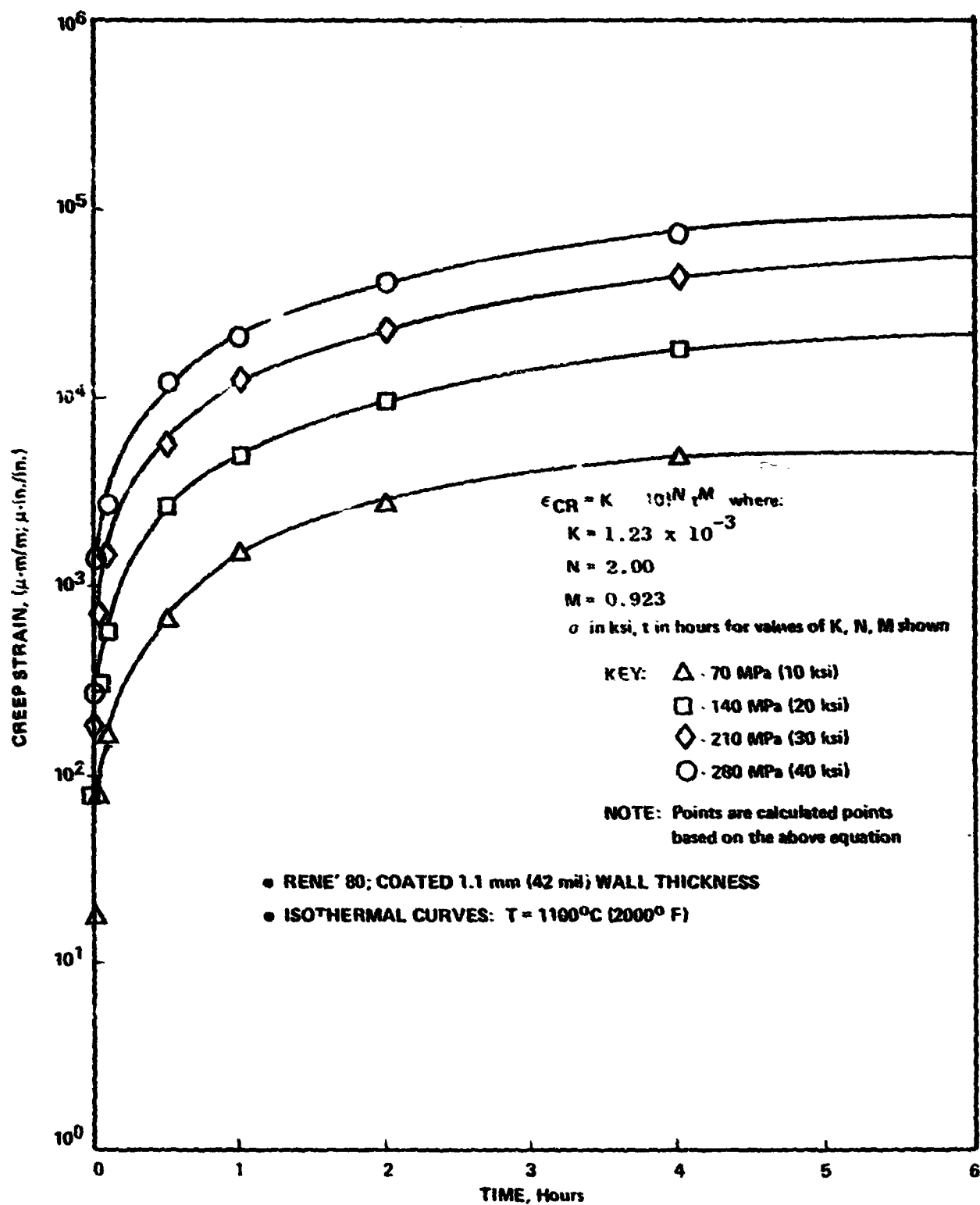
Figure 4.3-10. Creep Strain vs. Time for René 80.
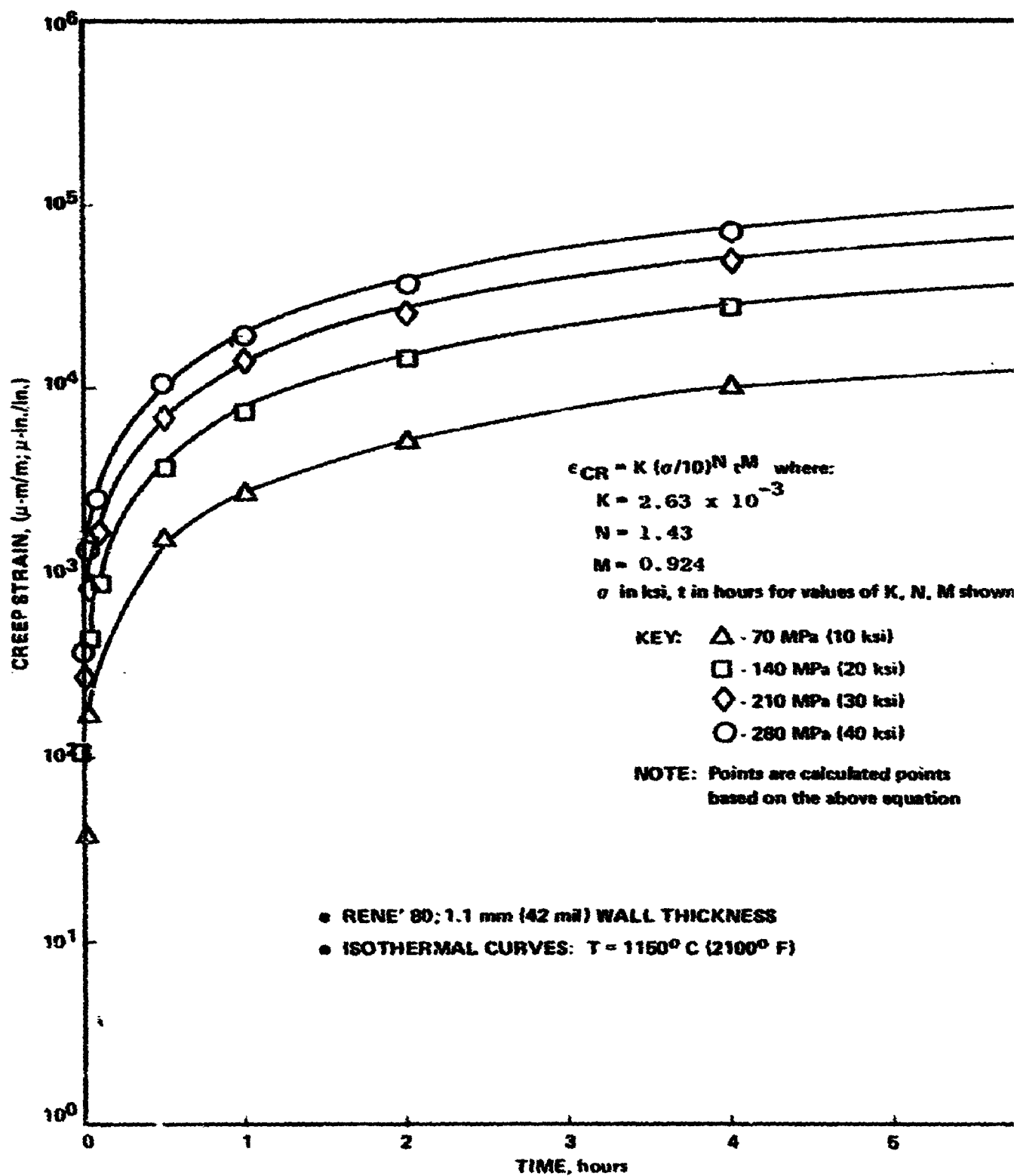
Figure 4.3-11. Creep Strain vs. Time for René 80.

and a load vector that is modified after each iteiation so that the stress
calculated in the next iteration approaches the stress that the material can
support at that strain. Each time-step consists of a sufficient number of
iterations, based on a single set of boundary conditions, so that convergence
criteria are met. Plasticity convergence criteria are met whenever the ratio
of the plastic strain increment to the elastic strain for all elements is less
than 1% (recommended). Reversed loaJing with plasticity was modeled using the
ANSYS kinematic hardening option. This practice assumes that the total elastic
stress range is equal to twice the yield stress, which is a close approximation
to the real-world Bauschinger effect.

For creep analyses, the creep rates are determined from the elastic
stresses computed after the plasticity solution has been calculated. The
creep law equation is of the form:

$$\varepsilon_{creep} = K \bar{\sigma}_e^n t^m$$

where

$$\bar{\sigma}_e = \sigma_e/100,000; \quad \sigma_e = \text{effective stress in psi}$$

$$t = \text{time, hours}$$

$$K, m, n = \text{material-dependent and temperature-dependent creep}$$
$$\text{coefficients (Figures 4.3-5 through 4.3-11)}$$

Creep calculations are handleJ by an incremental technique similar to that
used for plasticity. The iterative procedure is completed when the ratio of
the creep strain increment to the elastic strain for all elements is less than
0.25 (recommended).

The cyclic ineͳastic analysis was performeJ for a sufficient number of
cycles to adequitelv stabilize the stress-strain hysteresis loop at the criti-
cal crack initiation location. For the elastic stress-strain analysis or
alternate snortcut method, a stress analysis was performed using MASS (Mechan-
ical Analysis of Space Structures), an in-house finite-element analysis system
capable of handling large structural problems. An elastic three-dimensional
analysis was done using the same model as that used for the cyclic nonlinear
inelastic analysis. Strain-range data and other required crack initiation and
cyclic life analysis parameters were obtained from this procedure.

Boundary conditions obtained from the three-dimensional model were used
to analyze the crack initiation critical area with a two-dimensional inelastic
program, CYANIDE, an economical, in-house system capable of performing incre-
mental plasticity and creep analysis. Results were used to gain insight into
both shakedown and LCF effects with respect to subsequent thermomechanical
fatigue testing.

4.5 RESULTS OF ELASTIC ANALYSIS

Subsequent to retrieval of the finite-element and heat-transfer models, an elastic steady-state hot-day takeoff condit'ɔ. checkout run was conducted using MASS. Results were compared with previou⹁ analyses to validate the completeness of the component model. Since cer·roidal t-⹏peratures were used for nodal values (i.e., no gradient exists across the w.l. thickness), the results represent only a relative magnitude of the effective stresses. However, it should be noted that high effective stresses are predicted at several squealer tip locations where cracking occurred during test (e.g., suction-side face near trailing edge; pressure-side face at 60% chord). The metal temperature distribution and stress analysis results are provided in Figures 4.5-1 through 4.5-4 for each spanwise slice.

The three-dimensional THTD heat-transfer model was updated with new film coefficients and boundary conditions based on test information as described in Section 4.1. This new model was used to make an updated steady-state heat-transfer analysis of the blade tip region. The THTD heat-transfer nodal centroidal temperatures were transformed to element face temperatures for input to the existing finite-element model using STP (Surface Temperature Program), which is capable of directly interfacing with THTD output. Due to modeling differences between the finite-element and THTD heat-transfer models, adjustments had to be made to the STP-generated element face temperatures. A time-sharing computer program was written to determine the corresponding temperatures for each of the finite-element nodes.

A combined thermal and mechanical linear elastic stress analysis of the blade tip model was made, incorporating the updated temperatures, using both MASS and ANSYS. The runs were made to serve as a stress validity check prior to making more expensive creep runs using ANSYS. Stress analysis results agreed within 5% between the two programs, with the MASS results being consistently higher than those determined from ANSYS. This comparison was made on the basis of surface stresses and the difference could be attributed to a number of different factors. These include how the programs handle temperature variations, how they calculate surface stresses, how they handle temperature-dependent material properties, and the integration order. Again, the most highly strained (compressive) regions are coincident with points where cracking was observed during test.

Mission cycle transient heat-tranfer analysis was also performed for the subject component for the 23 time points shown in Figure 4.5-5. Small increments were chosen to ensure that analytical error would not be introduced due to gross temperature changes between steps. Interfacing of THTD model results with the finite-element model was performed as previously described for each of the 23 time steps.

Linear elastic finite-element analyses (MASS) were made at selected time steps for the purpose of determining a strain and temperature history to be used in the testing of a smooth axially loaded, air-cooled, cylindrical specimen. Mission cycle transient points for which analysis was performed are

100% SPAN

98% SPAN

96% SPAN
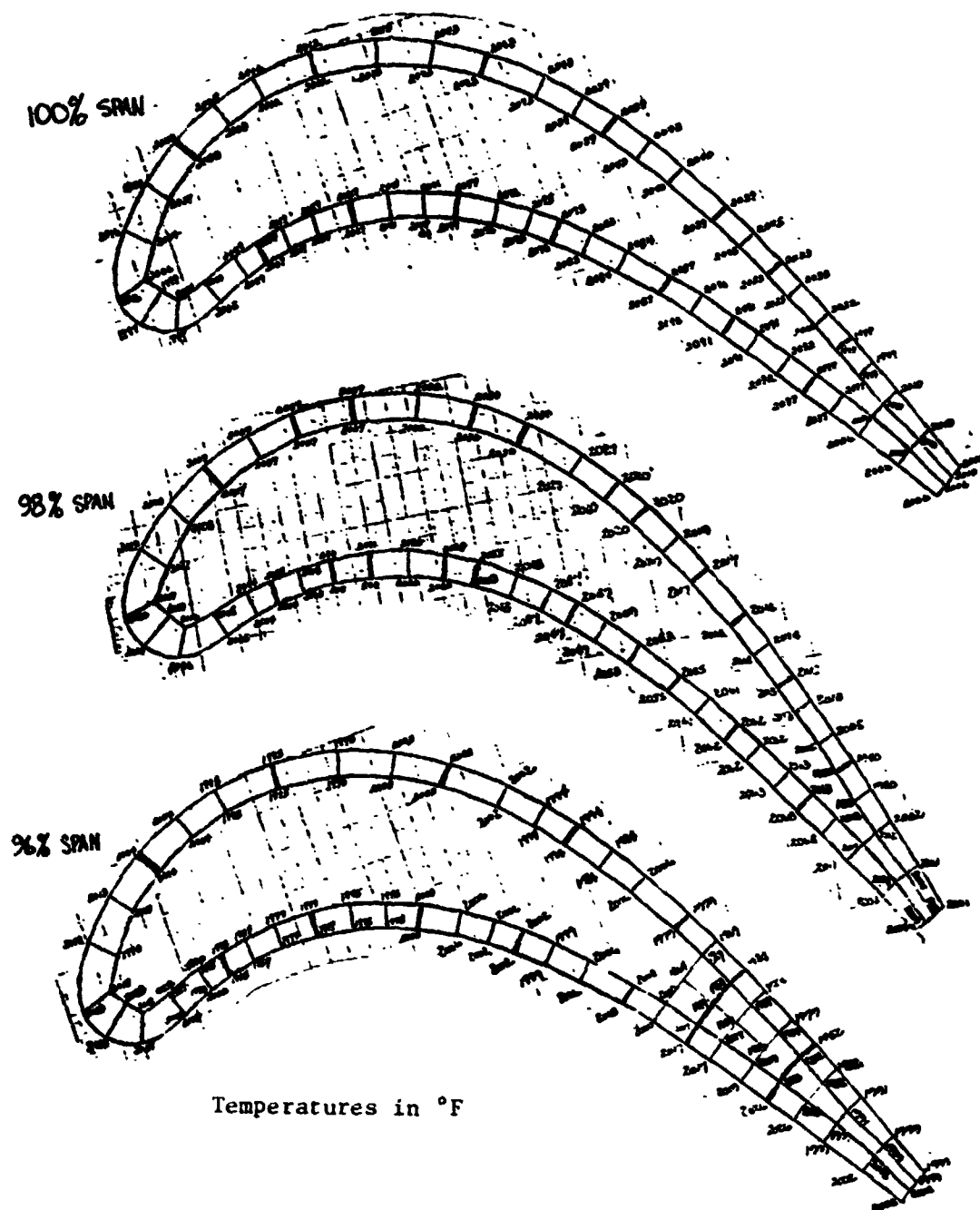
Temperatures in °F

Figure 4.5-1. Steady-State Temperatures for Hot-Day Takeoff
Condition - Squealer Tip Region.
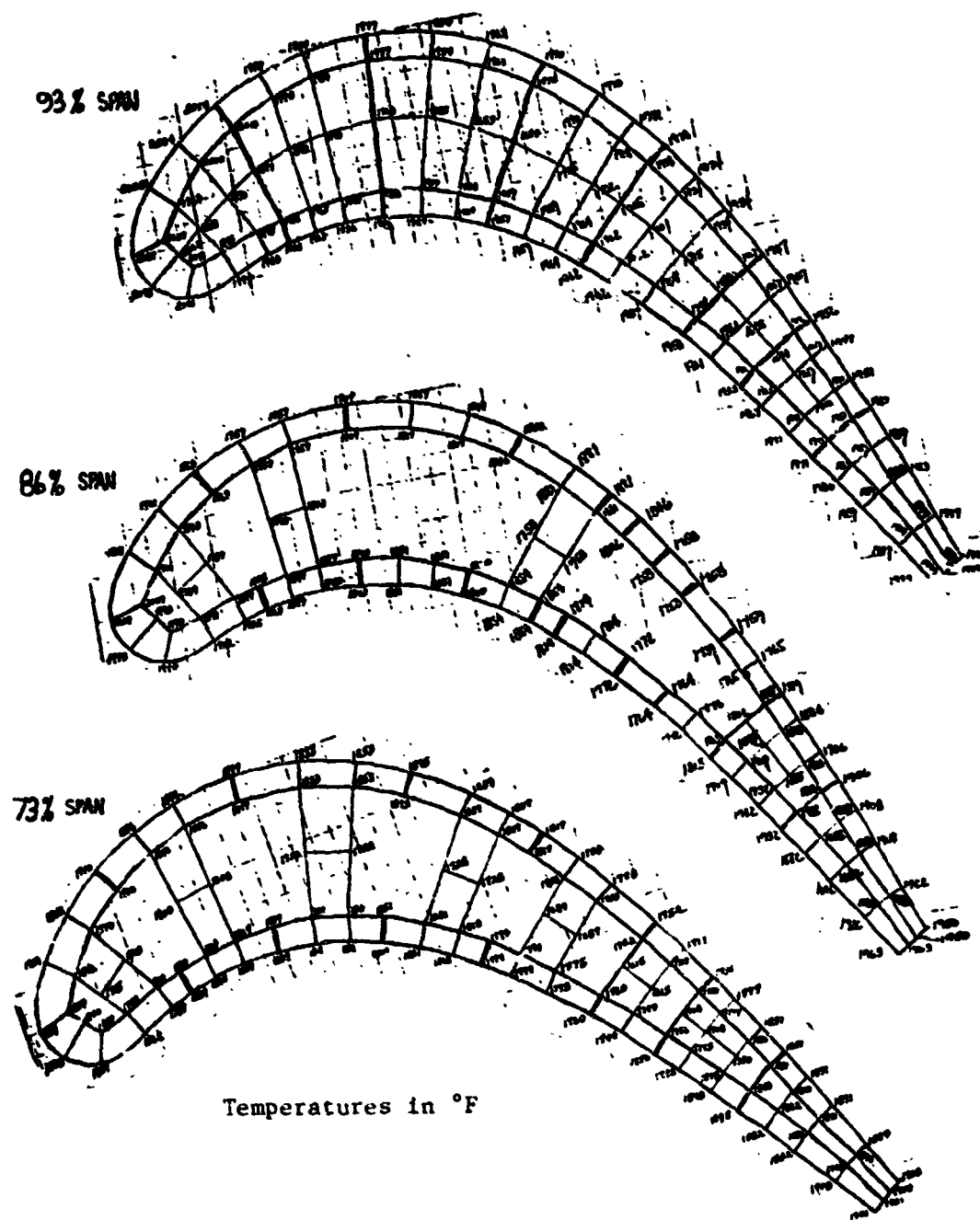
Temperatures in °F

Figure 4.5-2. Steady-State Temperatures for Hot-Day Takeoff
Condition - Tip Cap Region and Below.

Figure 4.5-3. 3-D Elastic Stress Analysis - Squealer Tip Region -
Chordwise Stresses.

STRESSES IN KSI
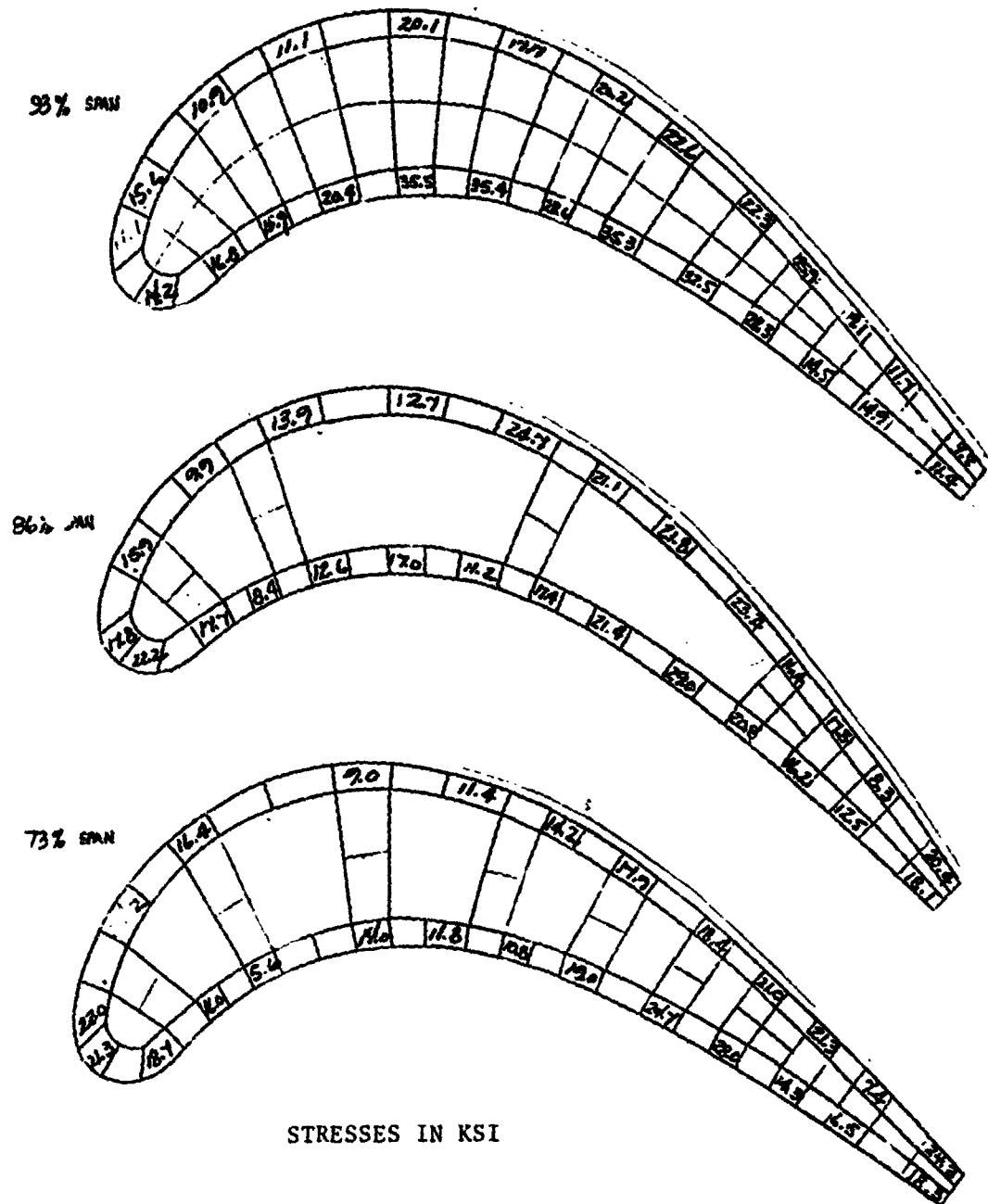
Figure 4.5-4. 3-D Elastic Stress Analysis - Tip Cap Region
and Below - Chordwise Stresses.
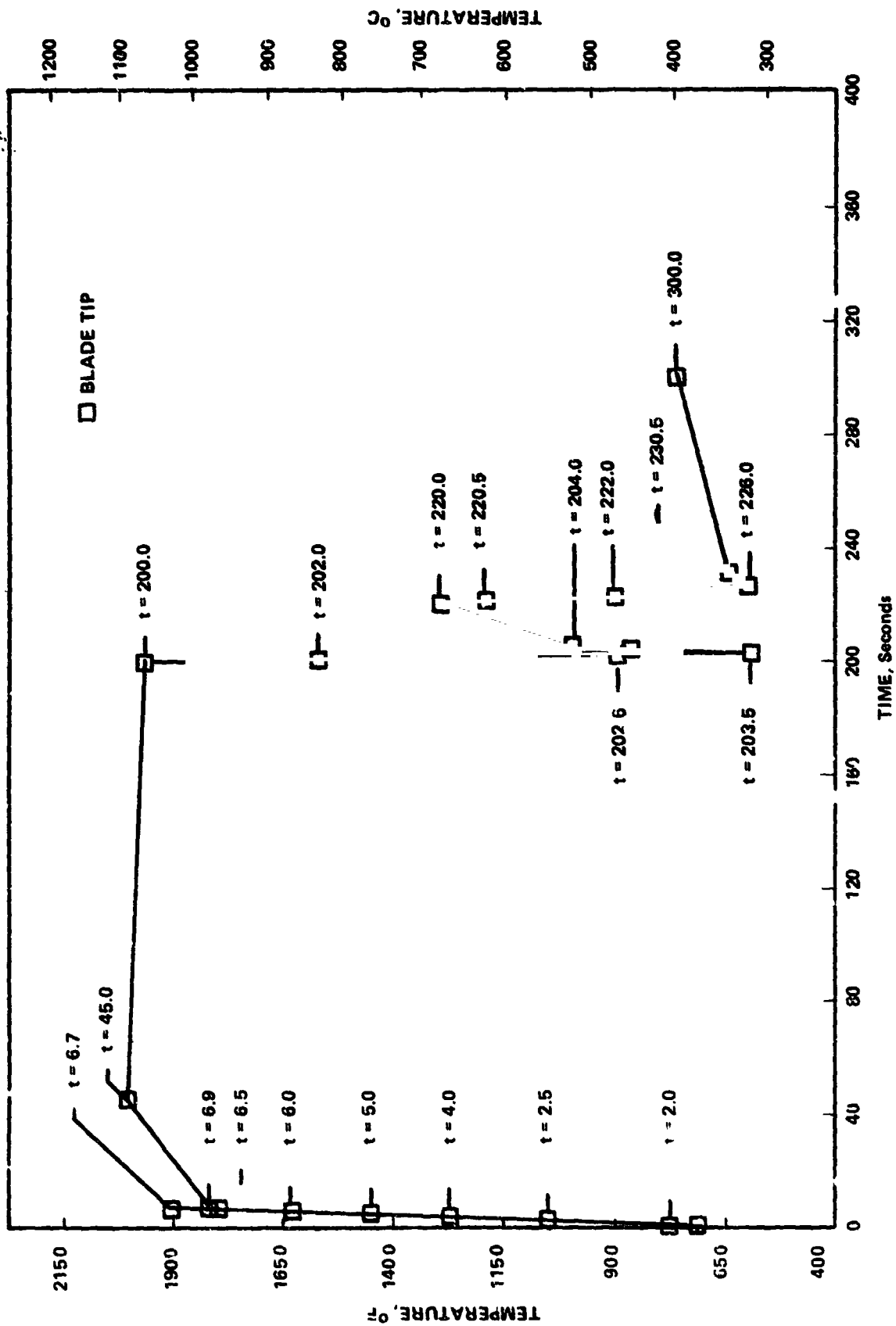
Figure 4.5-5. Time Points Chosen for Transient Analysis.

6.7 seconds (accel overshoot), 6.9 seconds (overshot dropoff), 45 seconds (steady-state), 203.5 seconds (thrust reverse), 220 seconds (burst), and 226 seconds (decel). The strain and temperature cycles were determined from the results at the critical area of the blade tip. The area is located on the suction side near the trailing edge and was selected because of good correlation between test-observed cracking and analytically predicted stress levels. Figure 4.5-6 shows the selected blade tip location. Plots of strain and blade metal temperature versus time are presented in Figures 4.5-7 and 4.5-8 for the critical location.

A newly developed and implemented postprocessing routine that allows the user to plot contour lines on a curved surface, with subsurface structure removed via hidden lines, has been used to assist in the blade tip model analysis. The model can be oriented in any desired fashion, permitting an efficient means of pursuing analysis results. Contour plots of transient analysis steady-state-condition temperature (Figures 4.5-9 and 4.5-10) and effective stress (Figures 4.5-11 and 4.5-12) are shown for both the pressure- and suction-side faces of the blade tip. Figure 4.5-13 depicts suction-side face principal stress levels for the same time point

4.6   INELASTIC ANALYSIS

Cyclic inelastic (creep and plasticity) finite-element stress analysis was conducted for the full blade tip model (580 elements, 1119 nodes) using ANSYS. An ANSYS deck generator was created and utilized to set up an inelastic model for the 23 mission cycle transient time points. The resultant data were read to tape and shipped to Houston, Texas, for processing on the CDC 176 computer.

Initially, nonlinear cyclic stress analysis was performed for one complete mission transient cycle including all 23 time points. One cost-reduction measure investigated was the elimination of unnecessary analysis points within the mission cycle transient. Upon completion of one pass through the cycle, using the 23 time points originally selected, it was observed that reducing the number of analysis points to those shown in Figure 4.6-1 would have an insignificant effect on the results, provided that a sufficient number of iterations would be allowed so that convergence criteria could be met. As verification, the initial cycle was rerun using only these points. Excellent agreement was found between analyses, and all subsequent runs were made with the "reduced" cycle.

The three-dimensional blade tip finite-element model was successfully run through seven thermal loading cycles. Contour plots of minimum principal strain are presented in Figures 4.6-2 and 4.6-3 for the pressure- and suction-side faces, respectively. Results in the form of stress versus strain at the previously chosen critical location (Element 19) are shown in Figure 4.6-4 for the first two cycles. Considering the initial loading cycle the stress-strain response can be described as follows:
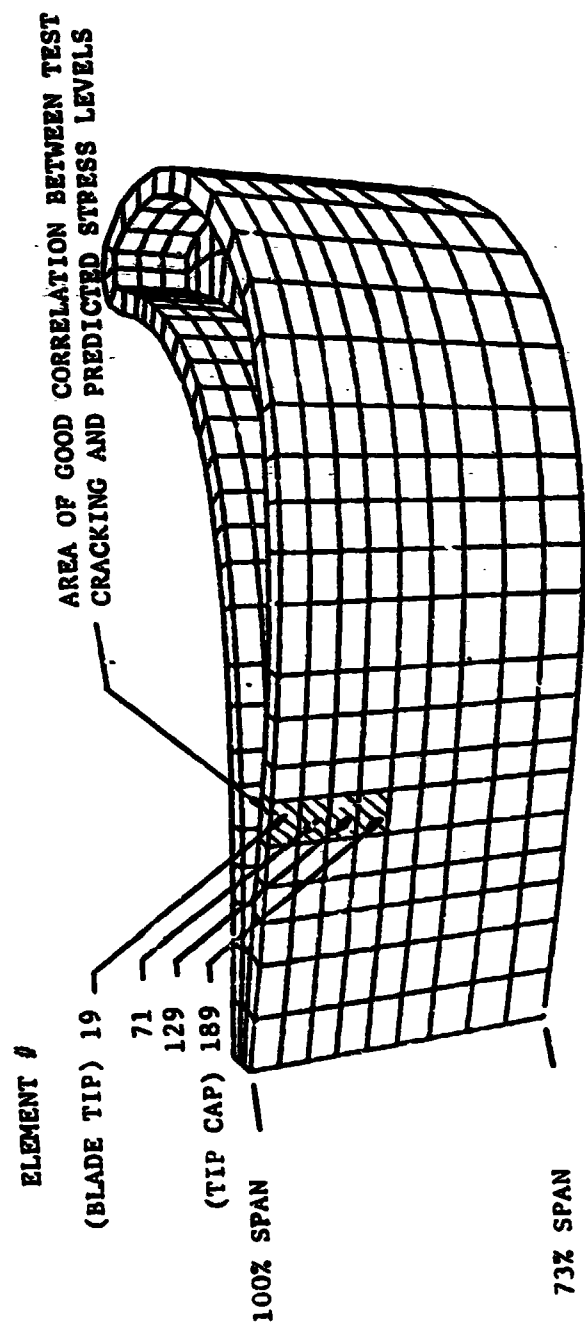
Figure 4.5-6. Blade Tip Location Chosen for Analysis.
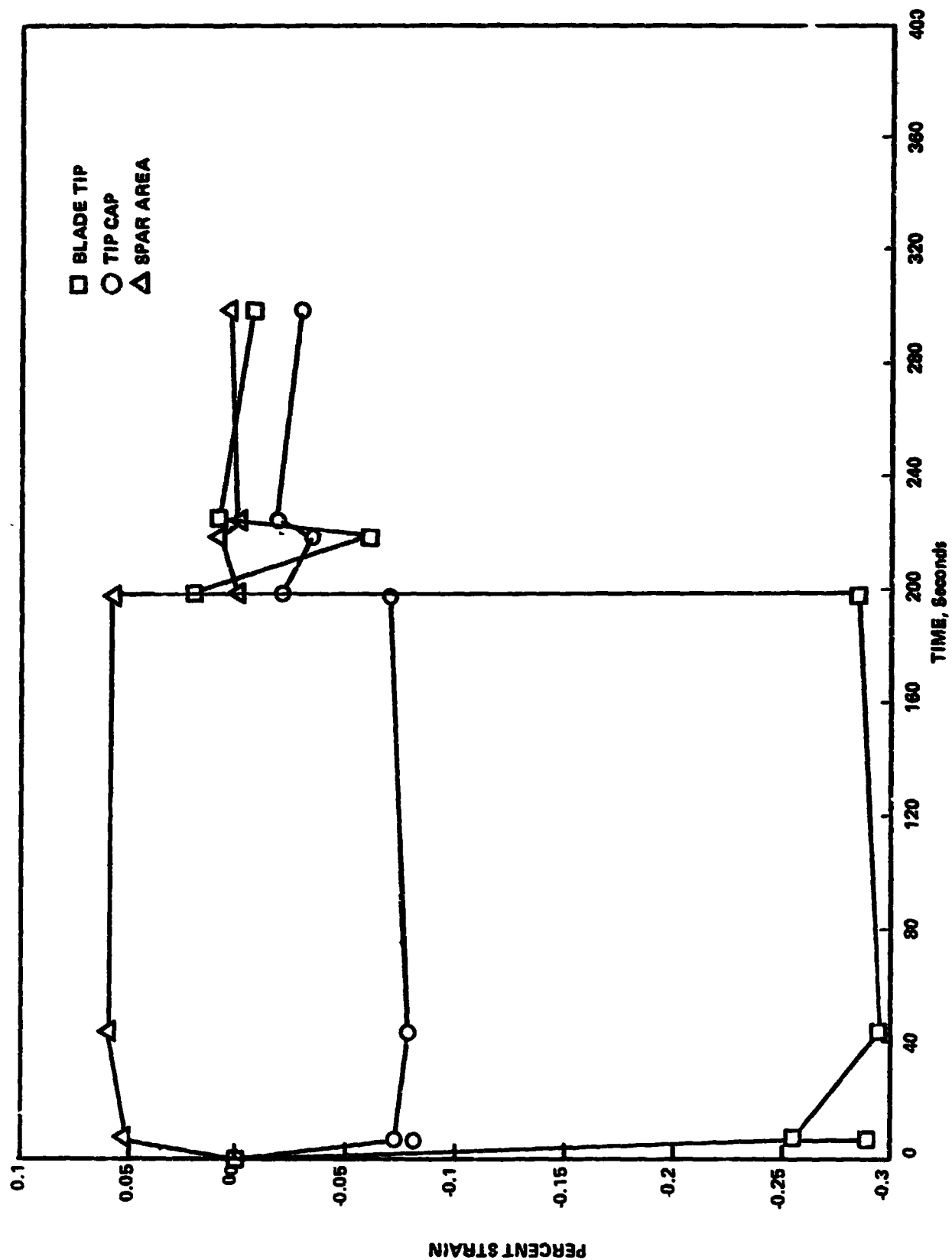
Figure 4.5-7. Principal Strain vs. Time for Critical Location (MASS Analysis).
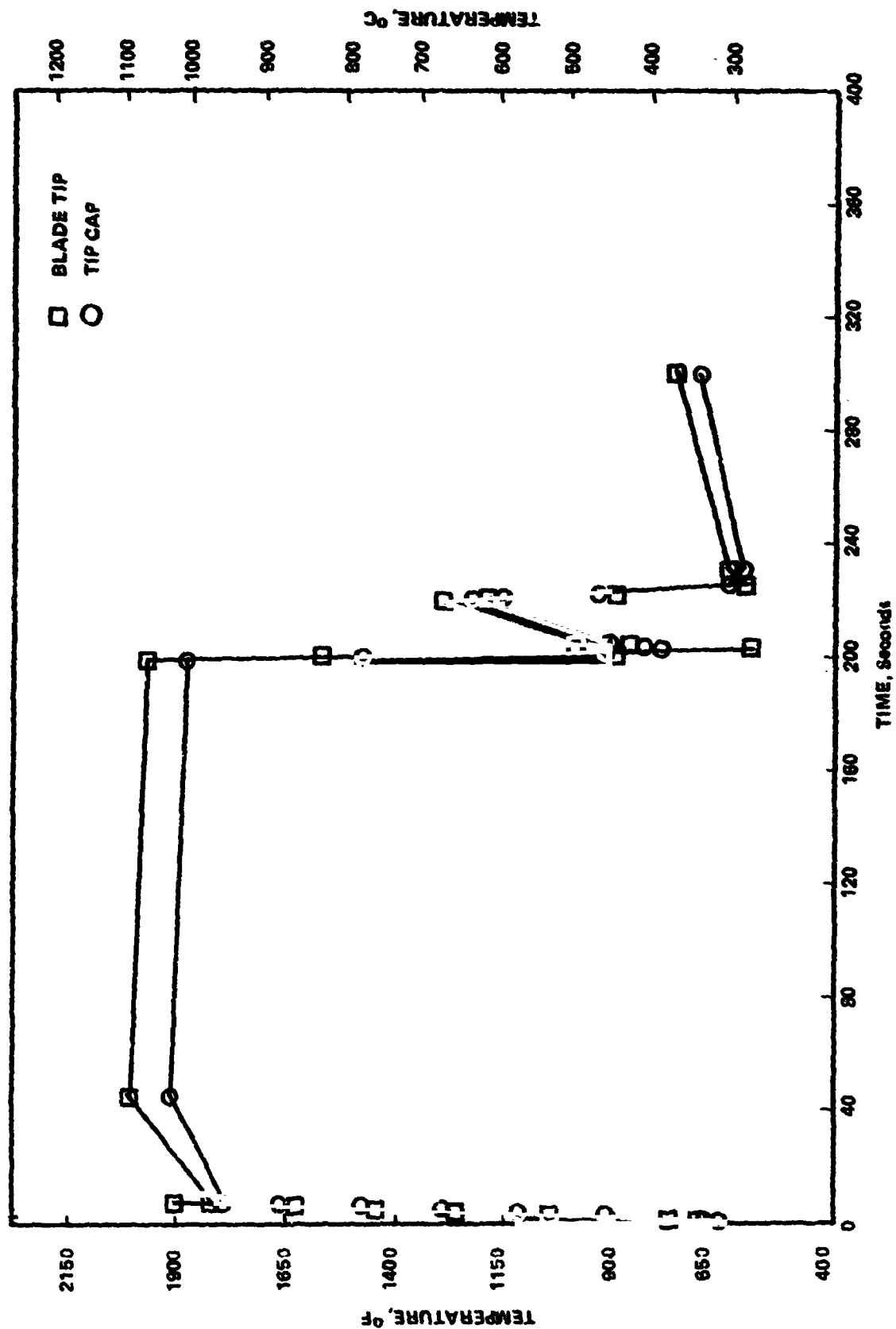
Figure 4.5-8. Blade Metal Temperature vs. Time for Critical Location.

BLADE TIP MODEL - TEMPERATURE CONTOUR PLOT

● MISSION CYCLE TRANSIENT - TIME = 45
  SECONDS (STEADY-STATE CONDITION)

-100% SPAN

-73% SPAN
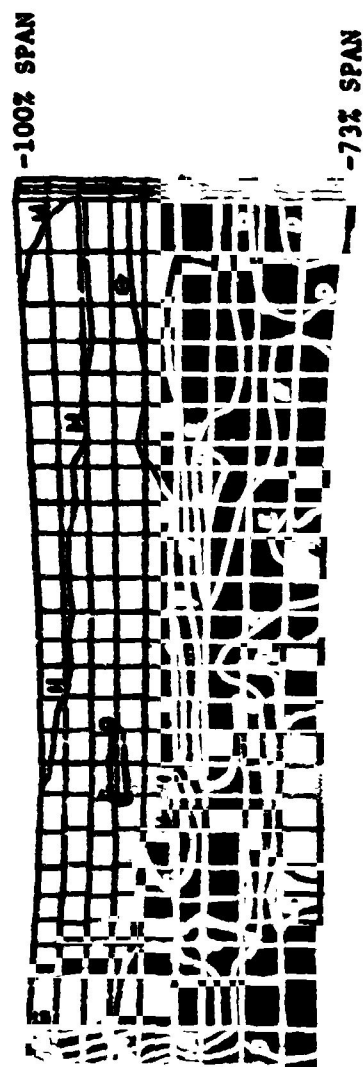
KEY:

H - 1120° C (2050° F)
G - 1070° C (1950° F)
F - 1010° C (1850° F)
E - 950° C (1750° F)
D - 900° C (1650° F)

Figure 4.5-9.   Blade Tip Model - Temperature Contour Plot -
                Pressure-Side Face.

37

● MISSION CYCLE TRANSIENT ANALYSIS –
TIME = 45 SECONDS (STEADY-STATE
CONDITION)

100% SPAN–

73% SPAN–

KEY:
G – 1120° C (2050° F)
F – 1070° C (1950° F)
E – 1010° C (1850° F)
D – 950° C (1750° F)
C – 900° C (1650° F)

Figure 4.5-10. Blade Tip Model – Temperature Contour Plot –
Suction-Side Face.

● MISSION CYCLE TRANSIENT ANALYSIS –
  TIME = 45 SECONDS (STEADY–STATE
  CONDITION)

100% SPAN—

73% SPAN—

KEY:

E   280 MPa (40 ksi)
D   210 MPa (30 ksi)
C   140 MPa (20 ksi)
B   70 MPa (10 ksi)
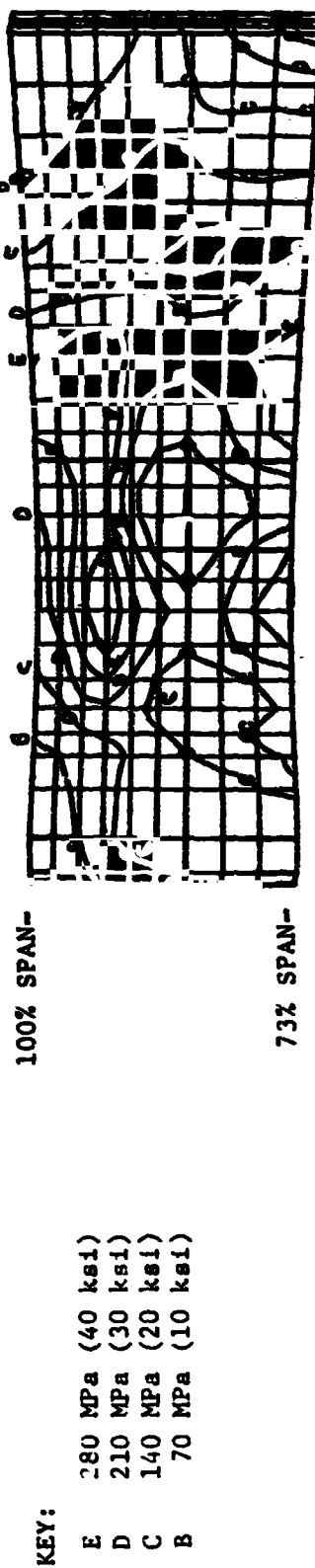
Figure 4.5-11. Blade Tip Model – Effective Stress Contour Plot –
Pressure–Side Face.

- MISSION CYCLE TRANSIENT ANALYSIS
  TIME = 45 SECONDS (STEADY-STATE
  CONDITION)

KEY:

E   280 MPa (40 ksi)
D   210 MPa (30 ksi)
C   140 MPa (20 ksi)
B   70 MPa (10 psi)
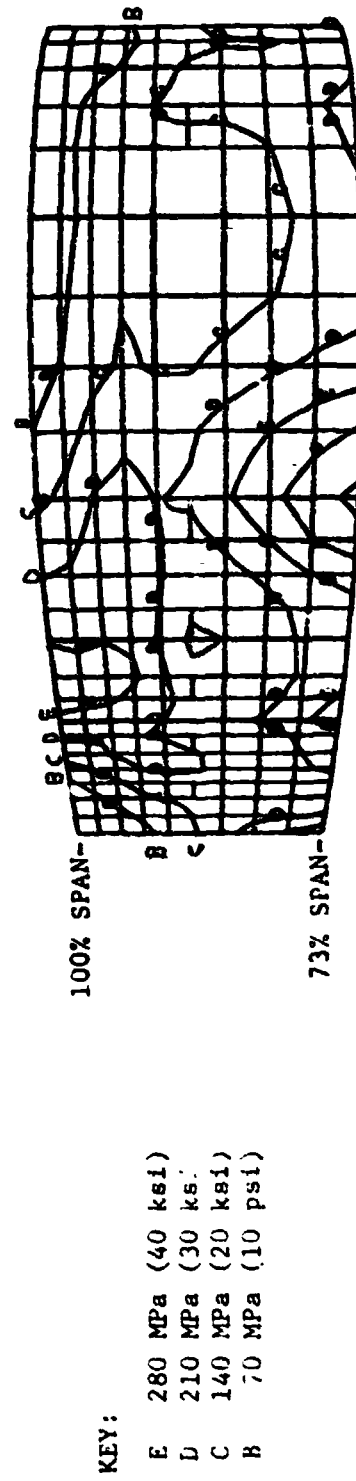
Figure 4.5-12.   Blade Tip Model - Effective Stress Contour Plot -
Suction-Side Face.

- MISSION CYCLE TRANSIENT ANALYSIS –
  TIME = 45 SECONDS (STEADY-STATE
  CONDITION)

100% SPAN–

73% SPAN–

KEY:

H	140 MPa	(20 ksi)
G	70 MPa	(10 ksi)
F	0 MPa	(0 psi)
E	-70 MPa	(-10 psi)
D	-140 MPa	(-20 psi)
C	-210 MPa	(-30 psi)
B	-280 MPa	(-40 psi)
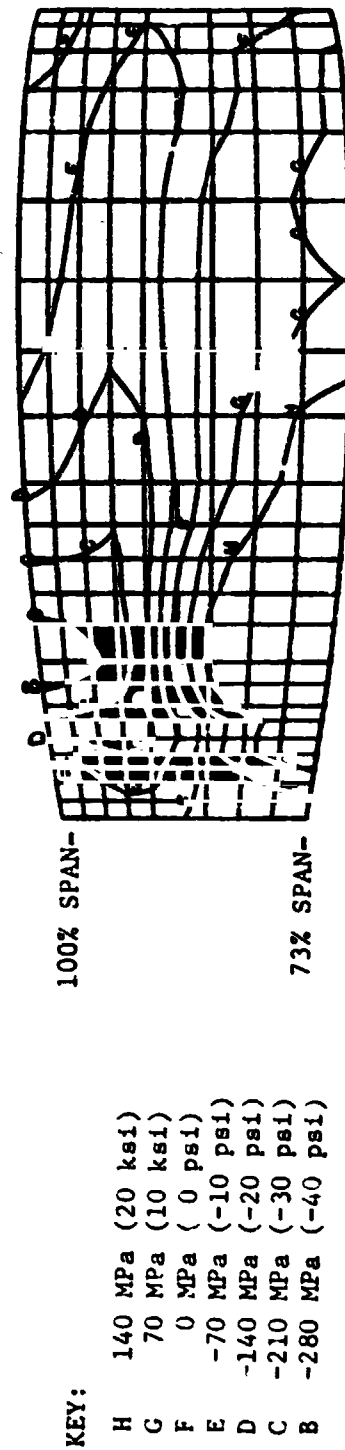
Figure 4.5-13. Blade Tip Model – Chordwise Stress Contour Plot –
Suction-Side Face.

Temperature (°C)

1200
1100
1000
900
800
700
600
500
400
300

Blade Tip
(Element 19)

● Time Points Chosen for Inelastic Analysis
● Darkened Squares Indicate Points Selected for the "Reduced" Cycle

t=6.7
t = 45.0
t=6.9
t=6.5
t = 5.0
t = 4.0
t = 2.5
t = 0.5
t = 0.2

t = 200.0
t = 202.0
t = 220.0
t = 220.5
t = 204.0
t = 222.0
t = 230.5
t = 226.0
t = 300.0

t =202.6
t=202.5

2150
1900
1650
1400
1150
900
650
400

Temperature (° F)

TIME (Sec)

0   40   80   120   160   200   240   280   320   360   400
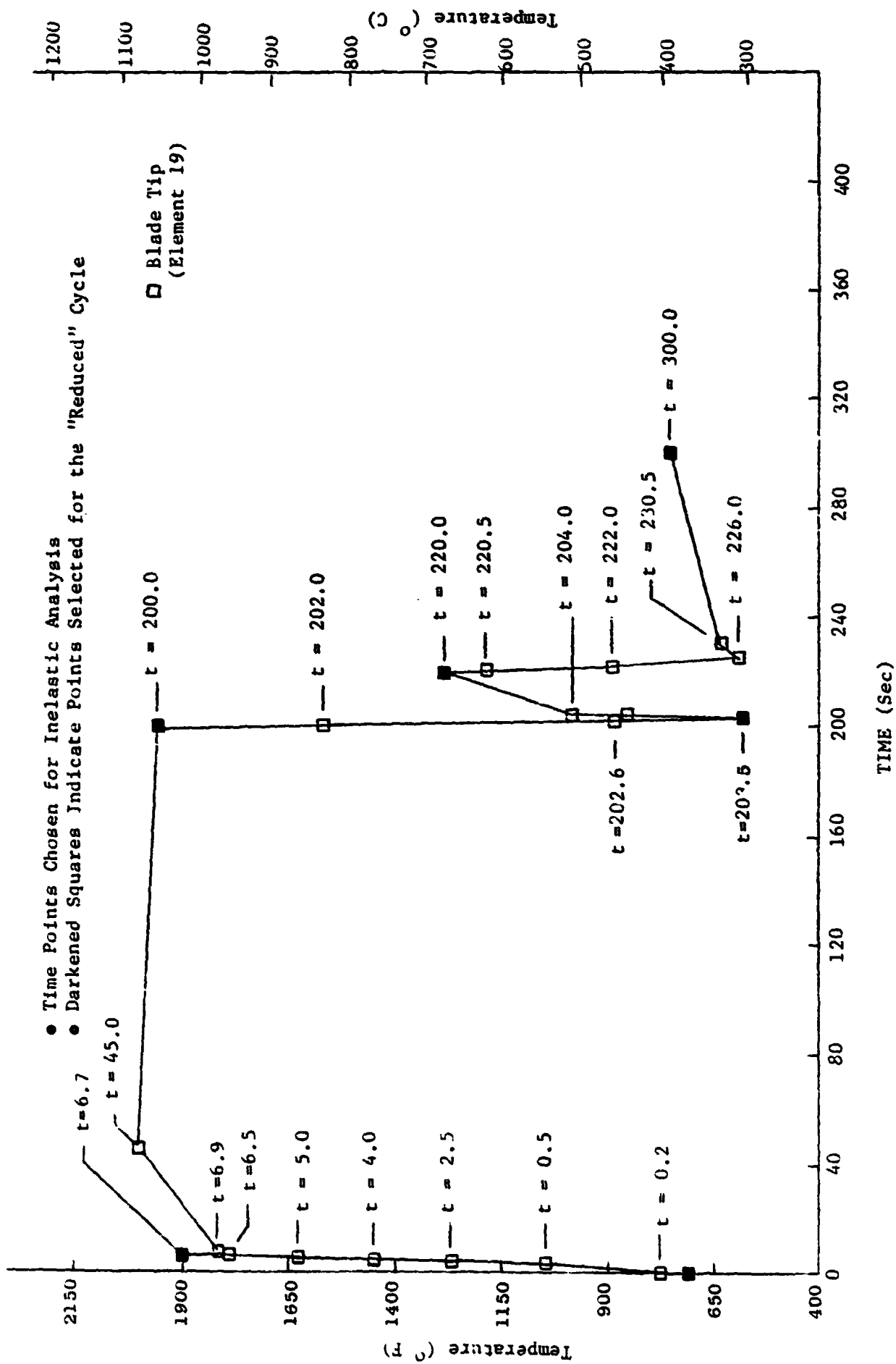
Figure 4.6-1. Blade Metal Temperature vs. Time at Critical Location.-

42

- INELASTIC ANALYSIS

- MISSION CYCLE TRANSIENT ANALYSIS - TIME = 45 SECONDS
  (STEADY-STATE POINT)

BLADE TIP

TIP CAP

KEY:

B = -0.0040
C = -0.0025
D = -0.0010

Figure 4.6-2. Blade Tip Model - Contour Plot of Principal Strains - Pressure-Side Face.

Figure 4.6-3. Blade Tip Model - Contour Plot of Principal Strains - Suction-Side Face.

- INELASTIC ANALYSIS
- MISSION CYCLE TRANSIENT ANALYSIS - TIME = 45 SECONDS (STEADY-STATE POINT)

KEY:

B = -0.0040
C = -0.0025
D = -0.0010

44
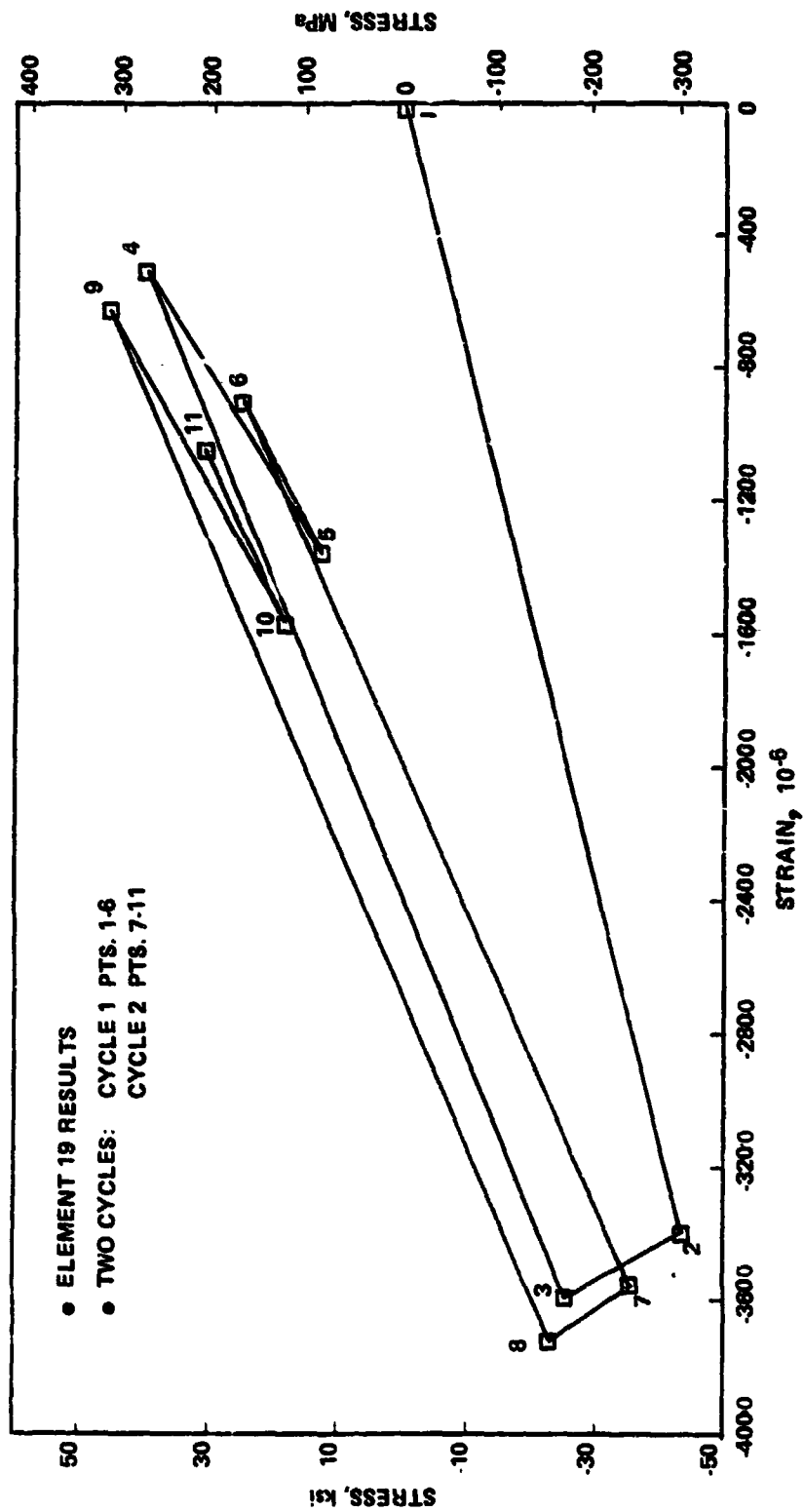
Figure 4.6-4. ANSYS Inelastic Analysis Results –
Initial Two Cycles.

Cycle Points	Response
1-2	Elastic-plastic response during heat-up (accel)
2-3	Essentially elastic-creep response at constant temperature (steady-state)
3-4	Elastic response during cool-down - no reverse plasticity was experienced (thrust reverse)
4-6	Elastic response during heat-up and cool-down (burst and decel)

It is observed that a large amount of plasticity occurs during the initial heat-up portion of the first cycle. Creep occurs during the subsequent steady-state hold time, reducing some of the plasticity. Reversed plasticity is not experienced in the cool-down segment, resulting in residual compressive strain and tensile stress at the end of the cycle. A stress-strain curve which contains a smaller amount of plasticity is generated by the second thermal loading. As shown in Figure 4.6-5, subsequent cycles will produce hysteresis loops that move progressively in the negative strain direction, with larger peak tensile stresses during the cool-down portion of the cycle. This is consistent with the fact that the progressively higher peak tensile stresses cause a longer elastic range to be traversed [because of the shape of the low-temperature (320° C, 600° F) stress-strain curve] before yielding can occur due to the heat-up portion of the cycle. Additionally, the predicted creep strain, while still increasing, does so at a slower rate with each increasing cycle as the stress level at the hot end of the cycle stabilizes. While complete hysteresis loop stabilization has not occurred by the seventh cycle, the maximum change in strain between the sixth and seventh cycles for any comparable points is less than 35μ-m/m. The corresponding maximum stress change is less than 6.9 MPa (1 ksi) (Table 4.6-1). This is felt to be adequate stabilization for analysis requirements, and no additional inelastic cyclic analysis is needed.

In support of the thermomechanical fatigue (TMF) test program, an inelastic cyclic analysis was made for the simple model shown in Figure 4.6-6, using CYANIDE, to make some prejudgments on shakedown and LCF effects. The model represents an axial slice of Element 19 (Figure 4.5-6), the full model element located at the suction-side face of the blade tip, in the area selected for use in TMF test cycle definition. The 2-D representation consists of constant-strain triangular elements with loading applied in the R direction at Nodes 2 and 5. Displacements and temperatures conforming to TMF Cycle I (MASS elastic analysis results, Section 5.2) were imposed on the model as shown in Figures 4.6-7 and 4.6-8. The cyclic hysteresis loop (Figure 4.6-9) shows that after a large amount of plasticity incurred during the initial heat-up portion of the first cycle, a ratcheting effect is experienced with progressively higher tensile stresses during the cool-down portion of each cycle. This ratcheting effect will continue until a zero stress level is reached during the hot potion of the cycle. No change is seen in total strain range or the min/max strain values since it is held constant, as will be the case during TMF testing. However, Figures 4.6-10 and 4.6-11 show that during cycling a definite tradeoff occurs between plastic strain (which becomes progressively more positive) and creep strain (which becomes progressively more negative). The
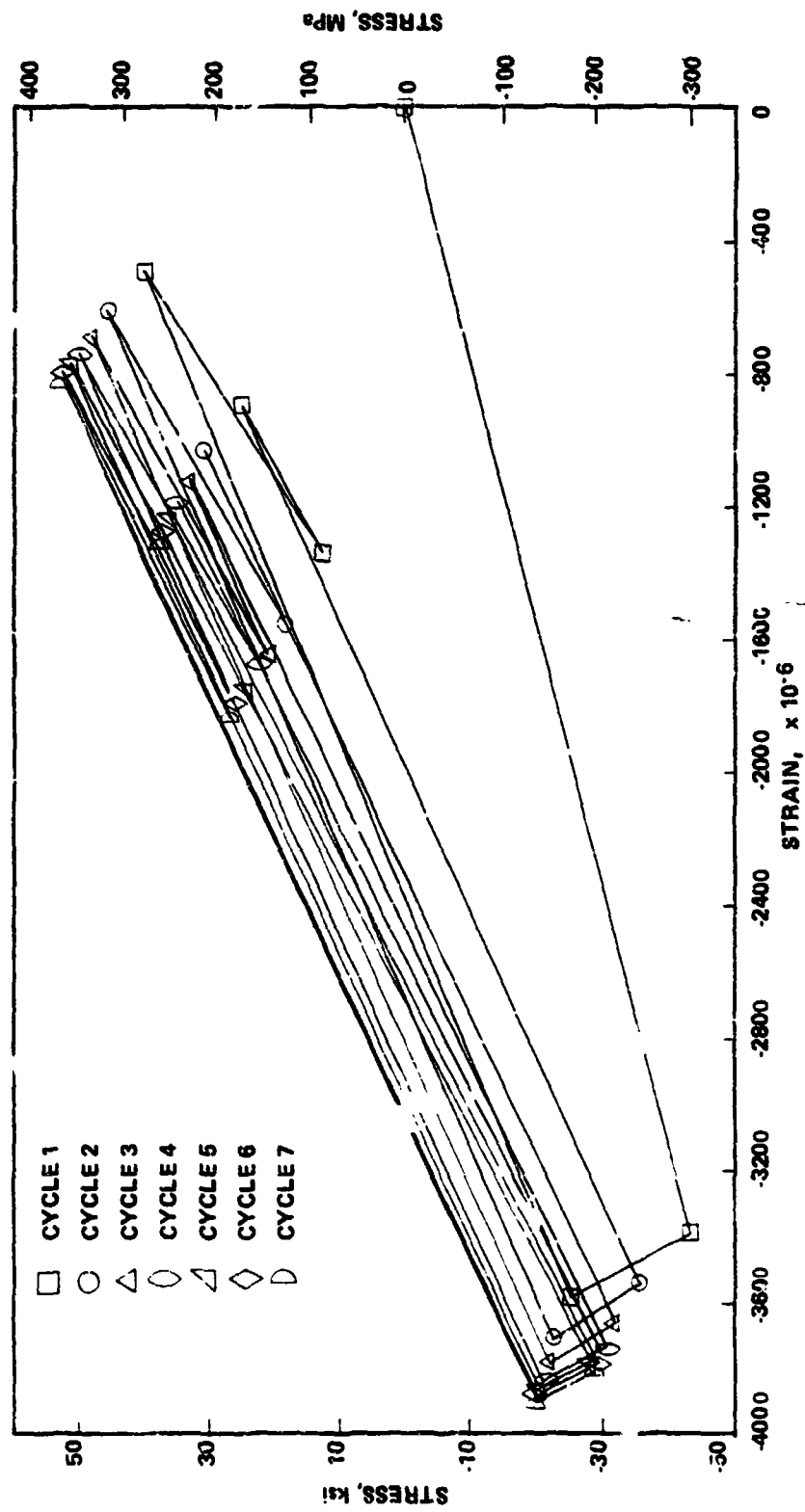
Figure 4.6-5. ANSYS Inelastic Analysis Results - Seven Cycles.

47

Table 4.6-1

ANSYS INELASTIC ANALYSES RESULTS

- Element 19 Results
- Stress vs. Strain

P_T	Strain, 10^{-6}	Stress (ksi)	Stress (MPa)
1	0	0	0
2	-338ċ	-43.52	-300.29
3	-3582	-25.?3	-174.78
4	-500	39.78	274.4̃
5	-1348	˙˙.50	86.25
6	-901	-34.73	-239.64
7	-3540	-35.74	-246.61
8	-3710	-22.82	-157.46
9	-620	45.50	313.95
10	-1560	18.02	124.34
11	-1040	30.40	209.76
12	-3663	-31.90	-220.11
13	-3787	-21.93	-151.32
14	-691	47.9G	330.51
15	-1648	20.56	141.86
16	-1131	33.10	228.39
17	-3741	-29.95	-206.66
18	-3839	-21.01	-144.97
19	-746	49.89	344.24
20	-1680	22.10	152.49
21	-1187	34.72	239.57
22	-3761	-29.87	-206.10
23	-3866	-20.48	-141.31
24	-775	51.10	352.59
25	-174?	23.89	164.84
26	-1243	35.81	247.09
27	-3777	-29.77	-205.41
28	-3889	-20.03	-138.21
29	-801	52.05	359.14
30	-1797	25.36	174.98
31	-1276	37.09	255.92

Cycle 1: 1–6
Cycle 2: 7–11
Cycle 3: 12–16
Cycle 4: 17–21
Cycle 5: 22–26
Cycle 6: 27–31

Table 4.6-1 (Concluded)

ANSYS INELASTIC ANALYSES RESULTS

- Element 19 Results
- Stress vs. Strain

	P_T	Strain, 10^{-6}	Stress (ksi)	Stress (MPa)
	32	−3788	−29.69	−204.86
	33	−3918	−19.78	−136.48
Cycle 7	34	−829	53.01	365.77
	35	−1825	25.99	179.33
	36	−1308	38.00	262.20
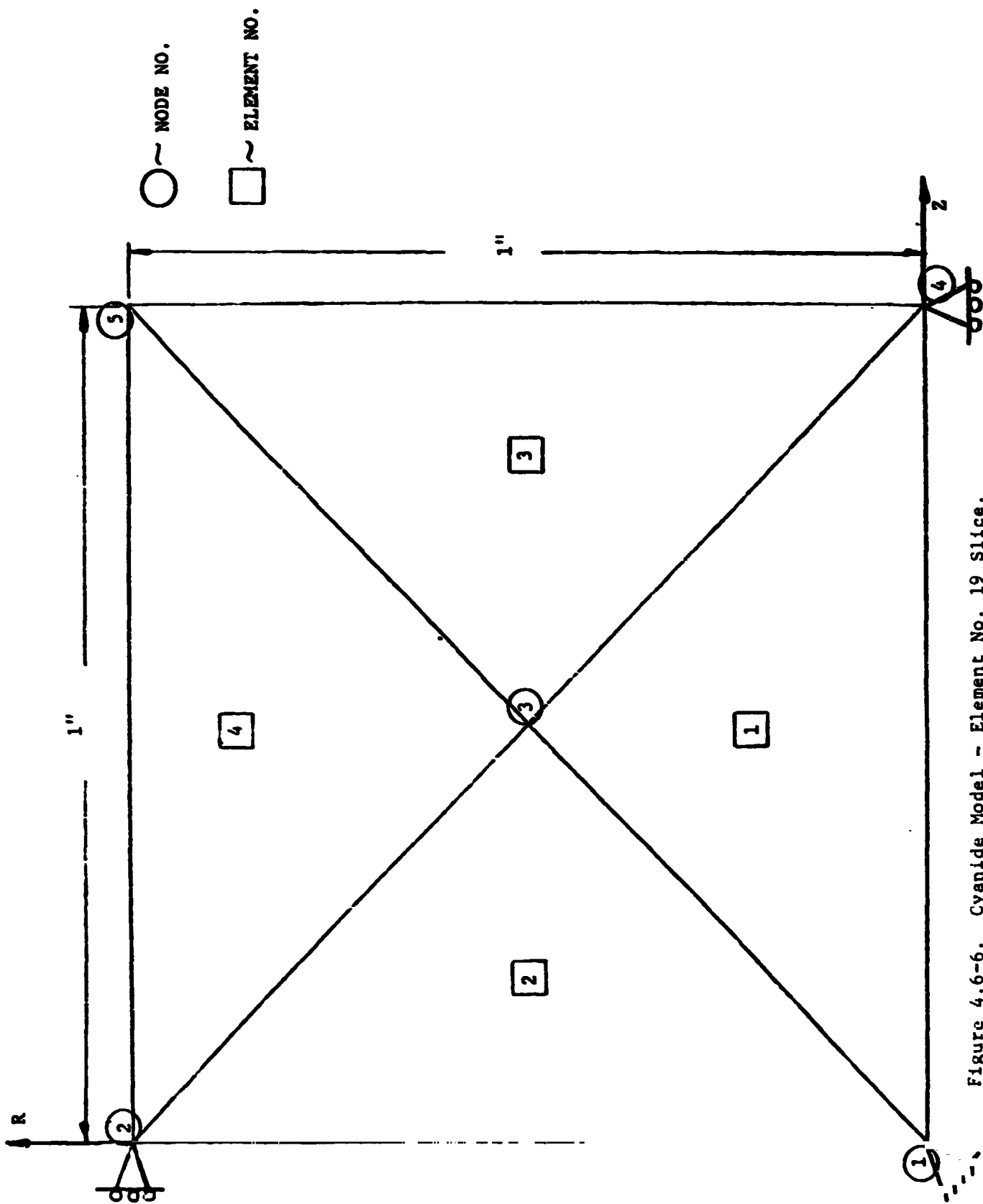
Figure 4.6-6. Cyanide Model – Element No. 19 Slice.
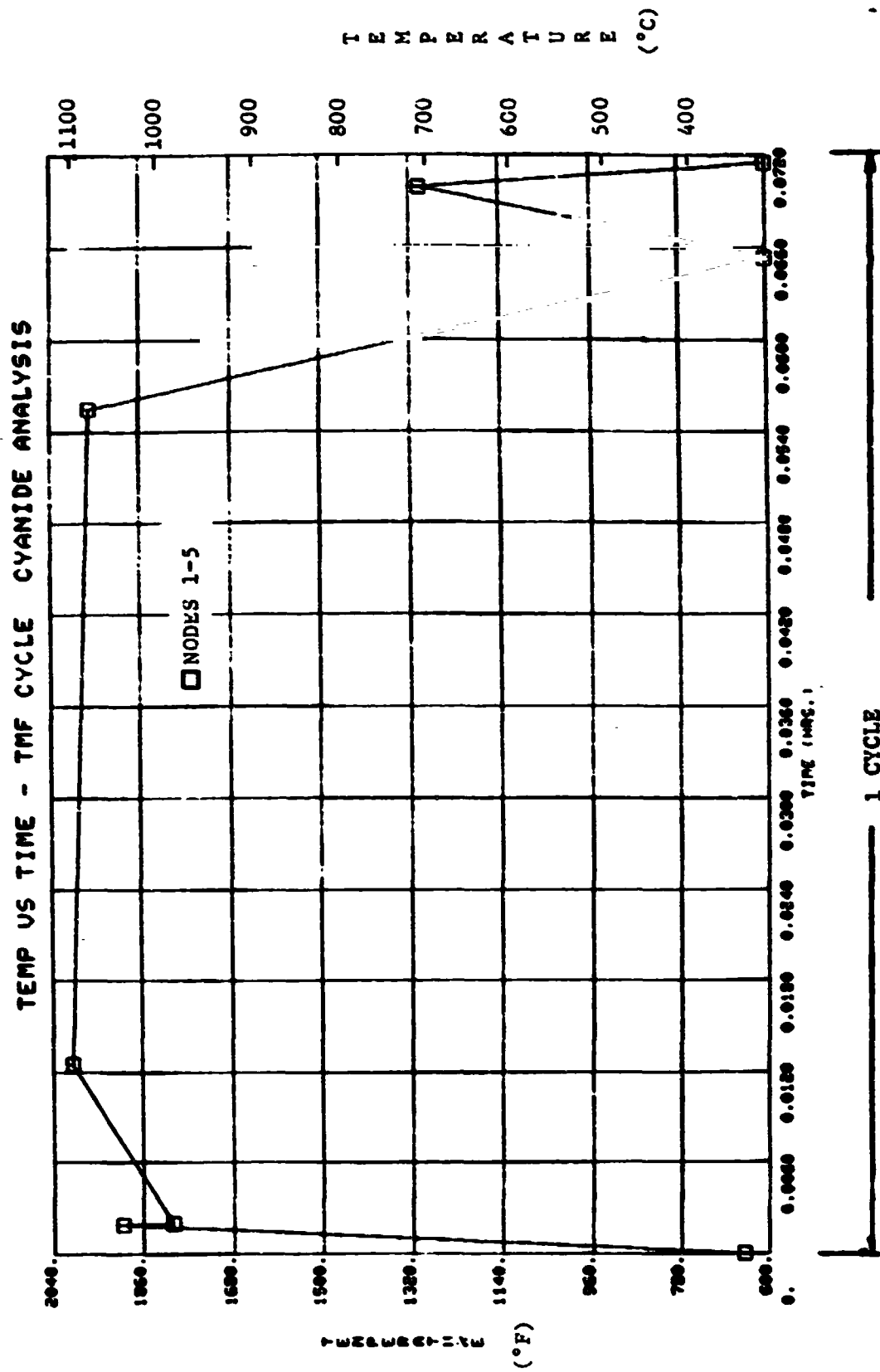
Figure 4.6-7. Transient Temperature vs. Time - Element No. 19.

51
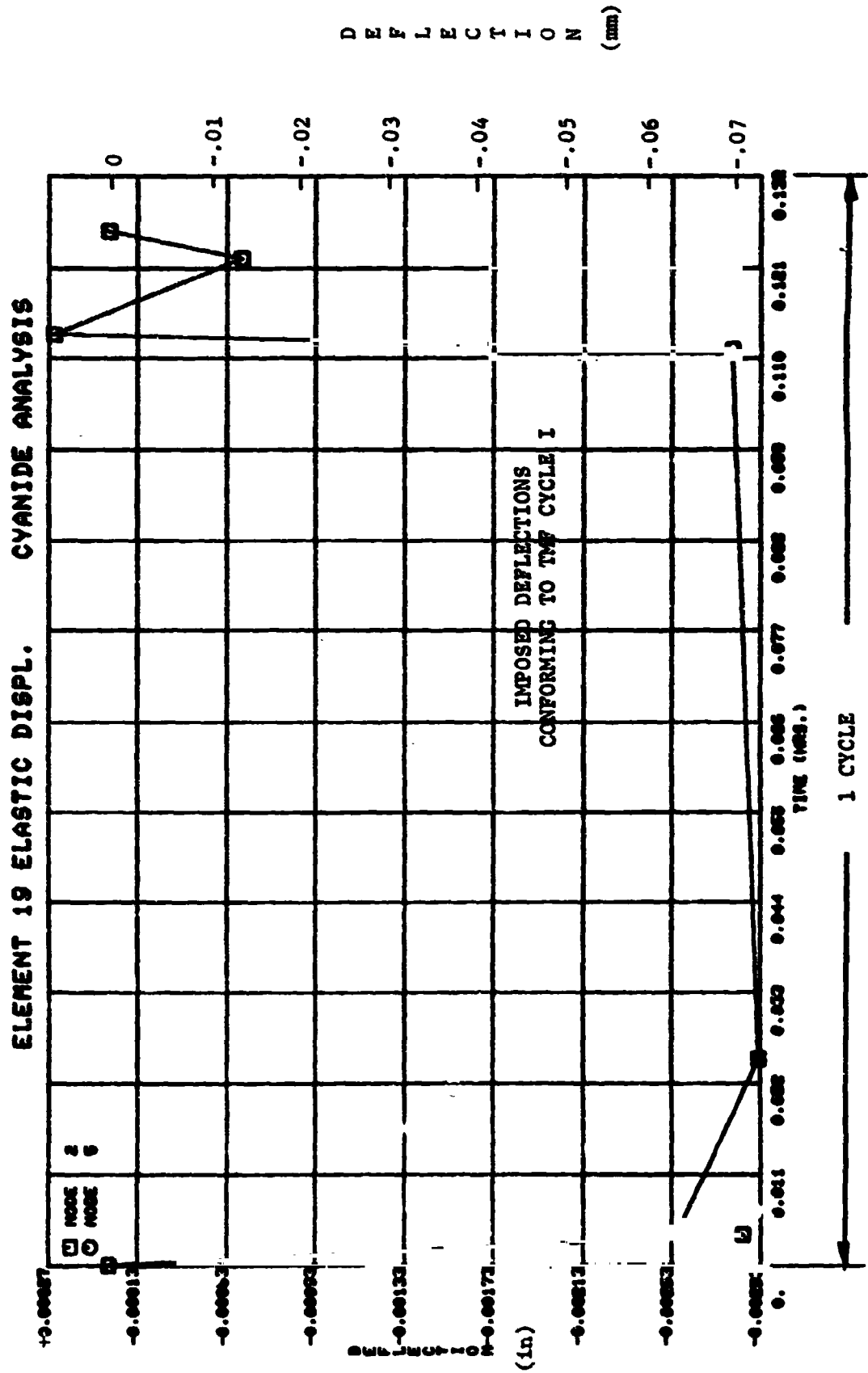
Figure 4.6-8. CYANIDE Model Deflections - Imposing Elastic Analysis Boundary Conditions.

o 14 CYCLES

o ELASTIC ANALYSIS RESULTS USED AS BOUNDARY CONDITIONS

o EACH LOOP REPRESENTS 2 CYCLE APPLICATIONS

ELEMENT 19 ELASTIC DISPL.   CYANIDE ANALYSIS

Total Strain, 10^{-6} in "R" Direction
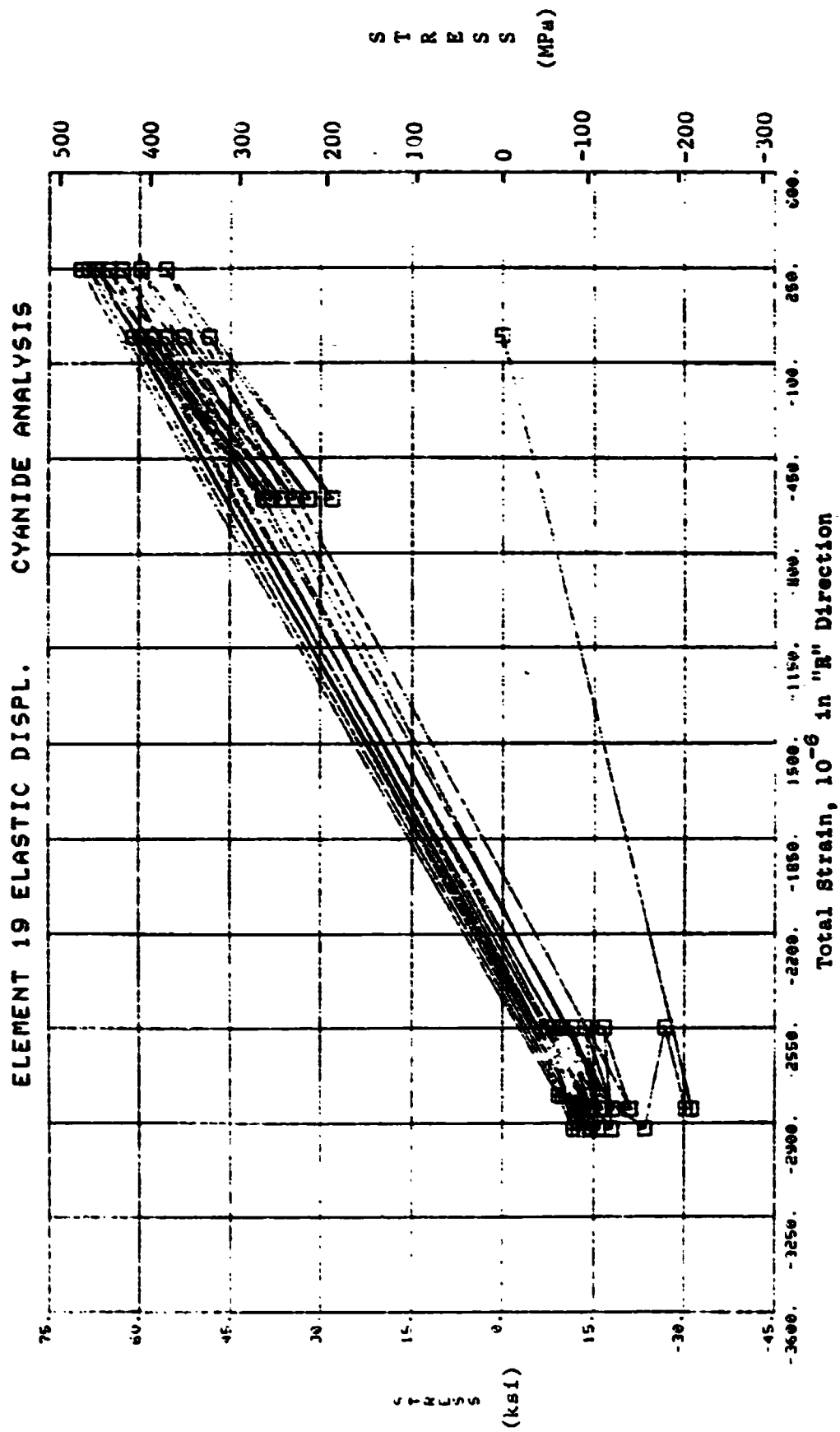
Figure 4.6-9.   CYANIDE Model Stress-Strain Response - Imposing Elastic Analysis
Boundary Conditions.

o 14 CYCLES

o ELASTIC ANALYSIS RESULTS USED AS BOUNDARY CONDITIONS

o EACH LOOP REPRESENTS 2 CYCLE APPLICATIONS

ELEMENT 19 ELASTIC DISPL.   CYANIDE ANALYSIS

Plastic Strain, 10^{-6} in "R" Direction
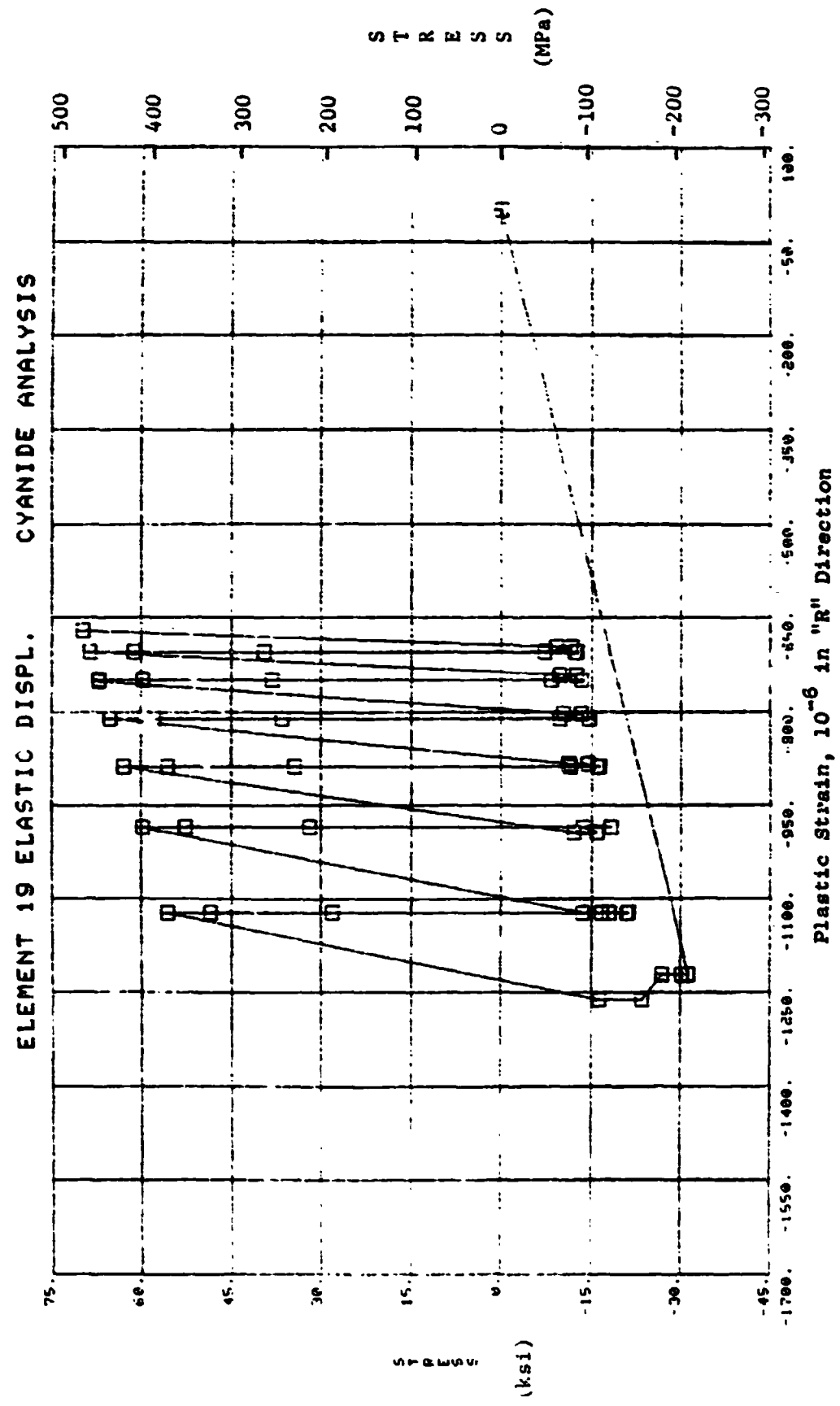
Figure 4.6-10.   CYANIDE Model Plastic Strain vs. Stress - Imposing Elastic Analysis
Boundary Conditions.

54

o 14 CYCLES

o ELASTIC ANALYSIS RESULTS USED AS BOUNDARY CONDITIONS

o EACH LOOP REPRESENTS 2 CYCLE APPLICATIONS

ELEMENT 19 ELASTIC DISPL.   CYANIDE ANALYSIS

Creep Strain, 10⁻⁶ in "R" Direction
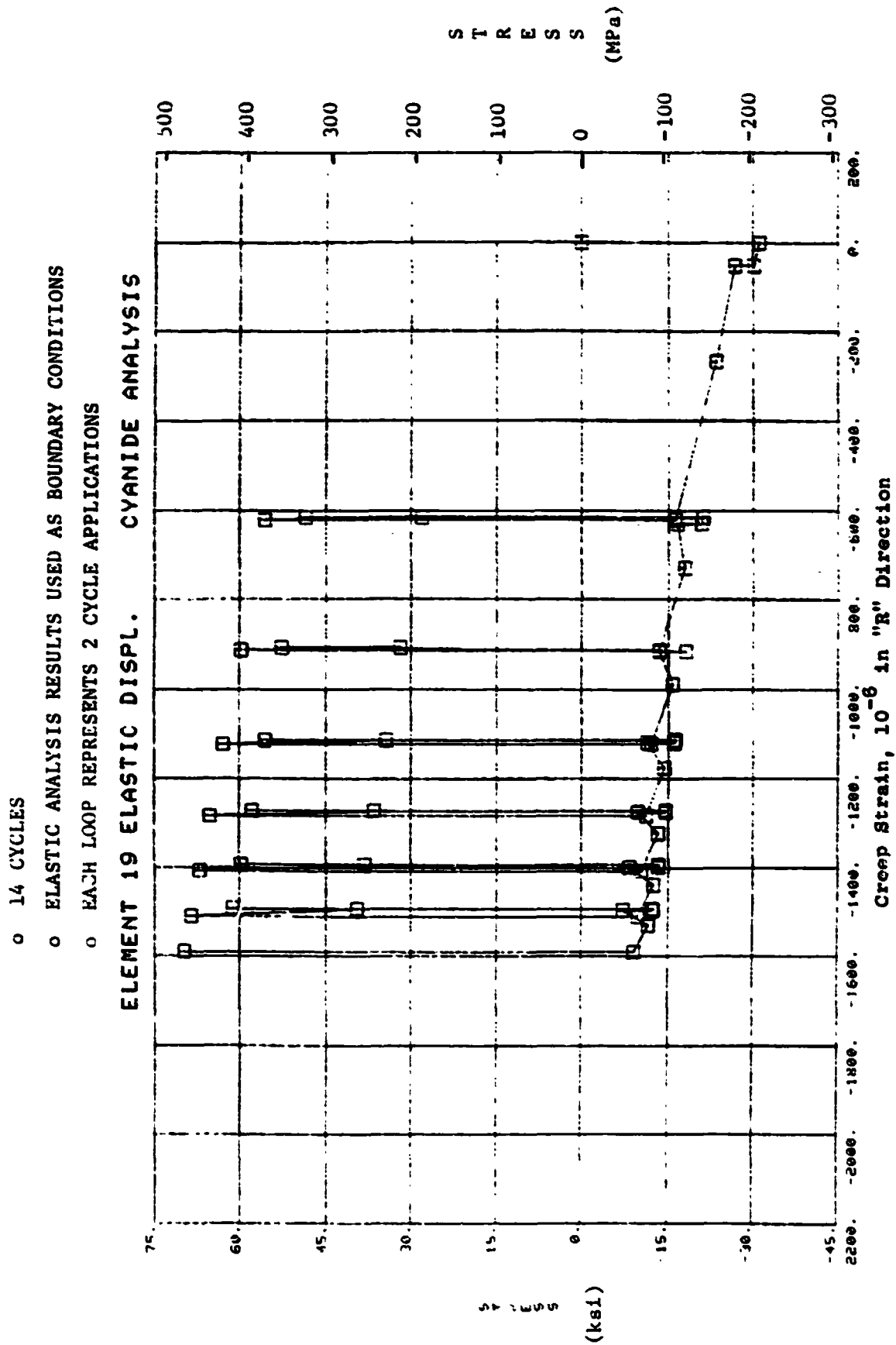
Figure 4.6-11.   CYANIDE Mode Creep Strain vs. Stress - Imposing Inelastic Analysis
Boundary Conditions.

55

change of plastic and creep strains with time is presented in Figures 4.6-12 and 4.6-13. It can be seen that by the sixteenth cycle the incremental change in both strain components is less than 10% of that occurring between start-up and the initial cycle. A similar analysis was performed imposing cyclic strains (in the form of displacements) obtained from the initial pass through the transient cycle of the ANSYS inelastic analysis for comparative purposes (Figures 4.6-14 through 4.6-16).

TMF testing as reported in Section 5.2 consisted of imposing both the elastic (MASS) and inelastic (ANSYS) analysis strain and temperature profiles (at the critical location) to a smooth axially loaded cylindrical specimen. The primary observation made from TMF test results was that stress relaxation occurred at a much faster rate experimentally than had been predicted. Figure 4.6-17 shows the correlation between CYANIDE analysis and test results for the first cycle of the elastic analysis profile. Stress relaxation (betwen Points 2 and 3) observed from testing is approximately three times greater than that of analysis. This indicates that the high-temperature creep properties and/or the creep damage model that was used require modification. It should be noted that only a small amount of short-time creep data exists at these stress-temperature levels due to the difficulty in performing such tests. The stabilized stress-strain loop which occurred by the fourth cycle experimentally is shown in Figure 4.6-18. Due to the differences in relaxation rates, CYANIDE analysis determined that 16 cycles would be required for stabilization to occur. Additionally, the peak tensile stress achieved from testing was slightly different from that predicted - 550 MPa (79 ksi) instead of 510 MPa (74 ksi). This could be due to differences in material properties (modulus of elasticity, etc.) and a slightly different test profile than the one originally defined (max at -0.333% to -0.293%). It was decided that in lieu of running interrupted creep tests at selected time points as initially intended, more knowledge would be gained by performing TMF cyclic testing and imposing the ANSYS analysis strain-temporal profile on the specimen. For convenience the first two analysis cycles were run, followed by and continuing with the seventh analysis cycle. A comparison of the seventh analysis and test cycles is presented in Figure 4.6-19. For comparative purposes both cycles have stabilized, and again the difference between predicted and actual stress relaxation during the initial cycle is evident.
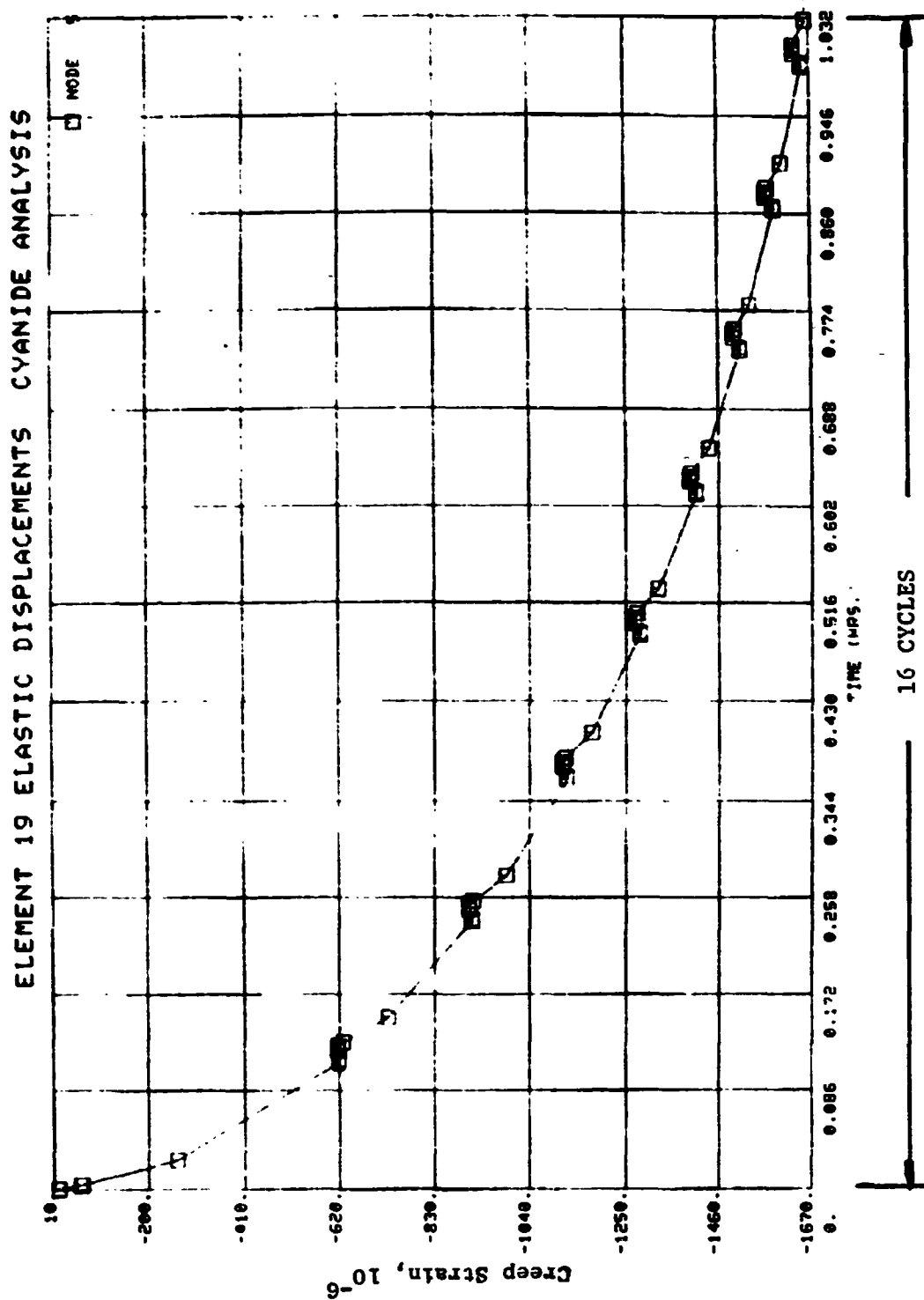
Figure 4.6-12. Cyanide Model Creep Strain vs. Time – Imposing Elastic Analysis Boundary Conditions.

57
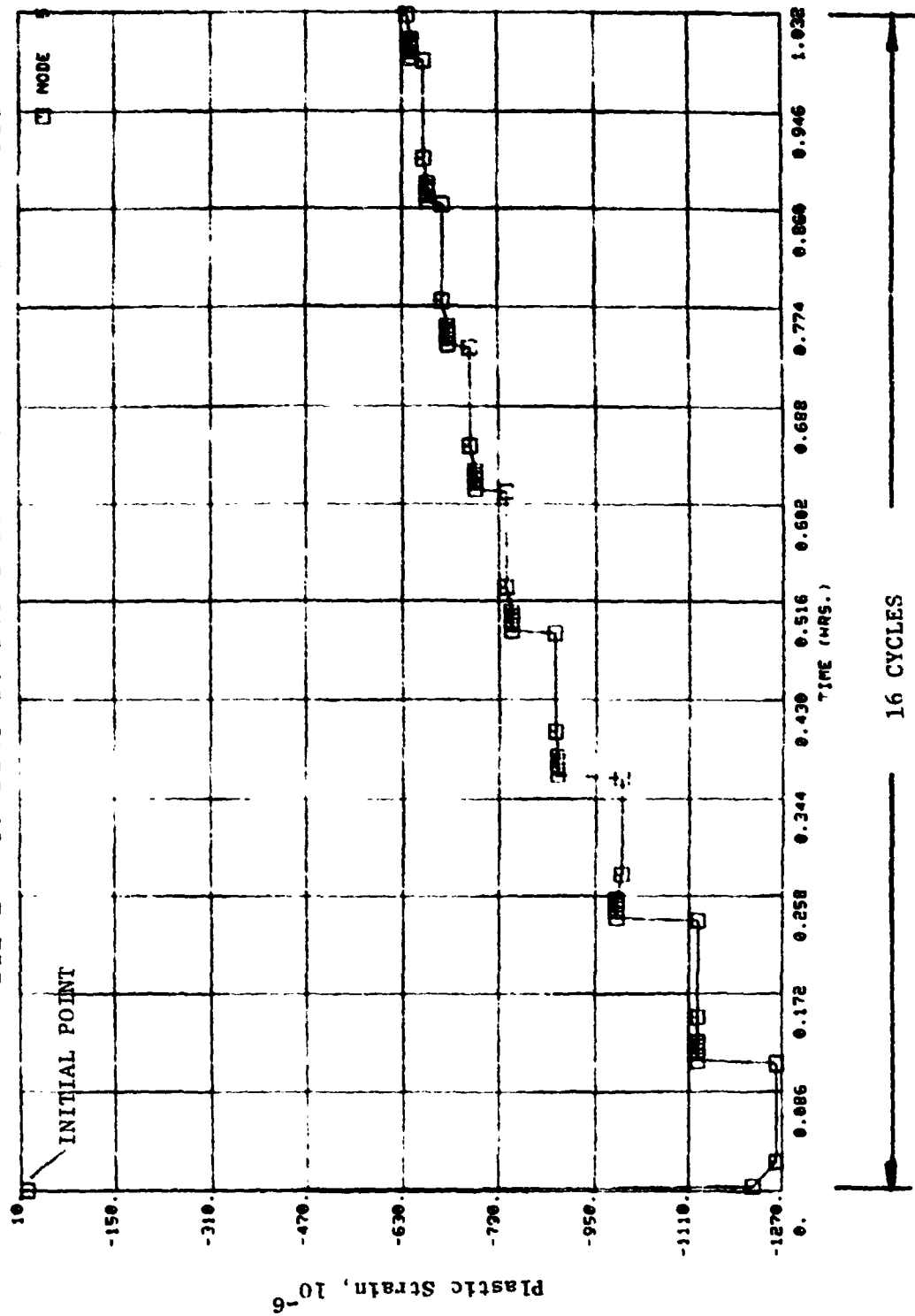
Figure 4.6-13. Cyanide Model Plastic Strain vs. Time – Imposing Elastic Analysis Boundary Conditions.

Figure 4.6-14. CYANIDE Model Stress-Strain Response – Imposing Inelastic Analysis
Boundary Conditions.

59

Figure 4.6-15. CYANIDE Model Plastic Strain vs. Stress – Imposing Inelastic Analysis Boundary Conditions.

o 14 CYCLES

o INELASTIC ANALYSIS RESULTS USED AS BOUNDARY CONDITIONS

o EACH LOOP REPRESENTS 2 CYCLE APPLICATIONS

ELEMENT 19 INELASTIC DISPL.   CYANIDE ANALYSIS
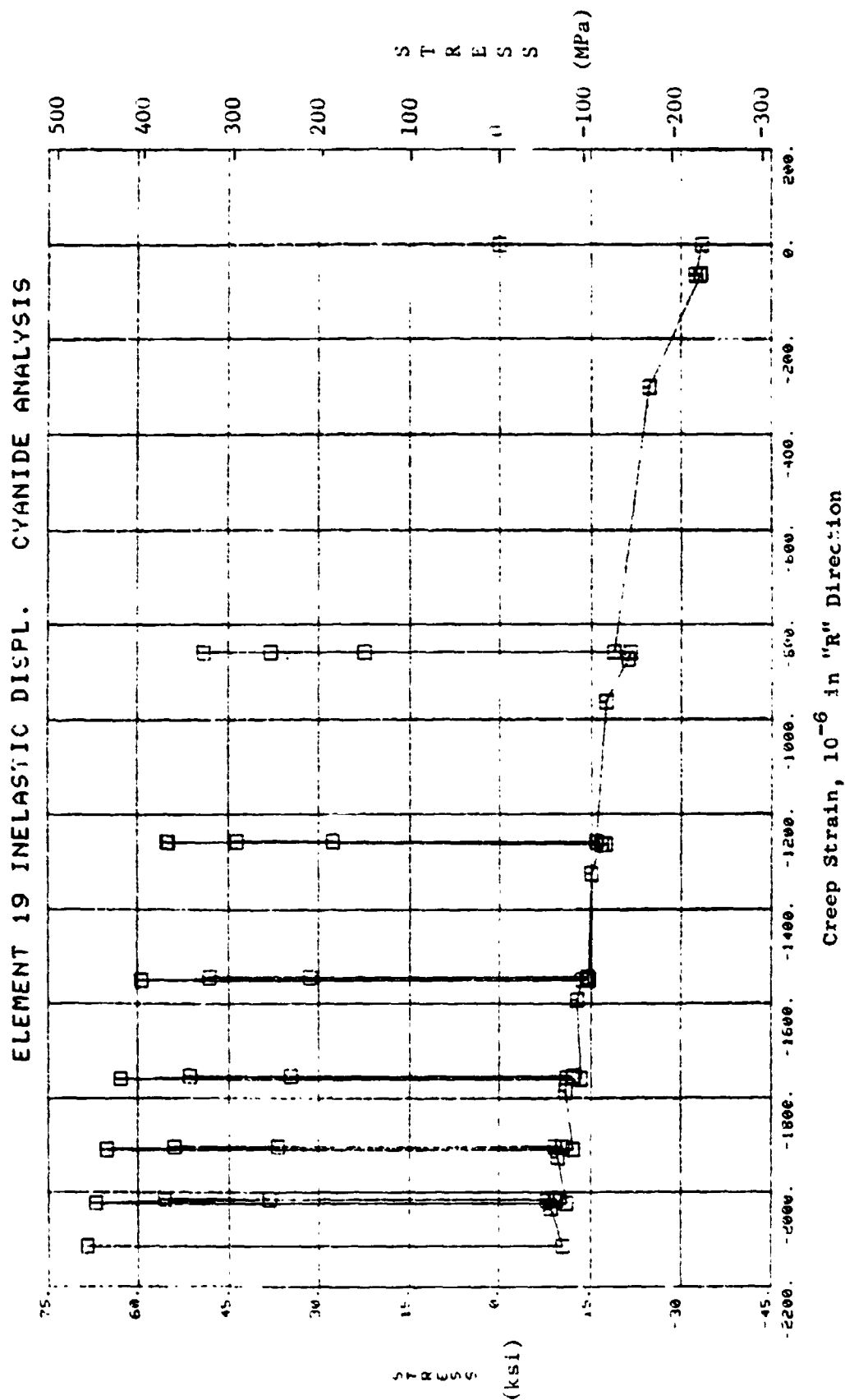
Figure 4.6-16. CYANIDE Model Creep Strain vs. Stress - Imposing Inelastic Analysis
Boundary Conditions.
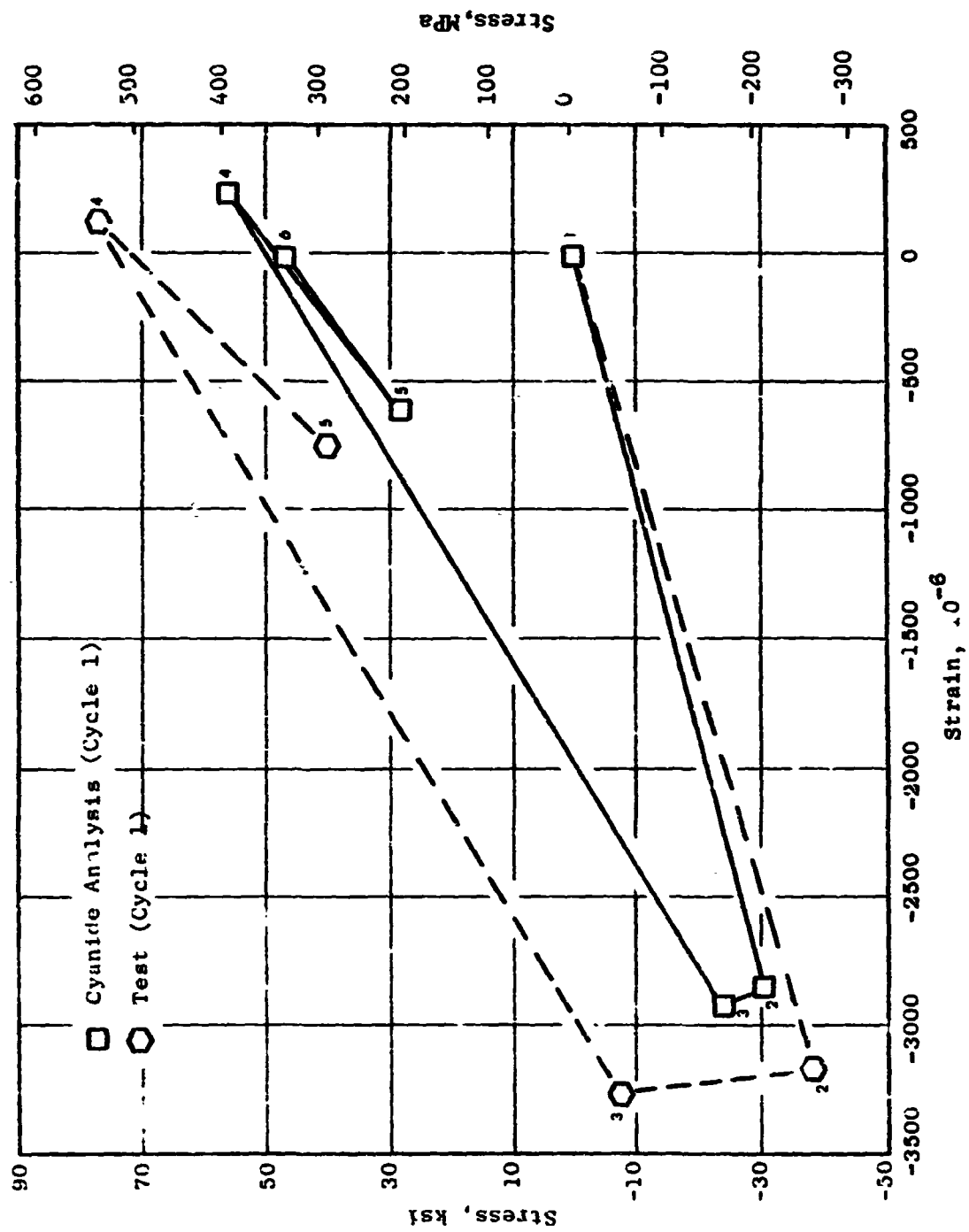
Figure 4.6-17. Stress Versus Strain – Elastic Analysis Profile.
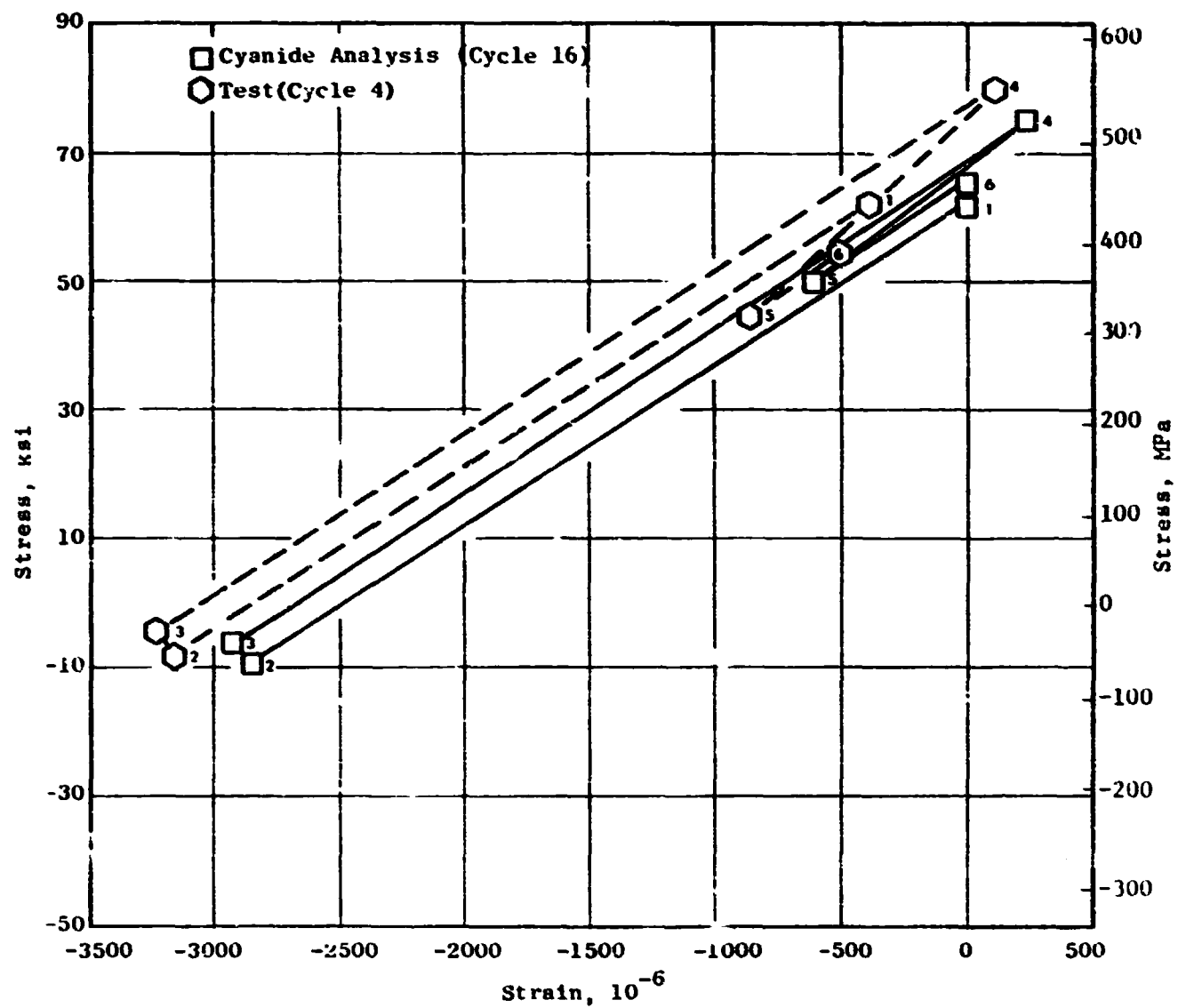
Figure 4.6-18. Stress Versus Strain - Elastic Analysis Profile.
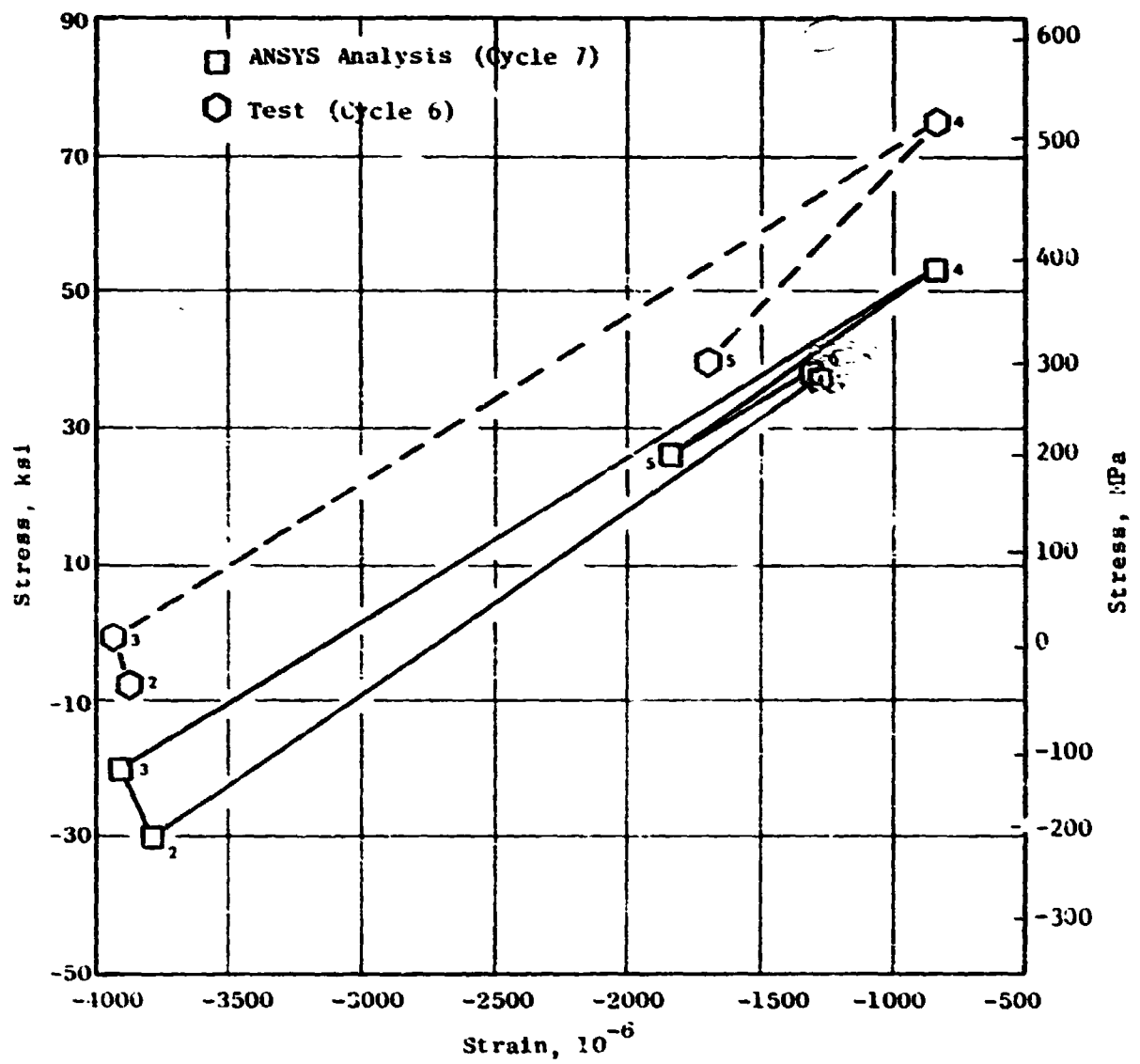
Figure 4.6-19.   Stress Versus Strain - Inelastic Analysis
                 Profile.

5.0 THERMAL MECHANICAL EXPERIMENTS AND LIFE ANALYSES

In this section results are presented for the thermal mechanical fatigue (TMF) experiments, crack initiation lifetime calculations, and crack propagation analyses. It is shown that the longest running TMF specimen (135 cycles) shows what appears to be many tight coating cracks when it is examined with a fluorescent penetrant. This in turn suggests that crack initiation is related to coating cracking at the lowest temperature of the TMF cycling and not to the fatigue of the substrate material (Rene 80). However, it is also shown that most of the life analysis techniques are capable of reaching reasonable conclusions about the structural lifetime of the analyzed blades. Nevertheless, none of the methods are satisfying when one compares these techniques to both the TMF stress-strain response and the total life calculation, including both initiation and propagation.

Recall the factory test cycle definition that was given in Figure 4.1-1, and the accompanying discussion that showed that only one of three chop-and-burst cycles in the factory test was modeled in the analysis phase of this program. In the subsequent life analyses, it was assumed that all three of these chop-and-burst cycles were identical and were composed of the time points from zero to 203.5 seconds in the analyses (see Figures 4.1-1 and 4.6-1). The subsequent reversals in strain and temperature which happened between the analyses times of 203.5 and 226 seconds occurred once per cycle in the factory tests.

The assumption that the three chop-and-burst cycles are equivalent is reasonable. The only question is the possibility that some of the transient temperatures (and hence strains) might be different during the other two cycles. However, the same ramp rate is used in the tests for all three cycles, and in any event, the steady-state portions of the three cycles should be identical. Hence, since the maximum compressive strain in the analyses occurs at the end of the steady-state takeoff setting (the 200-second point) this strain level should be accurately calculated. Finally, it is noted that the strain cycle between 203.5 to 226 seconds is very small, and is henceforth deleted from the initiation analyses (it is included in the propagation work).

Several factory tests were conducted using a myriad of cycle combinations and blade configurations; virtually all the factory test results as well as actual in-service experience showed blade distress in the tip region under study. The particular combination of factory cycles and blade geometry studied here involved 16 blades and 1000 factory cycles. At the end of the 1000 cycles, the blades were removed and the extent of cracking was documented. Of the 16 blades, one had cracked just to the tip cap; 10 had cracked below the tip cap, and 5 had cracked below the tip cap and the cracks had changed direction. Since the tip cap was 3.8 mm (0.15 in.) below the blade tip, this length and 1000 cycles were used as the criteria for judging the results of the crack propagation analyses. For the initiation analyses, the above-noted assumption of three cycles per mission cycle meant that 3000 was the maximum number of these chop-and-burst cycles which could occur.

5.1 SURFACE STRESS EXTRAPOLATION

Recall that all of the above-mentioned ANSYS stresses and strains were
element centroidal values. The centroid of the critical Element 19 was approx-
imately 0.5 mm (0.02 in.) removed from the free surface of the blade tip. In
order to provide a better basis for the life-assessment and crack-propagation
analyses, surface extrapolated stresses were obtained. This was accomplished
by applying the ANSYS nodal displacements in a reduced model of the critical
region using a three-dimensional version of the CYANIDE computer code. The
refined mesh was constructed such that nine times the number of elements was
used and interpolated boundary conditions were app..ed as required. Only the
seventh cycle was used from ANSYS, however total time was accumulated such
that at each mission point the elapsed time was the same as had elapsed at the
end of the seventh ANSYS cycle. In this way, the time (and temperature) depen-
dent creep strain was included in the reduced model.

The resulting stress distributions are shown in Figure 5.1-1. As shown,
the two analysis codes agree to within 10% in most locations. Subsequently,
the CYANIDE stress distribution is used in the crack propagation analysis
which is described later.

In a similar manner, the surface strains were obtained from the 3-D
CYANIDE analysis by extrapolating to the surface. These strains were used to
run repeated cycles in the simple four-element, two-dimensional CYANIDE model
previously described. The results of this analysis yielded a surface strain
range of about 0.33% with a maximum inelastic strain range of 0.013% on the
last cycle. These results were used in the crack initiation analyses.

5.2 THERMAL MECHANICAL EXPERIMENTS

Three thermal mechanical fatigue experiments were carried out at Material
Behavior Research Corporation. These tests were run to determine the actual
hysteresis response that resulted from imposing the strain-time history from
the analyses on a laboratory specimen. The first two tests modeled the elas-
tic analysis strain-temperature-time profile, while the third modeled the
strain profile from ANSYS. The purpose of the two tests that were based on
the elastic analysis was to establish the effect of the fast temperature
excursion from 340° C to 1040° C (650° F to 1900° F) in 6.7 seconds. This
excursion could not be obtained experimentally with standard laboratory induc-
tion heating which had a time of 75 seconds. It was shown that the lack of
fast heating was not critical as rapid creep occurred in the 1040° C to
1100° C (1900° F to 2000° F) temperatue range. Extreme care was required
in modeling the thermal expansion of the specimen since it was about 1.5%
while the mechanical strain range was on the order of 0.3%.

A schematic of the TMF setup is shown in Figure 5.2-1. As shown, three
function generators were required: temperature-time profile, mechanical
strain-time profile, and the measured thermal strain-time profile. The ther-
mal strain-time profile was measured by imposing the temperature-time profile
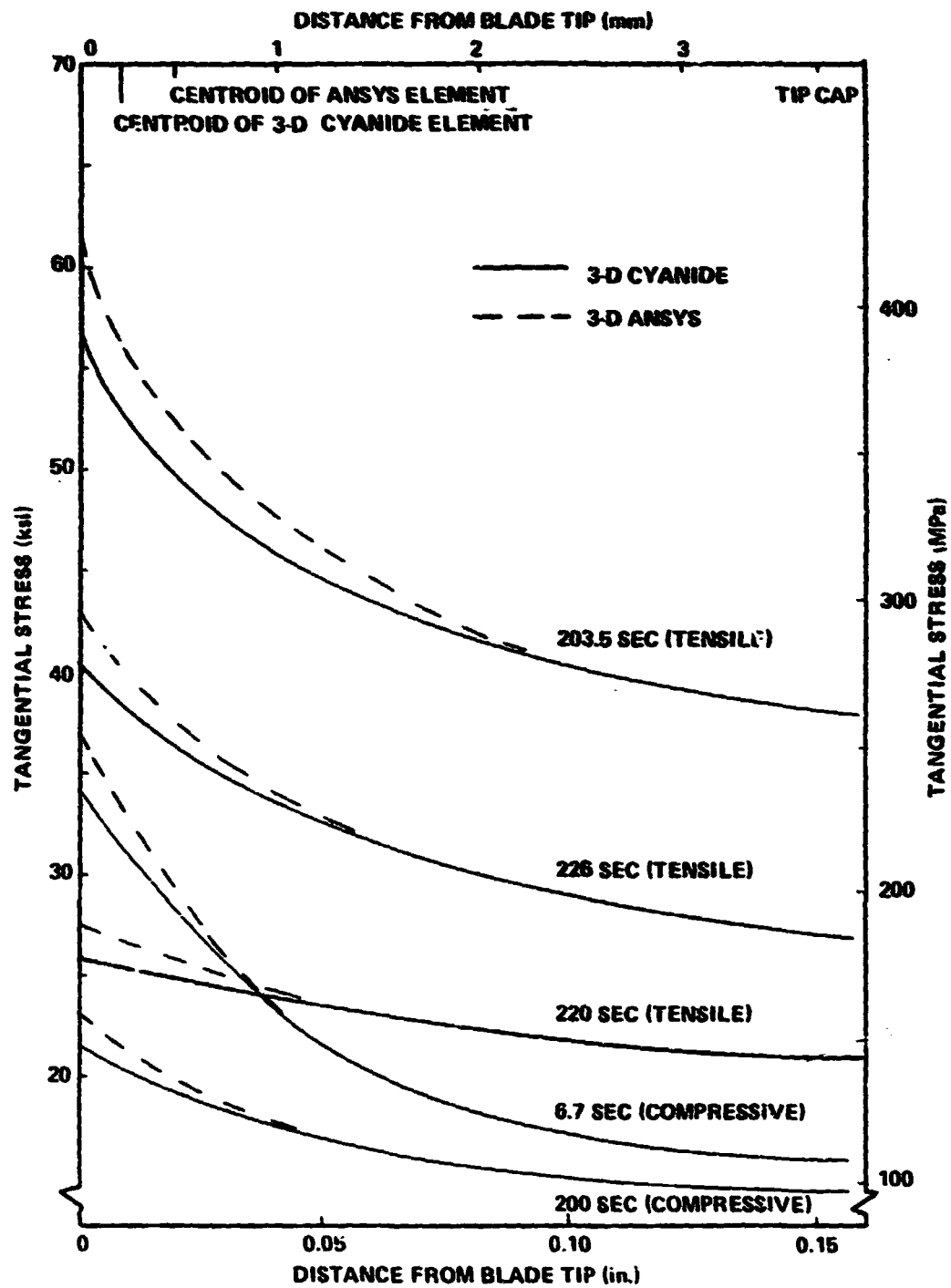
Figure 5.1-1. Comparison of Reduced 3-D CYANIDE Model with ANSYS Coarse Model.
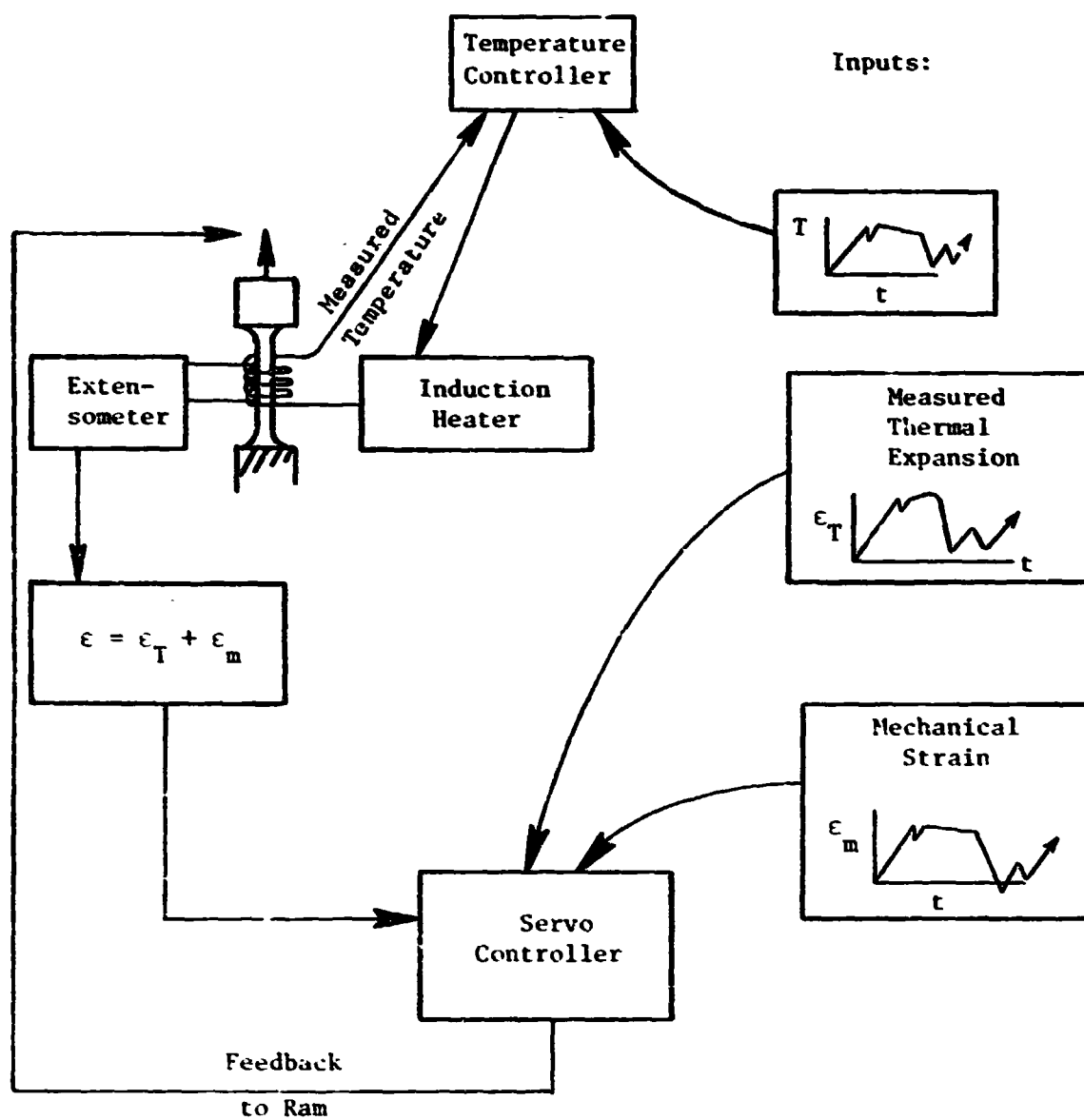
Figure 5.2-1.   Schematic of TMF Setup.

on the specimen in zero load control. After the response stabilized, the thermal strain-time history was carefully measured and converted to linear ramps for the digital computer which supplied the thermal strain command to the servo controller during the TMF experiments. The accuracy of the derived thermal strain command was verified by running the specimen in zero strain control and monitoring the load response. Typically, the control was within 0.01 to 0.03% strain throughout the cycle. The specimen that was used in these experiments is shown in Figure 5.2-2.

The strains derived from the elastic analysis were used in Test I (Figures 5.2-3 and 5.2-4). Note that Point 1 was reached in 75 seconds as compared to the 6.7 seconds in the blade analysis. Note further that the time from Point 2 to Point 3 was about 40 seconds, which was closely modeled in the experiment. During this latter time period the stress rapidly decayed, such that even had the initial fast excursion been modeled exactly, it is doubtful that the results would have been materially different. This was further verified by Test II (Figures 5.2-5 and 5.2-6). In this case, the initial strain excursion was applied at 1100° C (2000° F) in about three seconds, thereby simulating, at least, the initial total strain rate. Thereafter, the strain and temperature were cycled simultaneously as shown in the figures. Note that the hysteresis loops induced by the two tests were virtually the same.

Figures 5.2-7 and 5.2-8 detail the imposed condition and measured response, respectively, from Test III. In this case, the small ratchet strains predicted by the seven analytical ANSYS cycles were modeled by four cycles experimentally. The subsequent cycles repeated Cycle 4. As can be seen, these results are virtually the same as those from the other two tes ..

Test III was the longest test with 135 cycles. The specimen was removed and inspected for surface degradation using a fluorescent penetrant. The results showed severe instances of cracking, as seen in Figure 5.2-9. It was known that coating cracking could precede matrix cracking (as measured by a compliance technique) by a large percentage of life. However, for this CODEP coating, most previous studies showed such brittle behavior at temperatures below about 760° C (1400° F), while at higher temperatures above 760° C (1400° F) the coating had more ductility. It appeared that such coating cracking would require the lower temperature of the TMF cycle in order for it to be observed. Note that such a crack initiation mechanism could not be predicted by using isothermal test data at the higher temperatures of the TMF cycle. Crack initiation at such higher isothermal temperatures would occur through a more conventional substrate fatigue mechanism presuming the coating is more ductile.

5.3 CRACK INITIATION LIFE ANALYSES

In this section, the analysis of some René 80 fatigue data is presented followed by life predictions made by four different approaches. The derived strains for these analyses and the factory test cycles are discussed in the introductory portion of Section 5.
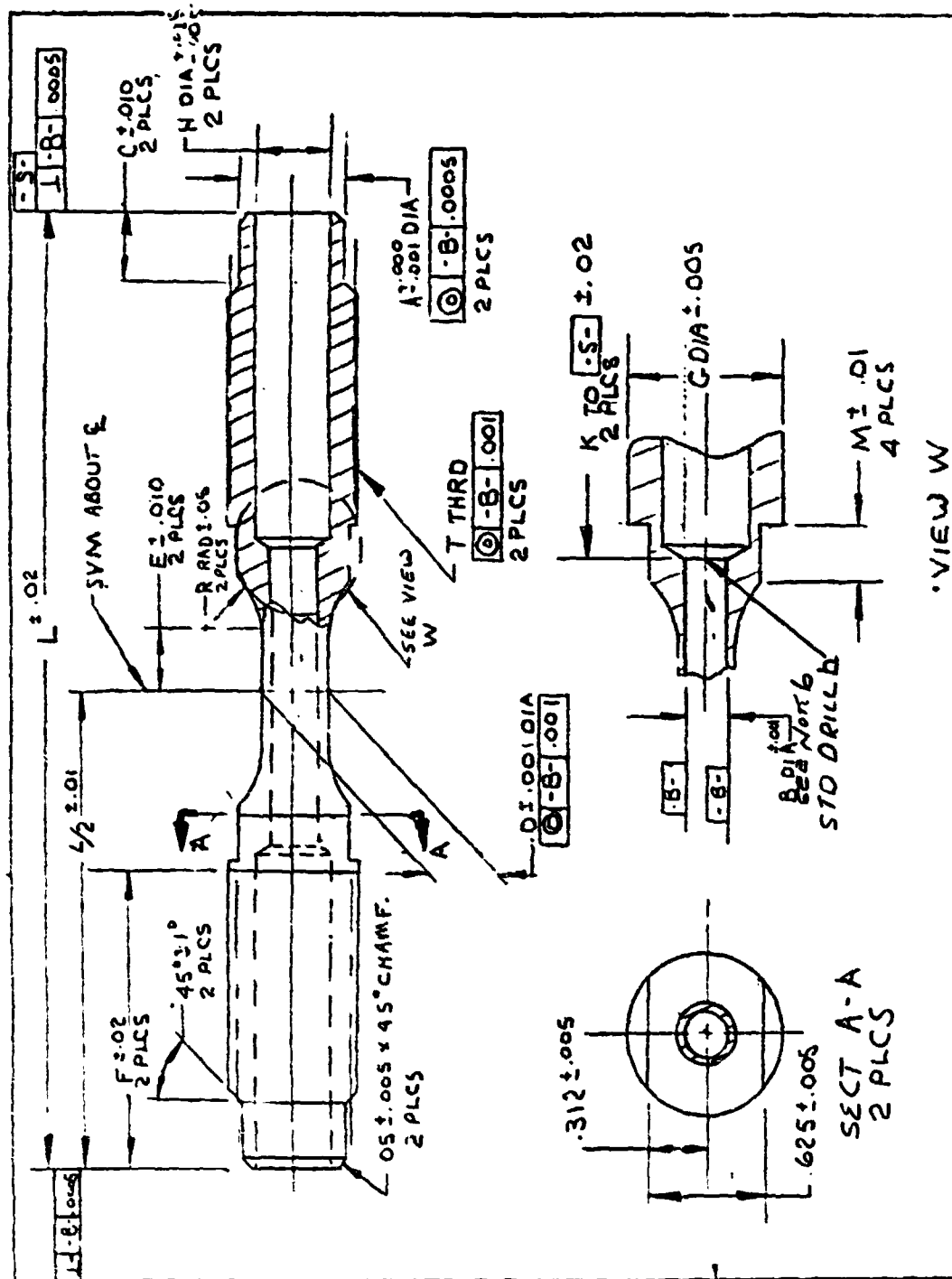
Figure 5.2-2. Specimen Geometry (Dimensions in inches).

70

T

1040
(1900)

1100
(2000)

1070
(1960)

980
(1800)

T, °C (°F)

700
(1300)

340 (650)

0   t_1 t_2 t_3 t_4 t_5 t_6 t_7 →Time*

-ε

* Note that the time
  axes are not to scale

0   t_1 t_2 t_3 t_4 t_5 t_6 t_7 →Time*

Point	Blade Time/Test Time (sec)	Blade Strain/Test Strain (%)
1	6.7/75	-0.285/-0.33
2	6.9/84	-0.255/-0.295
3	45/126	-0.293/-0.333
4	200/327	-0.28 /-0.32
5	203.5/672	+0.025/+0.02
6	220/891	-0.06 /-0.07
7	226/1116 (18.6 min)	0/0
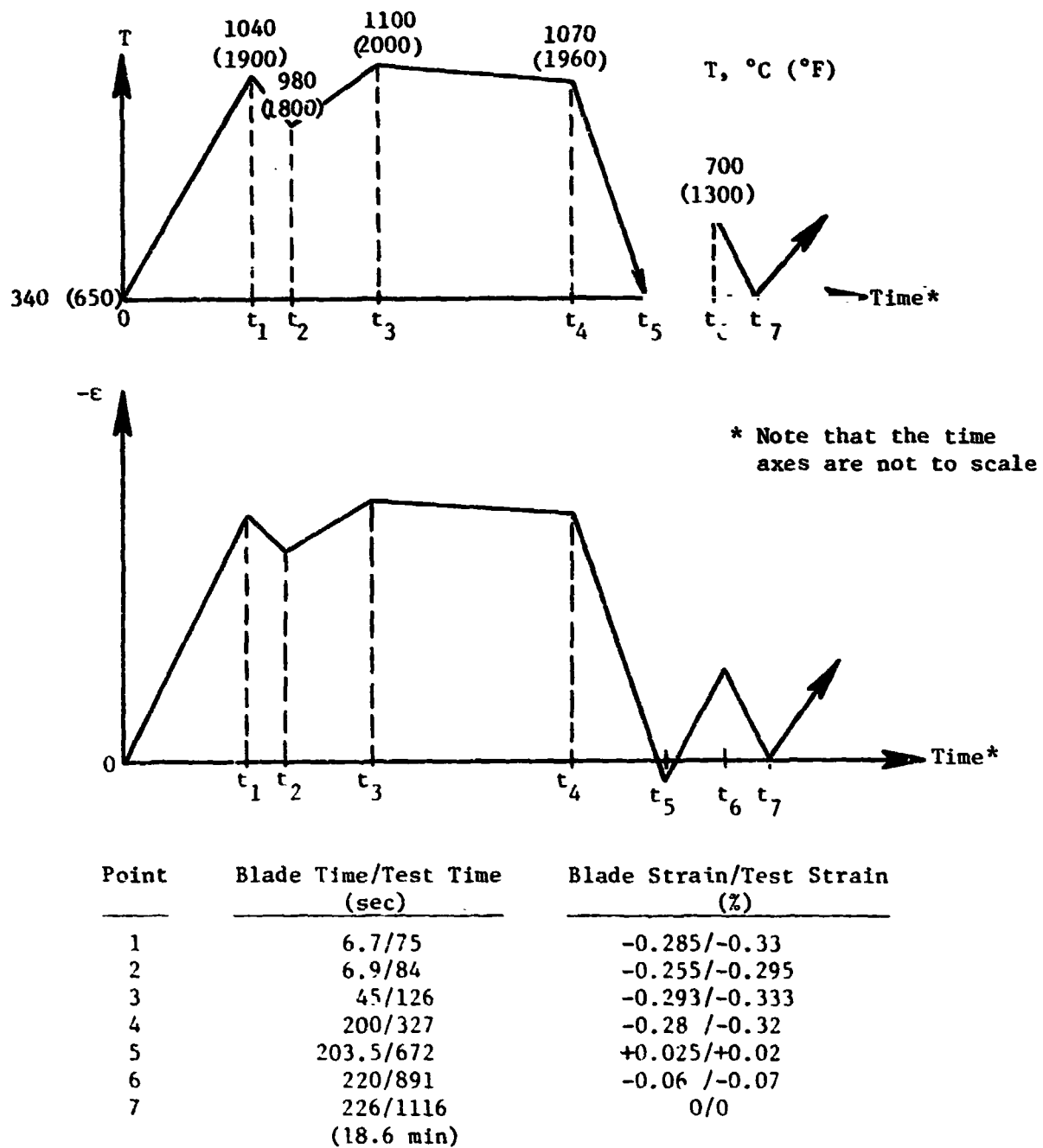
Figure 5.2-3. Schematic of the Imposed Temperature and Strain
History for Test I.

Figure 5.2-4. Mechanical Strain vs. Load – Test I.

72
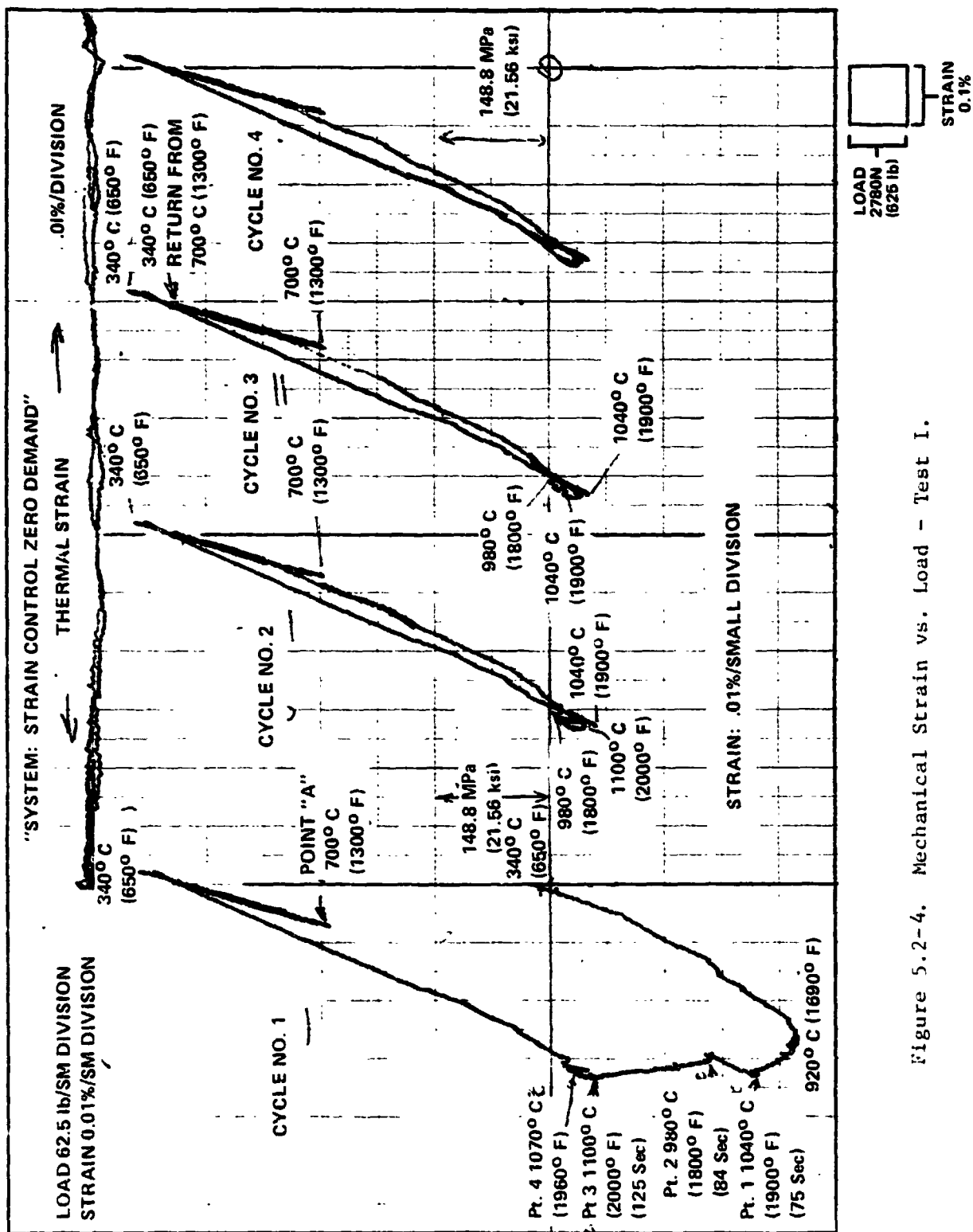
- Model Elastic Analysis
- Strain Applied in ~ 3 seconds at 1100° C (2000° F) on First 1/4 Cycle
- Strain and Temperature Imposed Simultaneously Thereafter
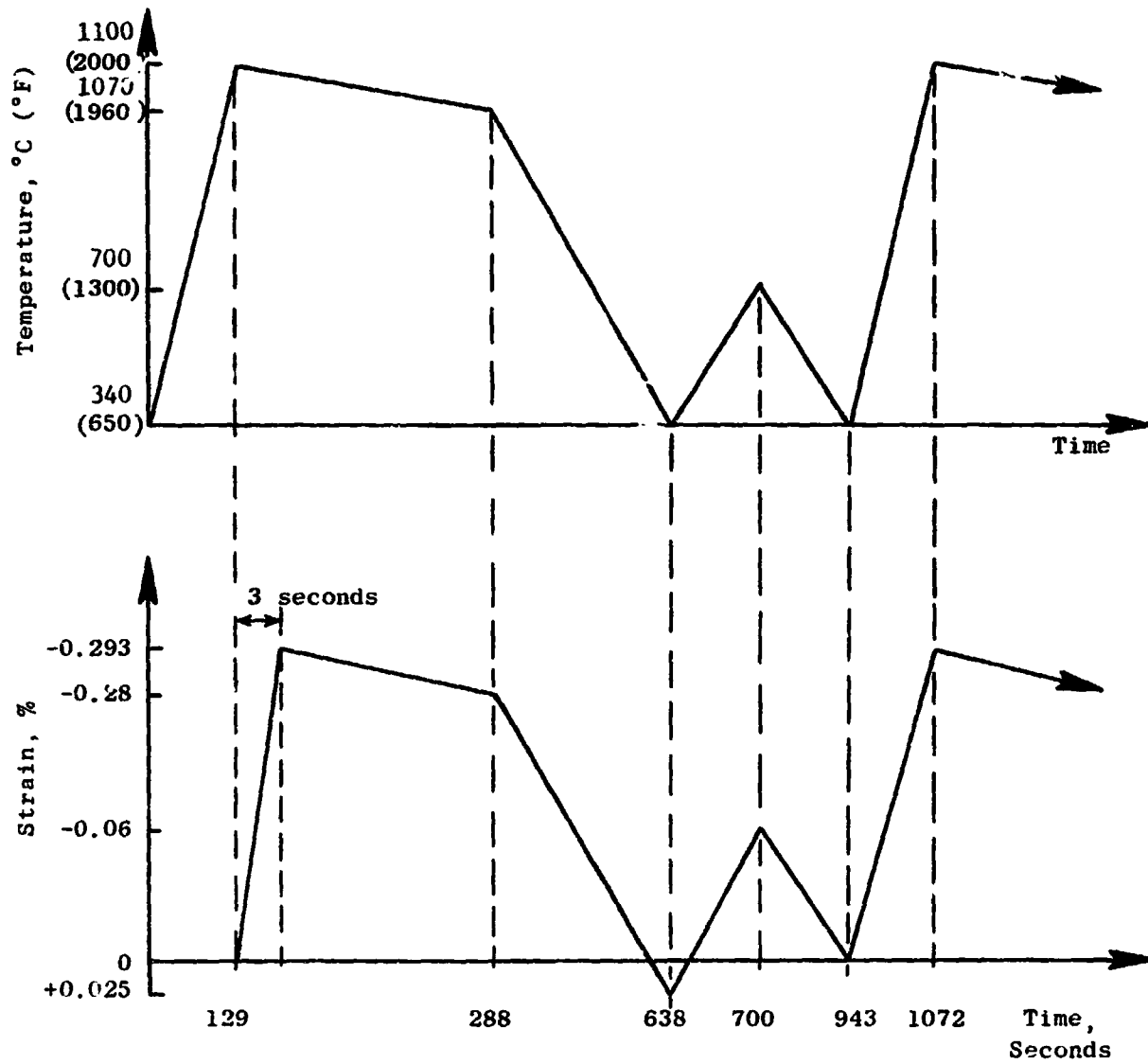
Figure 5.2-5. Schematic of the Temperature and Strain Cycle Imposed in Test II.
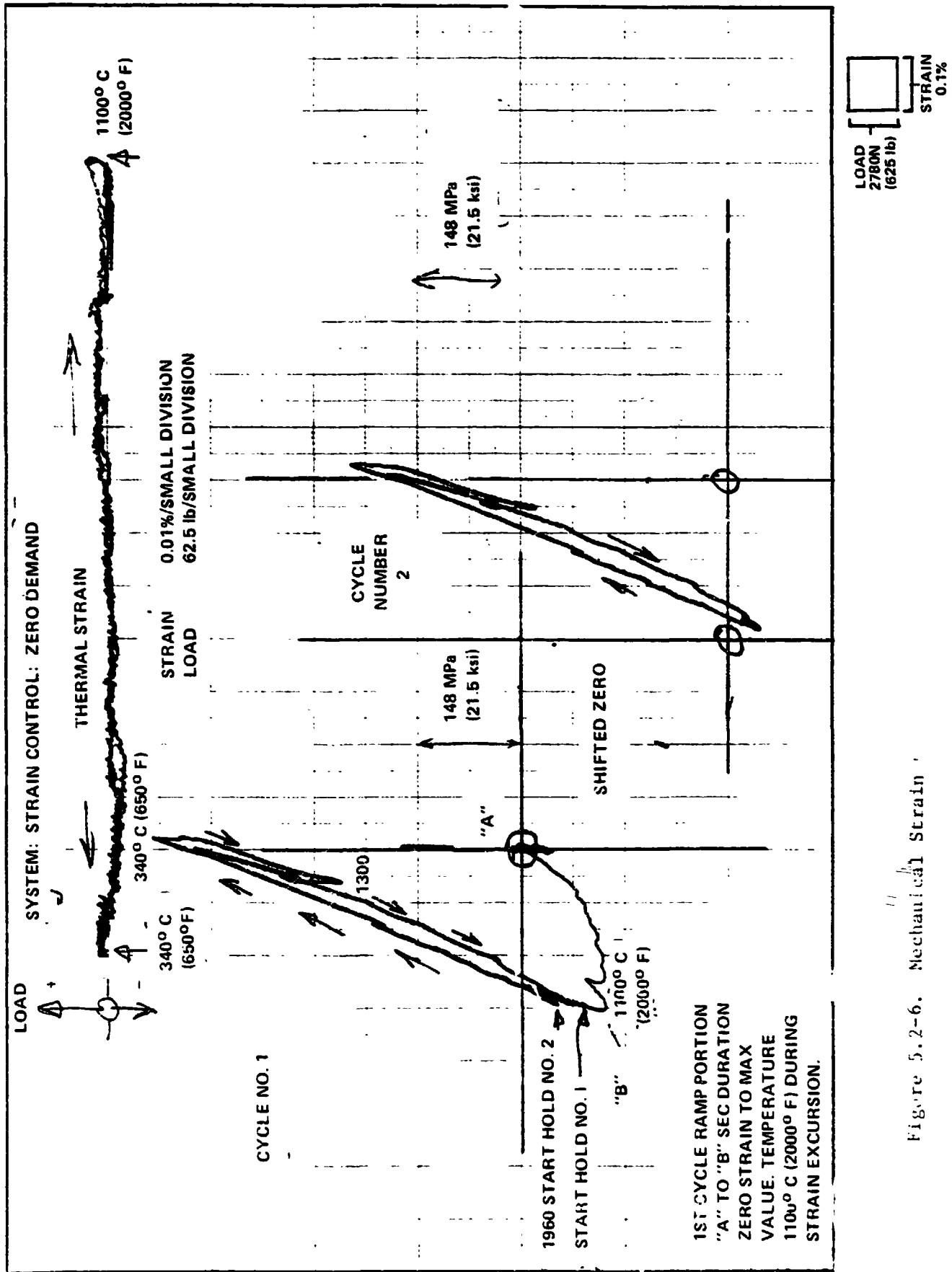
Figure 5.2-6. Mechanical Strain

LOAD
SYSTEM: STRAIN CONTROL: ZERO DEMAND

THERMAL STRAIN

1100° C
(2000° F)

340° C (650° F)

340° C
(650°F)

STRAIN   0.01%/SMALL DIVISION
LOAD   62.5 lb/SMALL DIVISION

148 MPa
(21.5 ksi)

148 MPa
(21.5 ksi)

CYCLE
NUMBER
2

SHIFTED ZERO

"A"

1300

"B"

1100° C
(2000° F)

CYCLE NO. 1

1960 START HOLD NO. 2

START HOLD NO. I

1ST CYCLE RAMP PORTION
"A" TO "B" SEC DURATION
ZERO STRAIN TO MAX
VALUE. TEMPERATURE
1100° C (2000° F) DURING
STRAIN EXCURSION.

LOAD
2780N
(625 lb)

STRAIN
0.1%

74

- **Mode' Analysis Strain Profile**
  - Small Ratchet Strain
  - Modeled with 4 Cycles - Thereafter the same
- **Strain and Temperature Imposed Simultaneously**
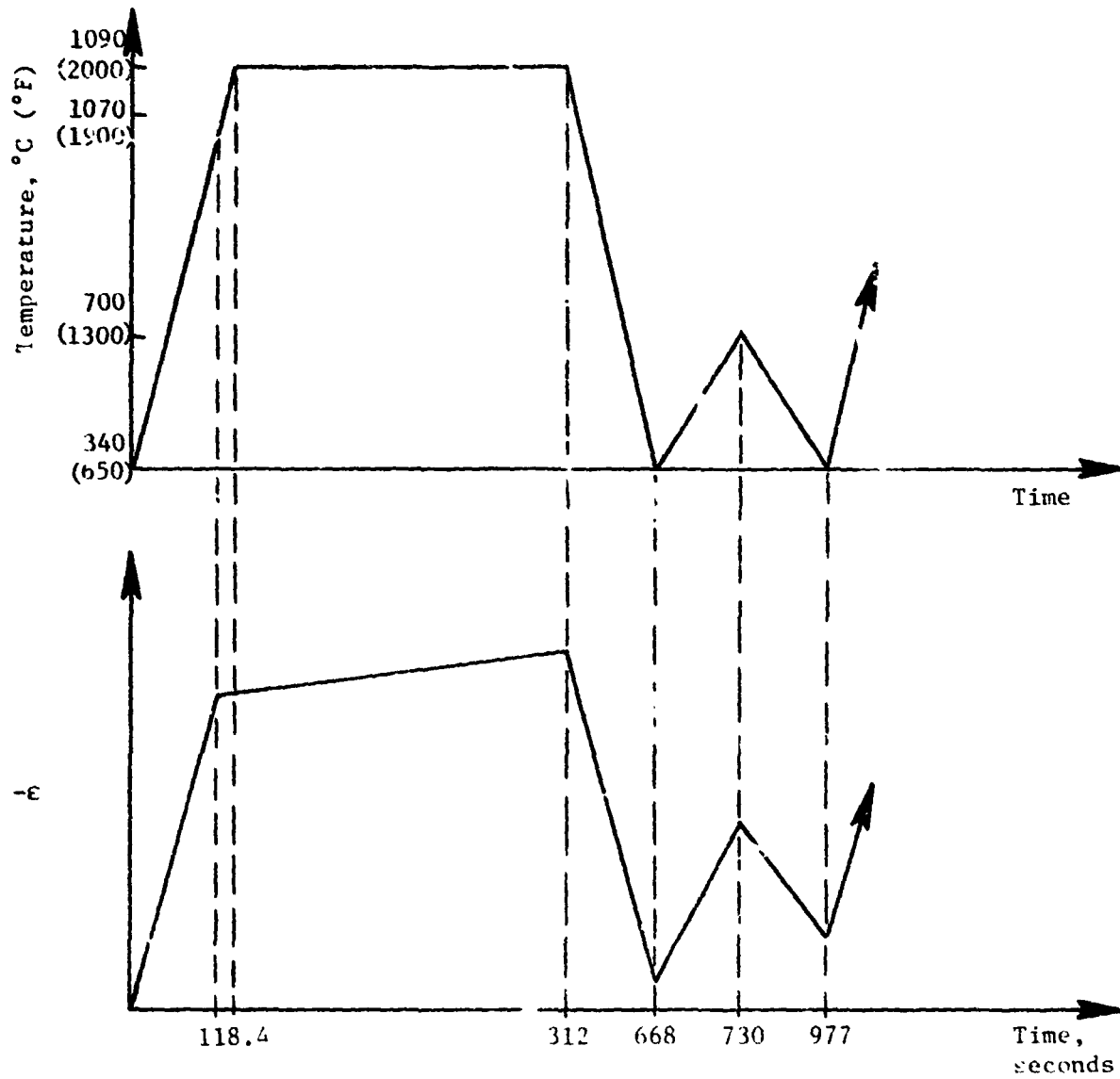
Figure 5.2-7. Imposed Cycles in Test III.
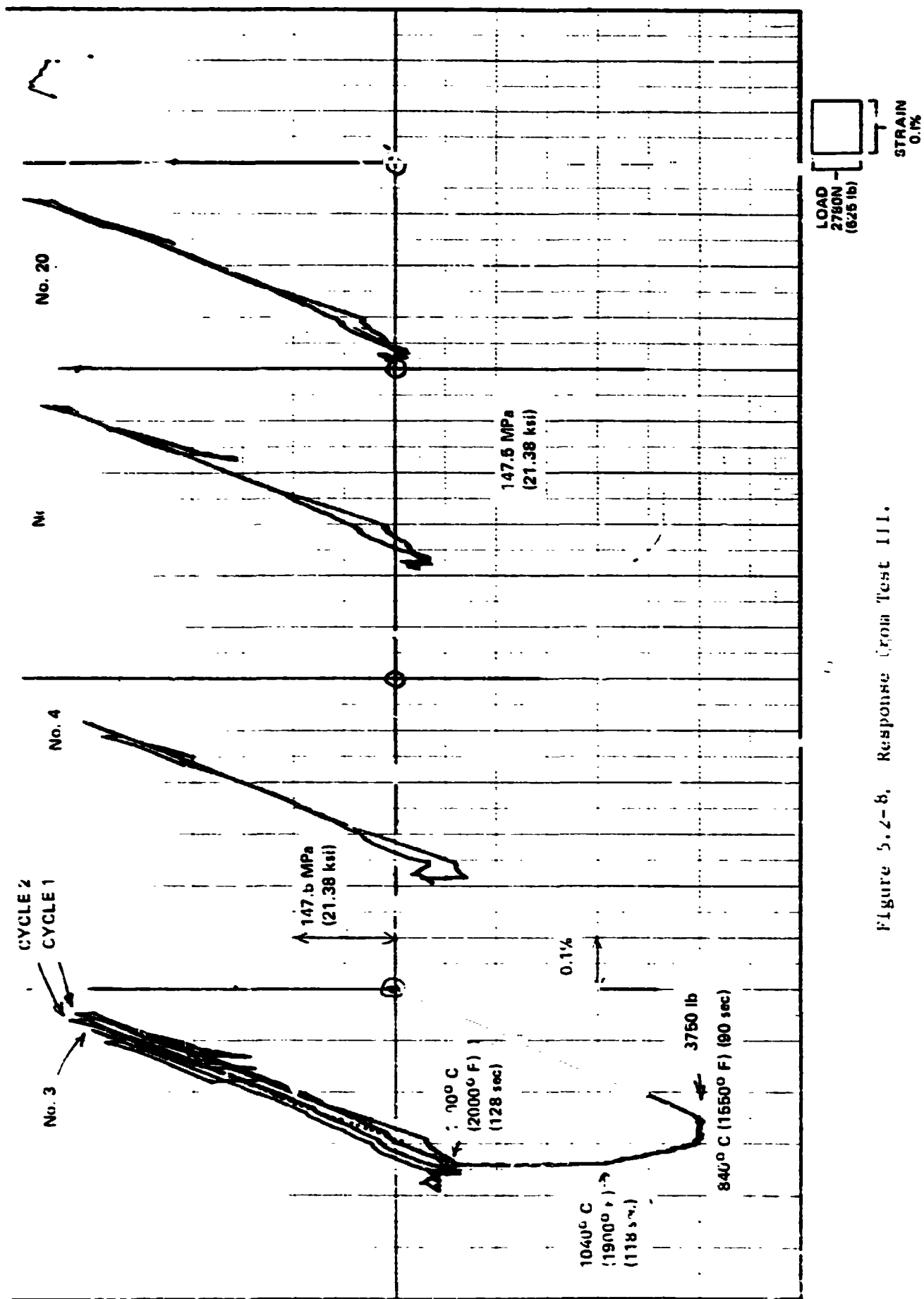
Figure 5.7-8. Response from Test 111.
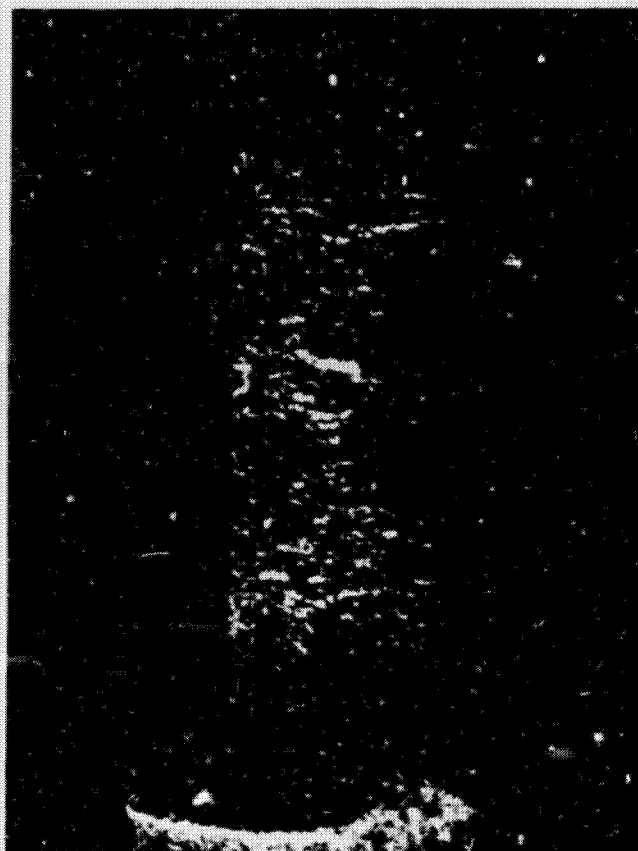
3X

Figure 5.2-9. Photograph of the Last TMF
Specimen After 133 Cycles
of Imposed Temperature and
Strain Cycling in Test III,
and After Zyglo Inspection.

77

5.3.1 Data Analyses

As stated earlier in this report, René 80 is a well characterized material, and considerable fatigue data exists. However, it was necessary to reanalyze the data to make it suitable for the various life prediction theories. The methods examined were Strain Range Partitioning (SRP) (References 2 through 9), Frequency Modified (References 9 through 11), and the conventional time and cycle fraction rules. In addition, the data were cast into a form suggested by current mean stress damage parameters (References 12 through 15).

Most of the data [540° C to 980° C (1000° F to 1800° F)] are from experiments by Mar-Test, Cincinnati, Ohio, under an earlier contract to the General Electric Company. Other data [1040° C to 1100° C (1900° F to 2000° F)] are from early (circa 1969) work using noncontact, laser-based strain control. These data are somewhat suspect in that the measured hysteresis loops, at times, show concavities in the stress response, a tendency which may indicate that the control was less than desirable. Nevertheless. The high-temperature data suggest trends that are useful in extrapolating from 980° C to 1100° C (1800° F to 2000° F). Since the 980° C data is the largest set of the more reliable data, it is examined below in detail for interpretation by the Frequency Modified (FM) method. Other René 80 data at 870° C (1600° F) have been reported by Coffin (Reference 9). SRP data for the subsequent analysis are taken from Reference 4 at 1000° C (1830° F).

Figure 5.3-1 shows the 980° C (1800° F) René 80 data. The cycles to crack initiation, N_i, are based on load compliance. These data are taken under strain control at strain rates from 0.2%/min. to 10%/min. In addition, three A_ϵ ratios (A_ϵ = $\epsilon a/\epsilon m$, where ϵa and ϵm are the alternating and mean strain, respectively) are included. In total, there are 50 points, 20 at A_ϵ = +1, 20 at A_ϵ = -1, and the rest at A_ϵ = ∞. Only six of the data are at the lower strain rate and none of these data is for the A_ϵ = ∞ data set. For the purposes of the FM analysis, the cyclic frequency, ν, is calculated from the formula

$$\dot{\epsilon} = 2 \Delta\epsilon \nu \tag{5-1}$$

where $\dot{\epsilon}$ is the total strain rate and $\Delta\epsilon$ is the total strain range. Note that this formula is exact since the data are generated using a triangular wave form. When this formula is applied, the range of ν is from 0.05 to 25 cp.

The FM equations from Reference 9 are given by

$$\Delta\epsilon = \frac{A'}{E} N_i^{-\beta'} \nu^{K_1'} + C_2 N_i^{-\beta} \nu^{\beta(1-K)}, \tag{5-2}$$

where E is Young's modulus and A', β', K_1', C_2, β, and K are independent constants from which all subsequent equations can be derived. The first term on the right-hand side of Equation 5-2 represents the elastic strain range ($\Delta\epsilon$ = $\Delta\epsilon/E$) while the second term represents the plastic strain range ($\Delta\epsilon_p$). Eliminating the cycles to crack initiation, N_i, between these two terms, one has an equation for the cyclic stress-strain curve.
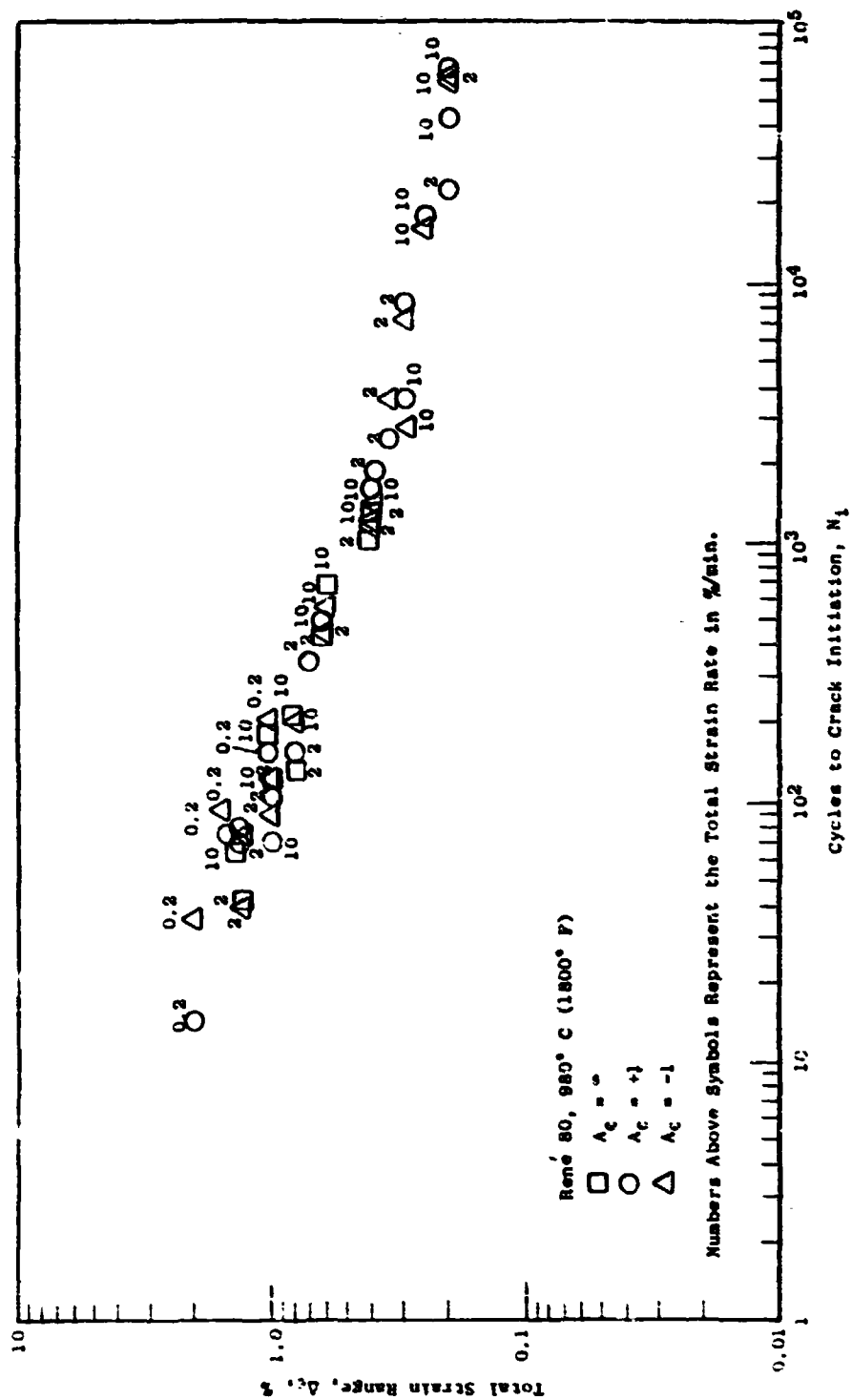
Figure 5.3-1. René 80 Data Base at 980° C (1800° F).

René 80, 980° C (1800° F)

$A_\epsilon = \infty$ (square)
$A_\epsilon = +1$ (circle)
$A_\epsilon = -1$ (triangle)

Numbers Above Symbols Represent the Total Strain Rate in %/min.

Cycles to Crack Initiation, N_1

Total Strain Range, $\Delta\epsilon_t$, %

$$\Delta\sigma = A(\Delta\varepsilon_p)^{n'} {}_\nu K_1, \qquad\qquad (5\text{-}3)$$

where $n' = \beta'/\beta$, $A' = A\ C_2{}^{n'}$, and $K_1 = K_1' + \beta'(K-1)$.

Equation 5-3 was fit to all of the René 80 980° C (1800° F) data by using a standard linear-regression technique. The results were as shown in Figure 5.3-2, where the lines were obtained from the resulting regression analysis with A = 486 MPa (70.4 ksi), n' = 0.183, and K_1 was 0.0951. As was observed, there appeared to be considerable scatter in the stress response when plotted on the basis of frequency. The cyclic stress-strain curve defined by the above noted range quantities was assumed to not be a function of the A_ε ratio. This assumption appeared to be in agreement with the results of recent work by T.S. Cook (Reference 16) on Inconel 718 response data.

The rest of the constants for Equation 5-2 were determined by linearly regressing the $\Delta\varepsilon_p$ line as a function of ν and N_i. These data were fit several ways, as summarized in Table 5.3-1. Many different approaches were used in this regression analysis because K was greater than unity. Although this was consistent with the results presented by Coffin (Reference 9), it indicated a reverse frequency effect such that the predicted life was longer as frequency was reduced at short lives (see Figure 5.3-4). Since the resulting elastic lines were as expected, the trend reversed at longer lives such that raising the frequency increased the life. These results were found for the total data set, $A_\varepsilon = +1$ data, and the $A_\varepsilon = -1$ data. The $A_\varepsilon = \infty$ data showed K<1, but were based on fewer data, and only the two higher strain rates were used in the experiments. Consequently, two sets of analyses were used: (1) K was assumed to be unity and the data were fit this way; and (2) K was allowed to be greater than unity. Both analyses were based on all the data and the results are given in Table 5.3-1.

The resulting data fits are shown in Figures 5.3-3 through 5.3-6. Note the reverse frequency trend in the first two of these figures for short lives. The last two of these figures show the results for K=1; the tendencies are more as expected. Unfortunately, as the data analysis suggests, there is enough scatter in the data to make either interpretation plausible.

A brief description of an analysis of "low temperature" data is given below. The lower temperature data were analyzed because of the extreme temperature variation at the critical blade tip location. This analysis shows that since the ductility is lower at lower temperatures, the plastic strain-life curve is correspondingly lower. The higher strength as temperature is lowered improves the life with respect to high-temperature data at longer lives. The lowered ductility suggests that methods based on plastic strain alone (e.g., SRP) may require the low-temperature characteristics for analyzing TMF situations if it can be assumed that the TMF cycle does not introduce interactive effects.

Figures 5.3-7 through 5.3-9 show the results of the lower-temperature linear regression analyses. The plastic strain-life line was derived by assuming that it was independent of temperature and strain rate (the strain
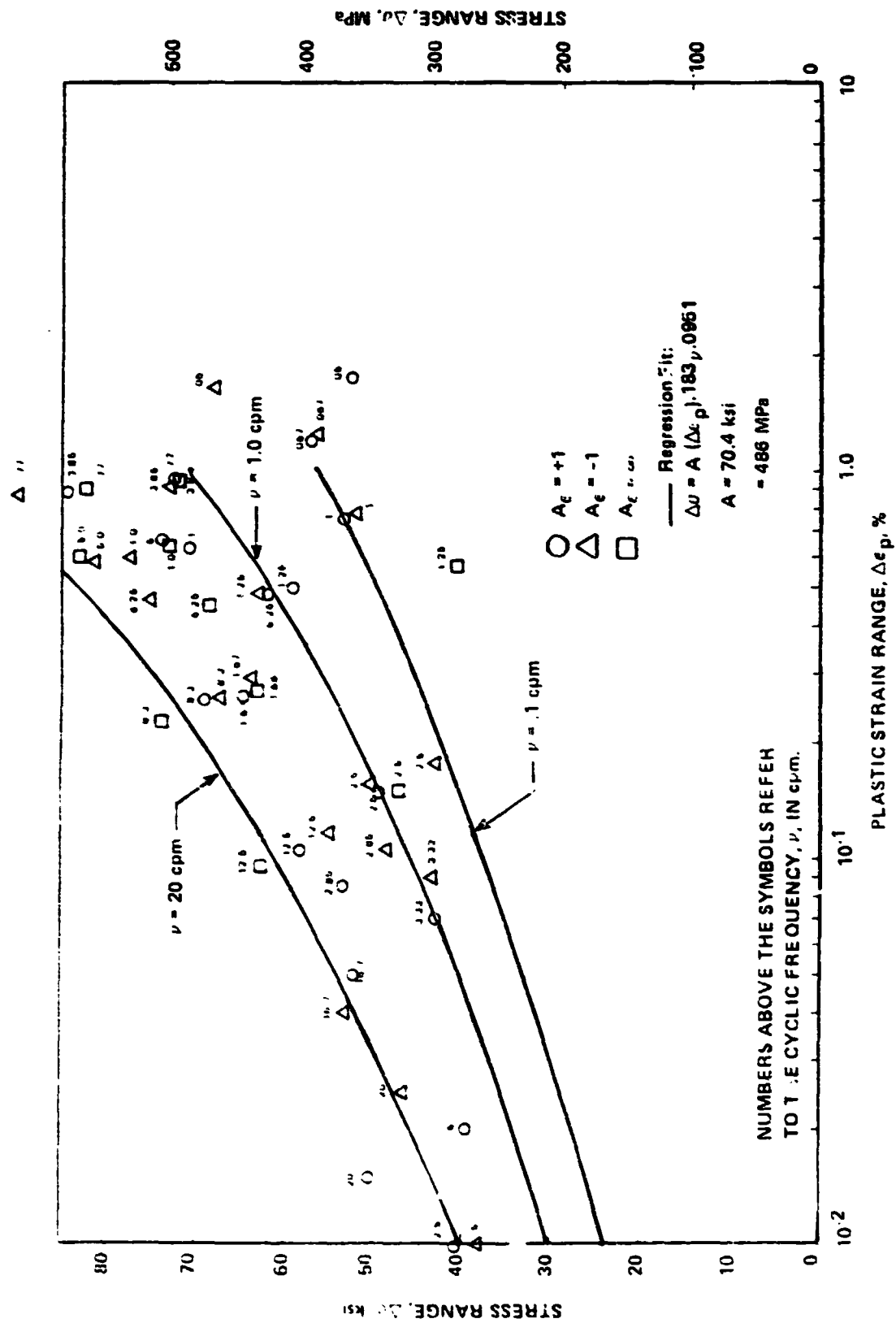
Figure 5.3-2. Pené to 980° C (1800° F) FM Cyclic Stress-Strain Curve Fit.

Table 5.3-1. Results of FM Regression Analyses Fit of 980 (1800° F)
Rene 80 Data (ν in cpm, and ε in %)

Fit of Plastic Data

Method	C_2	β	K
$A_\epsilon = \infty$ Data Only	14.825	0.6773	0.919
$A_\epsilon = +1$ Data Only	10.878	0.604	1.156
$A_\epsilon = -1$ Data Only	12.658	0.6116	1.229
All Data	12.17	0.614	1.169
All Data ($K \equiv 1$)	15.34	0.666	1.0

Resulting Elastic Fit

Method	A' (MPa/ksi)	β'	K_1'
All Data	767.5/111.2	0.112	0.0761
All Data ($K \equiv 1$)	800.63/116.03	0.122	0.0951
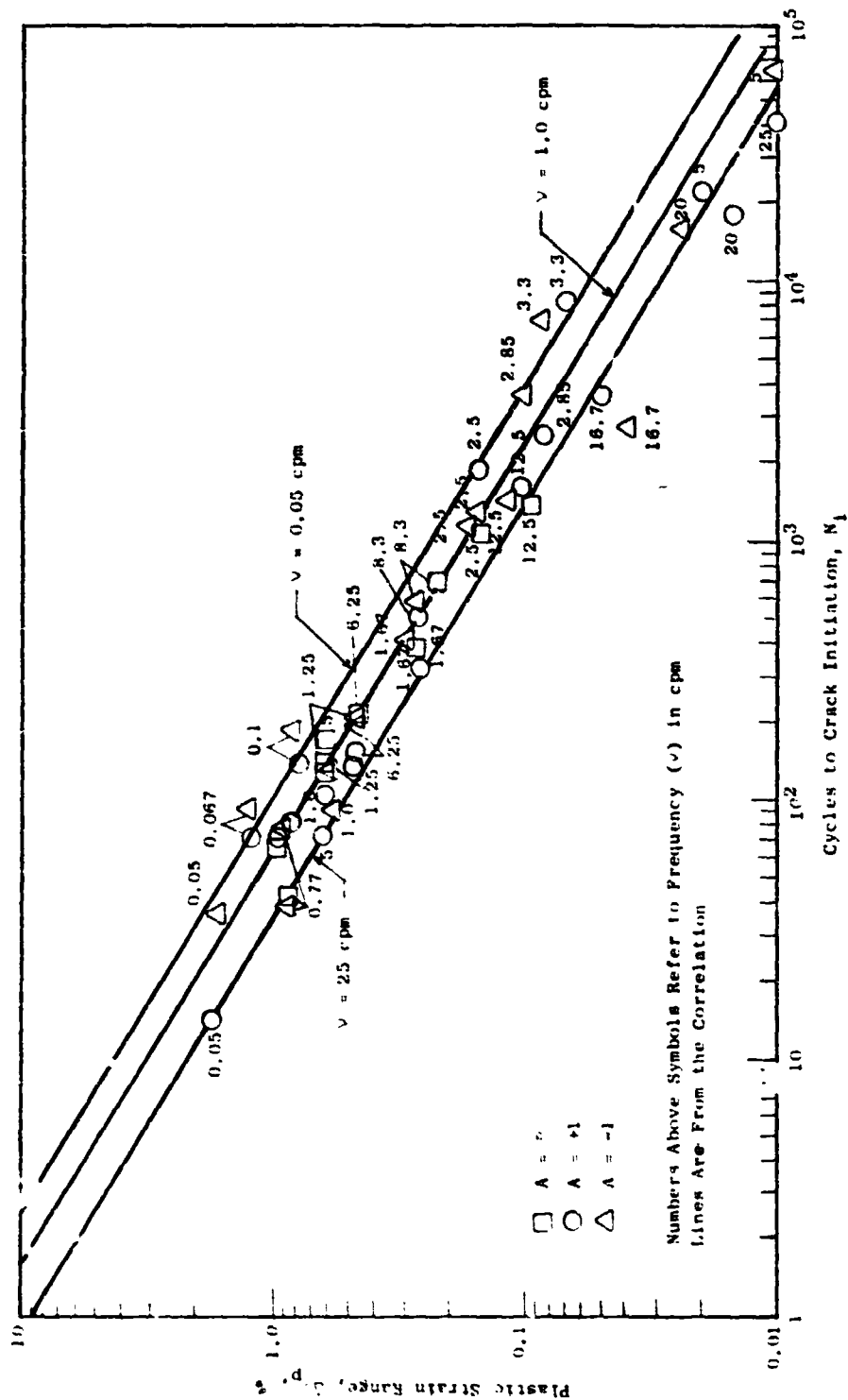
Figure 5.3-3. Full FM Method - René 80, 980° C (1800° F).

Figure 5.3-4. Full FM Method — René 80, 980° C (1800° F).

Figure 5.3-5.   FM Method with K = 1, René 80, 980° C (1800° F).
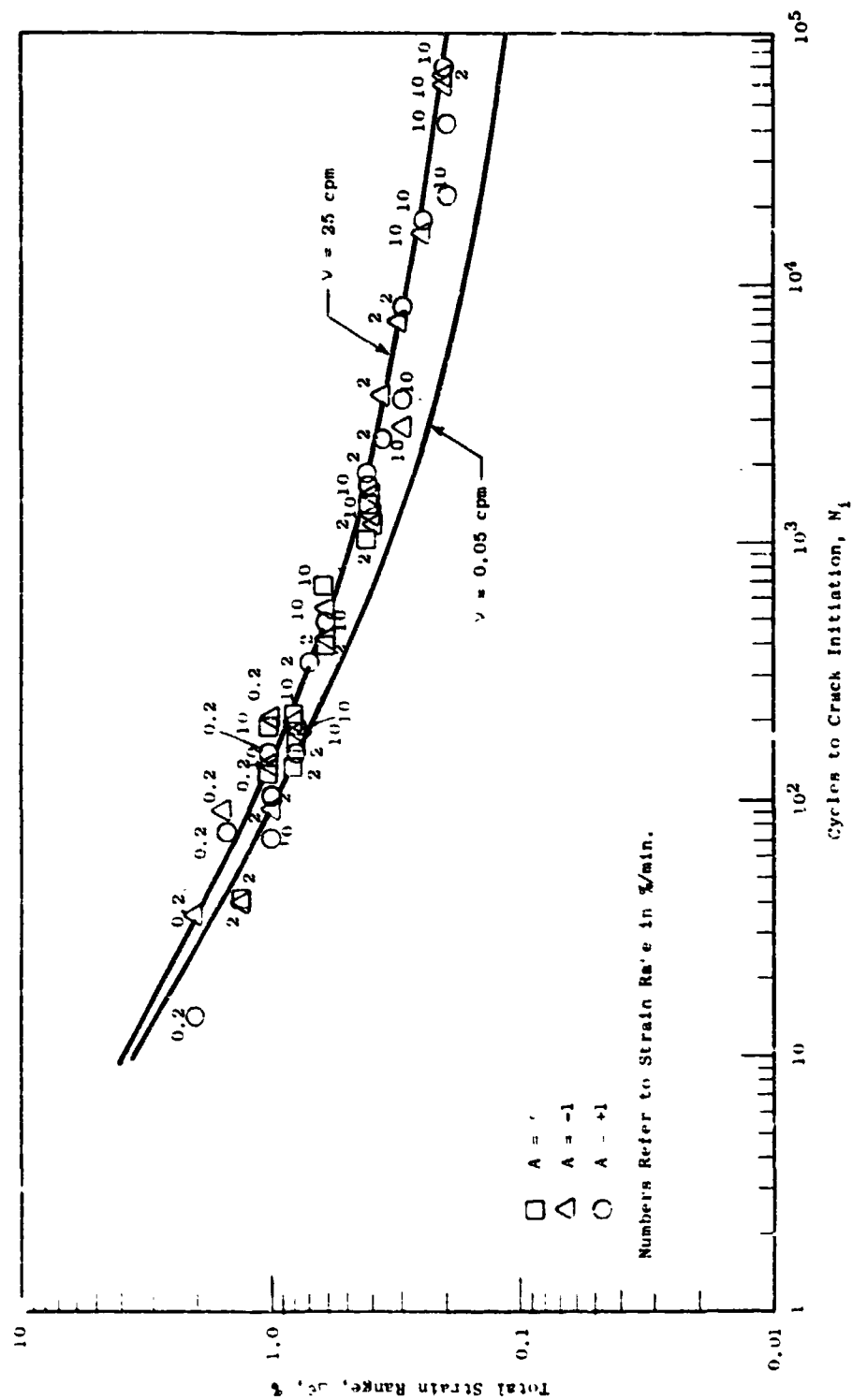
Figure 5.3-6. FM Method with K = 1, Rene' 80, 980° C (1800° F).
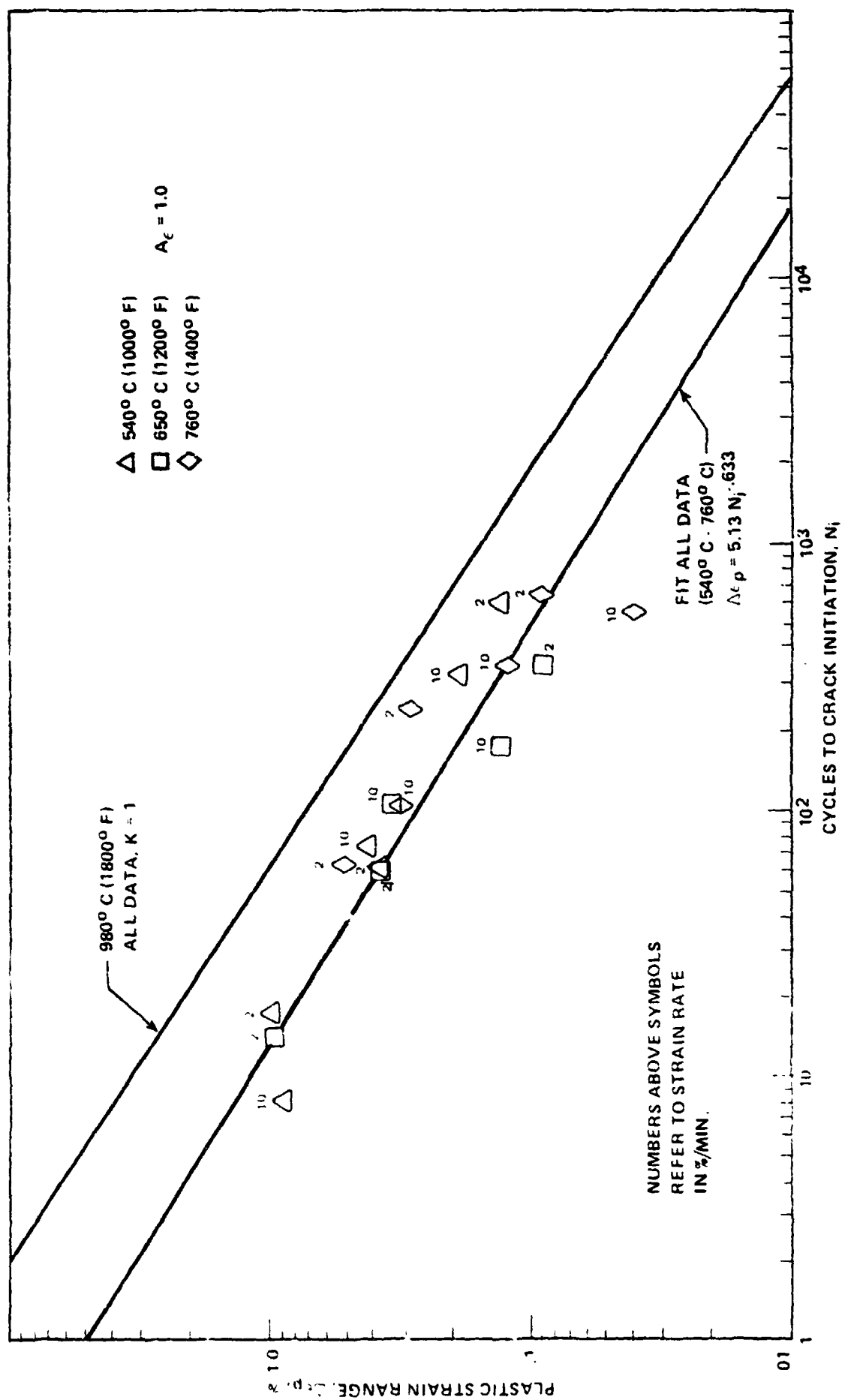
Figure 5.3-7. Plastic Strain Characteristics at Lower Temperatures - René 80.

87
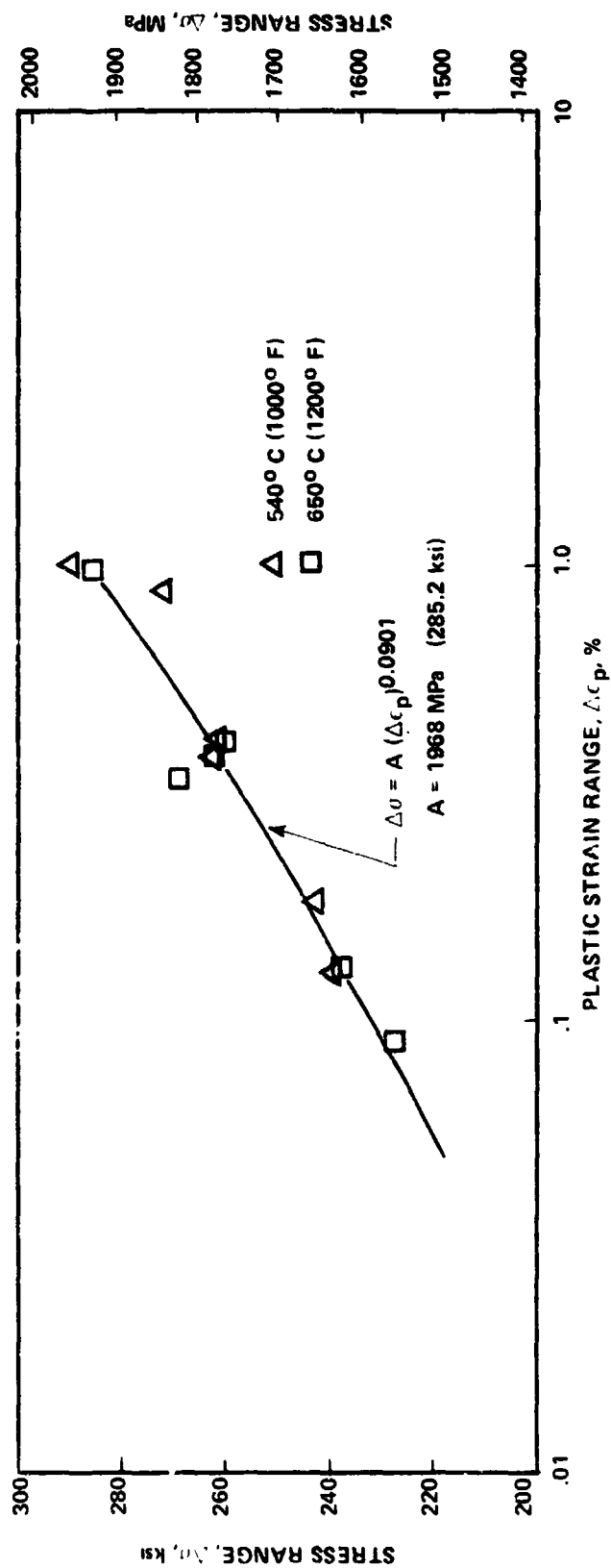
Figure 5.3-8. Fit of $\Delta\sigma$ vs. $\Delta\varepsilon_p$ at Low Temperatures -
René 80.

xx
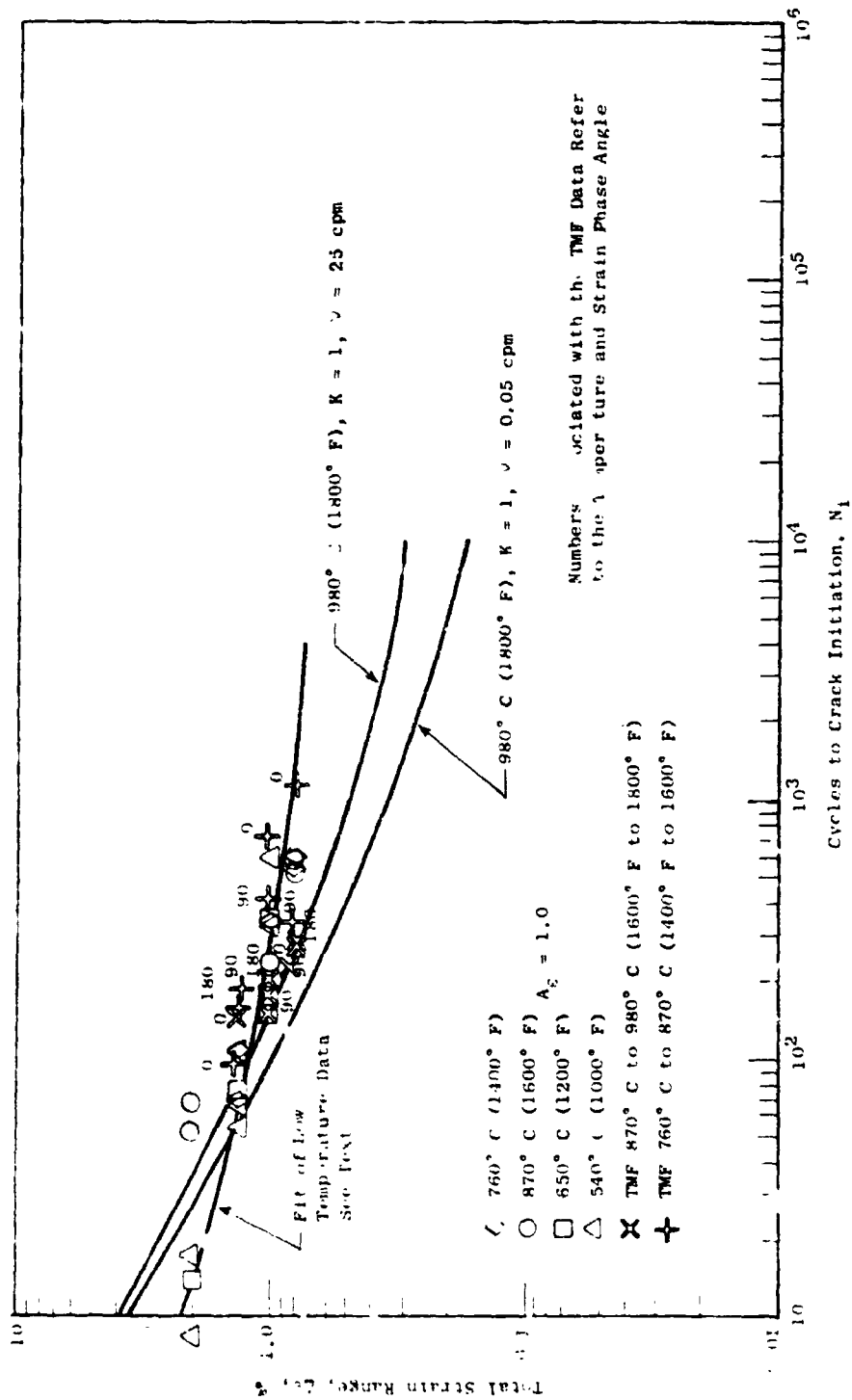
Figure 5.3-9. Summary of Data Analyses - René 80, 540° C to 980° C (1000° F to 1800° F).

rate varied from 2%/min to 10%/min). There appeared to be some layering of the data, with the lower-temperature data apparently somewhat stronger. However, the tensile ductility curve dropped continuously as the temperature decreased, so it was decided to treat the variation as scatter. It also appeared that the two-slope interpretation suggested by Coffin (Reference 9) for the data in Figure 5.3-7 might be warranted. However, this was not investigated further. Only the 540° C (1000° F) and 650° C (1200° F) cyclic stress-strain curves were analyzed (Figure 5.3-8) since they were comparable. Thus the resulting fit is for the lower temperatures of the data set which are still higher than the lowest temperature in the blade.

The analyses in Figures 5.3-7 and 5.3-8 were combined as was done previously fc the 980° C (1800° F) data into the comparison plot of Figure 5.3-9. Ac itional TMF data were included in this plot to show that over the limited temperature ranges involved in those tests, the TMF cycle did not introduce any drastic effects. It should be noted that the effects of temperature were as described above. The results of the lower temperature data analysis were used in making life predictions with the FM and SRP methods.

In Figure 5.3-10 the previously noted suspect 1040° C (1900° F) and 1100° C (2000° F) data are compared with the 980° C (1800° F) data on the basis of plastic strain. As shown, the effect of temperature in this range is small. In addition, a comparison based on total strain range shows the same result. Therefore, it is subsequently assumed that the change in temperature from 980° C (1800° F) to 1040° C (1900° F) results in little change in the life characteristics. Given the nature of these data above 980° C, further work is necessary to establish this trend.

With these data analyses completed, we now turn to the prediction of the life of the subject blade.

5.3.2 Time and Life Fraction Rule

Probably the oldest and still the most widely used approach for assessing creep-fatigue damage in practical applications is the linear-time-fraction approach. Though there are a multitude of forms for this rule, it can be generally stated as

$$\phi_f^a + \phi_c^b = 1, \tag{5-4}$$

where

ϕ_f = fatigue damage

ϕ_c = creep damage

a, b = material constants.

90

C-2

Figure 5.3-10. Comparison of High-Temperature Data - René 80.
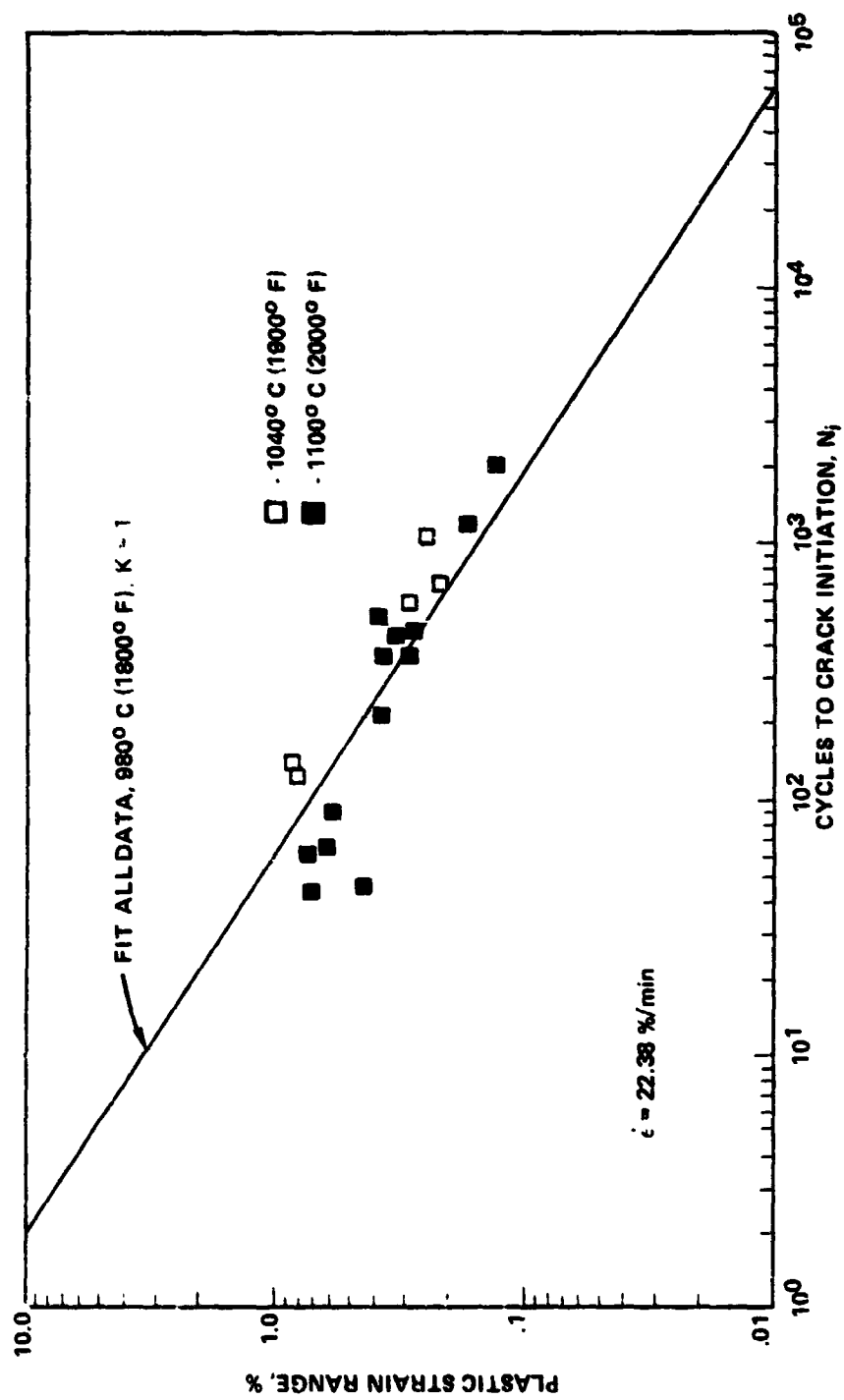
ϕ_f and ϕ_c are normally defined as follows:

$$\phi_f = \sum_{i=1}^{p} \frac{1}{N_{fi}} \quad , \tag{5-5}$$

and

$$\phi_c = \int \frac{dt}{t_r(\sigma,T)} \tag{5-6}$$

Equation 5-5 is merely a Palmgren-Miner rule summation, where N_{fi} is the cycles to failure for the i_{th} loading cycle. Thus, during a variable-amplitude strain history (as opposed to a constant-strain-range history), damage that occurs in each cycle is summed independently into the fatigue damage term, ϕ_f. Definition of a cycle in such a strain history is not always straightforward even though there are a variety of so-called cycle counting methods. This is because these cycle counting methods were developed expressly for proportional cycling - a circumstance which seldom occurs under variable-amplitude loadings which induce coupled creep-fatigue damage.

Equation 5-6 is frequently called Robinson's rule and represents the creep damage. The term $t_r(\sigma,T)$ is the time-to-rupture from a monotonic creep rupture test conducted at constant stress, σ, and temperature, T. In applications where the stress and temperature change, the fractions of the creep rupture life consumed during the time spent at each of the conditions are added together (integrated) until rupture is predicted when $\phi_c = 1$. Thus, if the stress and temperature are constant for a time period, t, Equation 5-6 yields

$$\phi_c = \frac{t}{t_r(\sigma,T)} \quad , \tag{5-7}$$

where ϕ_c is the creep damage (fraction of creep life) incurred during that time period for the given conditions.

This approach received much early support (References 17 through 23) until further research showed that it was generally unreliable (e.g., References 24 and 25). In what follows it was assumed that $a=b=1.0$, that the stress-time history could be described by an equation of the form $\sigma = Z_1 + Z_2t$, and that the temperature of the blade was 1100° C (2000° F). Creep damage was assumed to occur only during the compressive portion of the cycle (i.e., the analysis times of 45 seconds to 200 seconds), and compressive damage was assumed to be the same as tensile. Finally, estimates of the rupture characteristics of René 80 at 1100° C with a wall thickness of 1.1 mm (0.04 in.) were available from curve fits of a large population of thin-wall rupture properties. These data were accurately cast into the form

$$t_r = A\sigma^{-n} \tag{5-8}$$

92

Using Equations 5-6 and 5-8 and the assumed stress-time history, the creep damage was given as

$$\phi_c = \int_0^{t_h} \frac{dt}{t_r(|\sigma|)} = \frac{1}{Z_2 A(n+1)} \left[|Z_1 + Z_2 t_h|^{n+1} - |Z_1|^{n+1} \right] \tag{5-9}$$

where t_h was the hold time of 155 seconds. This equation represented the damage per one chop-and-burst cycle which was assumed to occur three times per mission cycle.

Recall that the extrapolated surface strain range at the blade tip is 0.33% which, according to Figure 5.3-1, predicts the value of N_i to be about 3000 cycles. Using this value and the predicted stress-time history during the time from 45 seconds to 155 seconds in Equation 5-4 yields

$$3n = \frac{1}{\frac{1}{N_i} + \phi_c}$$

or $n = 8.7$ cycles since ϕ_c was found to be 0.038.

Now, recall that the TMF tests showed much more relaxation than was predicted analytically. If this fact was taken into account, the life would drastically change since the creep damage was overestimated. Accordingly, the TMF results were reviewed, which showed that the stress might have been as high as 35 MPa (5 ksi) in those tests during the peak compression time period. If it were assumed that this stress lasted throughout the initiation life time of the blade tip, then the revised calculations yielded a predicted life of 431 cycles.

However, it is doubtful whether such a stress can be maintained, and indeed the last TMF test shows that by Cycle 20 the stress is lower than 35 MPa (see Figure 5.2-8). If one assumes that the stress quickly dies to zero, then the mission life prediction of this method is bounded by the crack initiation lifetime of 1000 cycles. Note in this case that the use of lower-temperature data would make the predicted lifetime longer since the lower-temperature data would predict an even larger value of N_i ($N_1 \sim 10^4$) cycles.

5.3.3 Frequency Modified Approaches

In this case, several approaches are available. First, assume that the full FM prediction given in Table 5.3-1 (with K>1 for all data) is correct. The frequency, ν, is given by $\nu = 60/203.5 = 0.295$ cpm. Using the strain range of 0.33% and Equation 5-2 with these constants, N_i is found to be (by iteration) about 2350 cycles. Thus, the crack initiation life time of the blade is predicted to be 783 cycles. Next, assume that the FM approach with K=1 is correct. Then following the same procedure, the predicted life is 500 cycles.

Next, assume that the frequency separation approach (Reference 9) is correct. The appropriate formulas are given by

$$N_i = \left(\frac{C_2}{\Delta\epsilon_p'}\right)^{1/\beta} \left(\frac{\nu_t}{2}\right)^{(1-K)} \tag{5-10}$$

$$\Delta\epsilon_p' = \left[\frac{\Delta\sigma_{tc}}{A} \left(\frac{2}{\nu_t}\right)^{K_1}\right]^{1/n'} \tag{5-11}$$

and

$$\sigma_{tc} = A(\Delta\epsilon_p)^{n'} \left[\left(\frac{\nu_t}{2}\right)^{K_1} + \left(\frac{\nu_c}{2}\right)^{K_1}\right] , \tag{5-12}$$

where ν_t and ν_c are the tension and compression-going frequencies, respectively, and the rest of the constants are those in Equation 5-2. Following this procedure requires the use of the actual inelastic strain range, $\Delta\epsilon_p$. Here there are two choices: use either $\Delta\epsilon_p = 0.03\%$ from the maximum width of the experimental hysteresis loops, or the value 0.013% found in the surface strain extrapolation. We choose $\Delta\epsilon_p = 0.03\%$ and utilize the constants with $K \sim 1$. Using Equations 5-11 and 5-12, $\Delta\epsilon_p'$ is found to be 0.0116% (with $\nu_t = 60/3.5 = 17.1$ cpm and $\nu_c = 60/200 = 0.3$ cpm). Equation 5-10 then predicts $N_i = 5.76 \times 10^4$ cycles, or a mission life of 19,200 cycles. The reason for the difference between this prediction and the previous FM results is that the actual value of plastic strain range (0.013% to 0.03%) is much less than what would be predicted by the 980° C isothermal data at a total strain range of 0.33%. (Either of the two initial FM approaches predict $\Delta\epsilon_p = 0.12\%$). That is, the use of the initial FM methods involves only the total strain range (of 0.33%) and the actual value of plastic strain range is not explicitly considered. The important point is that damage cannot be directly related to plastic strain when total strain is used in TMF predictions.

In passing, it is noted that Reference 9 gives a preliminary approach for predicting the life under TMF cycles. Using this approach and the lower-temperature data fits that are discussed in Section 5.3.1, it is found that the predicted value of N_i is even larger than that found by the frequency separation method. Thus, this approach appears unsuitable for at least this case.

5.3.4 Strainrange Partitioning (SRP) Predictions

To predict the life using the SRP method we use the experimental results for René 80 given by Halford and Natchigall at 1000° C (1830° F) (Reference 4). It is assumed that the inelastic strain range in the blade is that which is called $\Delta\epsilon_{pc}$ in SRP parlance (i.e., plasticity in tension reversed by creep in compression). This is the worst case given in Reference 4 for cycles to failure greater than about 10^3 cycles. The trend line from their experiments

94

is replotted in Figure 5.3-11, along with those predicted by the d ctility normalized SRP method (DN-SRP, Reference 2) in Reference 4. (The value of their reduction in area [RA] is larger than the average value found in our design handbook. However, it is within the bounds of the handbook curves.)

In Figure 5.3-11 several modifications are made to the basic SRP line based upon the notion of ductility normalization. According to the DN-SRP approach, the $\Delta\epsilon_{pc}$ component scales linearly with the tensile ductility. That is,

$$\Delta\epsilon_{pc} = .25 \ D_p N_{pc}^{-.60} \tag{5-13}$$

where $D_p = - \ln(1-RA)$. As a first step, assume that the slope in Equation 5-13 should be replaced by the one that is established by actual data analysis. The General Electric materials handbook shows that the RA decreases over the temperature range of $1000°$ C to $1100°$ C ($1830°$ F to $2000°$ F). Consequently, adjusting the actual data curve at $1000°$ C in accordance with Equation 5-13 the solid line in Figure 5.3-11 is obtained which is below the original line. The specimens that were used in developing the original curve were appreciably thicker than the blade tip region. Reviewing the results of thin specimen tensile tests on René 80 at $1100°$ C (Reference 26), it is possible to further reduce the solid line to the dashed one shown in Figure 5.3-11. This reduction is based on elongation measurements from bare and base pre-exposed specimens. Thus, to make this last reduction meaningful, it is necessary to assume that the coating cracks early in life, exposing the remaining substrate material.

Using the lowest line in Figure 5.3-11, then, the SRP method predicts a crack initiation life of about 2700 cycles by using the maximum width of the TMF hysteresis loops of 0.03%. Using the value of inelastic strain range that is predicted by analysis (0.013%), the life would be around 10,00. cycles. Accounting for the three chop-and-burst cycles per mission cycle, the minimum mission life that is predictable by this method is 900 missions. Note, that in making these ductility modifications it is assumed that the suspect $1040°$ C ($1900°$ F) and $1100°$ C ($2000°$ F) data in Figure 5.3-10 are invalid. Those data suggest that such ductility modifications must also consider changes in slope as they fall near the $980°$ C ($1800°$ F) data. However, without such modifications, the predicted life based solely on the $980°$ C data is much greater than 10,000 cycles.

Application of the SRP method to TMF cases is normally based on the idea that the SRP lines are independent of temperature. The above ductility normalization approach is one way of introducing potential temperature dependence; however, in Reference 8, it is mentioned that the SRP life might best be based on the temperature where the ductility is the least. In the current application, this is at the lowest temperature. Using the regression line in Figure 5.3-7, for the $540°$ C ($1000°$ F) curve, and the value of inelastic strain range of 0.03%, the life by this method would be 3300 cycles. In other words, the prediction by this approach is worse than before.
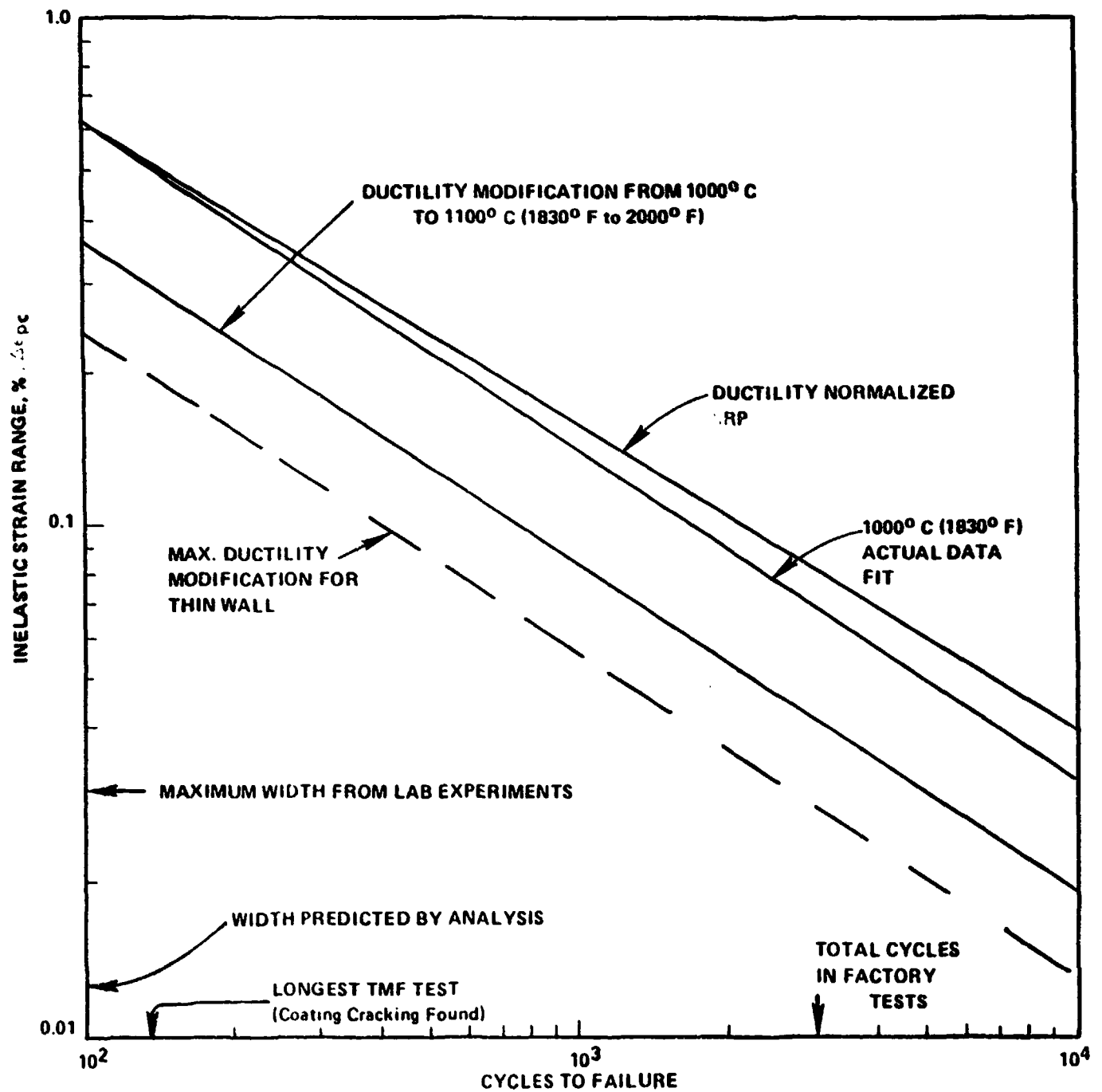
Figure 5.3-11.   SRP Analysis.

However, as with the 1100° C (2000° F) estimated curve (Figure 5.3-11) it is possible to use the tensile elongation measurements from Reference 26 to lower the plastic strain-line curve of Figure 5.3-7. This reduction is based upon bare thin specimen tensile tests at 760° C (1400° F) after pre-exposure at 1100° C (2000° F); the reduction is very dramatic such that only about 10% of the original elongation remains after pre-exposure. Using the ductility normalization concept with the lower temperature data curve (Figure 5.3-7) and assuming a plastic strain range of 0.03% results in a predicted crack initiation life of 90 cycles, or 30 factory cycles. These predictions depend heavily on the elongation measurements of Reference 26 which show scatter, depend on the pre-exposure conditions, and depend on whether or not the specimen was coated. Despite these additional considerations, there is strong support in the literature of the role of high temperature pre-exposure in reducing the lower temperature ductility of nickel-base superalloys (e.g. see References 27 and 28). Thus, while the reliability of these predictions can be questioned, there is little doubt that the effect of pre-exposure can be severe in reducing ductility.

5.3.5 Mean (Maximum) Stress Approaches

In References 12 through 15, methods are presented which attempt to take into account the influence of mean or maximum stress levels. In these cases, damage is assumed to be related to hysteresis loop energy. Of particular interest to this study are the results of Ostergren (Reference 13) and Jaske (Reference 15). Ostergren found for René 80 at 870° C (1600° F) that he could correlate the influence of tensile and compressive hold times simply by using the product of maximum stress and inelastic strain range. Jaske found for TMF tests on AISI 1010 steel that the Smith-Watson-Topper (SWT) parameter (given below) could correlate his results with isothermal data by using the maximum temperature and stress (not necessarily at the maximum strain) of the TMF hysteresis loop. Thus, it seems prudent to explore this approach.

Since the plastic strain range in the current case is small, it is assumed that total strain (rather than the plastic strain measure used by Ostergren) is the best basis. Further, it is assumed that the SWT method should work as suggested by Jaske. These two approaches are consistent since the SWT parameter, P, is given by,

$$P = E_{max.} \, \Delta\epsilon \tag{5-14}$$

Accordingly, all of the René 80 data were analyzed in this manner giving the results that are shown in Figure 5.3-12. All of the data at 980° C (1800° F) collapse reasonably well considering the scatter in stress response for René 80 at this temperature (see Figure 5.3-2). Note, too, that the parameter is a strong function of temperature, although the 1100° C (2000° F) data agree reasonably well with the 980° C data.

Using this approach to analyze the blade tip requires a definition of the modulus. Using the one at 980° C (1800° F) (the lower the temperature,
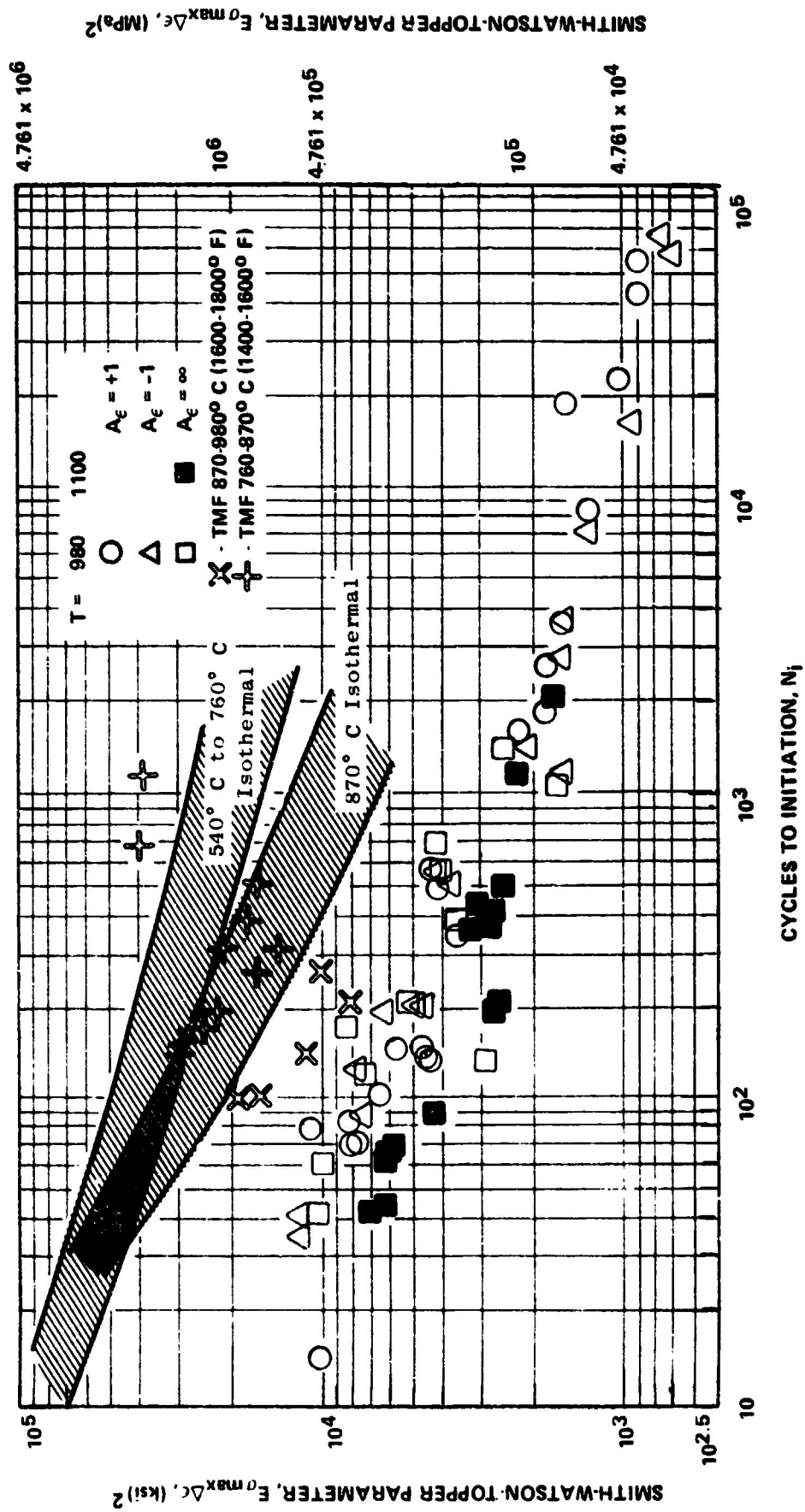
Figure 5.3-12. SWT Analysis – René 80.

the higher the parameter) and the surface extrapolated stresses result in an N_i prediction of about 250 cycles. For the experimental stresses and strains, the result is approximately 200 cycles. Considering the three chop-and-burst cycles, the results would be 83 mission cycles and 67 mission cycles, respectively.

Note that all of the variables (E, σ_{max}, and $\Delta\epsilon$) in Equation 5-14 increase in value as temperature decreases. That is, for example, the fatigue resistance to a given strain range, $\Delta\epsilon$, increases as temperature increases (at least over certain life ranges as shown in Figure 5.3-9). Also note that the TMF data in Figure 5.3-12 do not necessarily agree with the maximum isothermal temperature. Indeed, if a lower temperature isothermal curve is used the predicted life is greater than 1000 cycles. Based on these considerations, it is concluded that this approach does not appear promising for TMF application of René 80 at these temperatures.

5.4 CRACK PROPAGATION ANALYSES

A crack growth analysis was performed on the subjected blade by using an existing mission analysis computer code called MISKRA III (Reference 29). To analyze the blade, the side edge crack model (shown schematically in the insert of Figure 5.3-13) was selected. This model, which was based on Bueckner's weight function approach (Reference 30), took into account nonlinear gradients expressed as polynomial curve fits. Accordingly, the 3-D CYANIDE stress distributions shown in Figure 5.1-1 were fit using linear regression and used in the analyses. A 650° C (1200° F) René 80 crack growth rate curve was used in the analysis, which was akin to assuming that only the tensile stresses caused the crack to grow and that the 1100° C (2000° F) temperature had no interactive effects on the propagation rates. This crack growth rate curve was based on only one test. A mission was defined consistent with the applied stresses as schematically illustrated in Figure 5.3-14. (Note that all three chop-and-burst cycles were included along with the maximum reverse cycle).

The analysis assumes that the influence of mean stress on crack growth could be accounted for by the Walker relationship (Reference 31)

$$\overline{K} = K_{max}(1-R)^m \tag{5-15}$$

where $\overline{K}$ is the "effective" stress intensity factor, K_{max} is the maximum stress intensity level in a given cycle, R is the ratio of K_{min}/K_{max}, K_{min} is the minimum value of stress intensity in a given cycle (computationally it can be negative), and m is an empirical factor. It can be shown that Equations 5-14 and 5-15 would be consistent parameters in the elastic strain regime if the stress intensity symbols are replaced by stress levels and an empirical power is introduced by Equation 5-14.

Figure 5.3-13. Results of the Crack Growth Analyses.

Figure 5.3-14.   Schematic of the Assumed Mission Cycles for
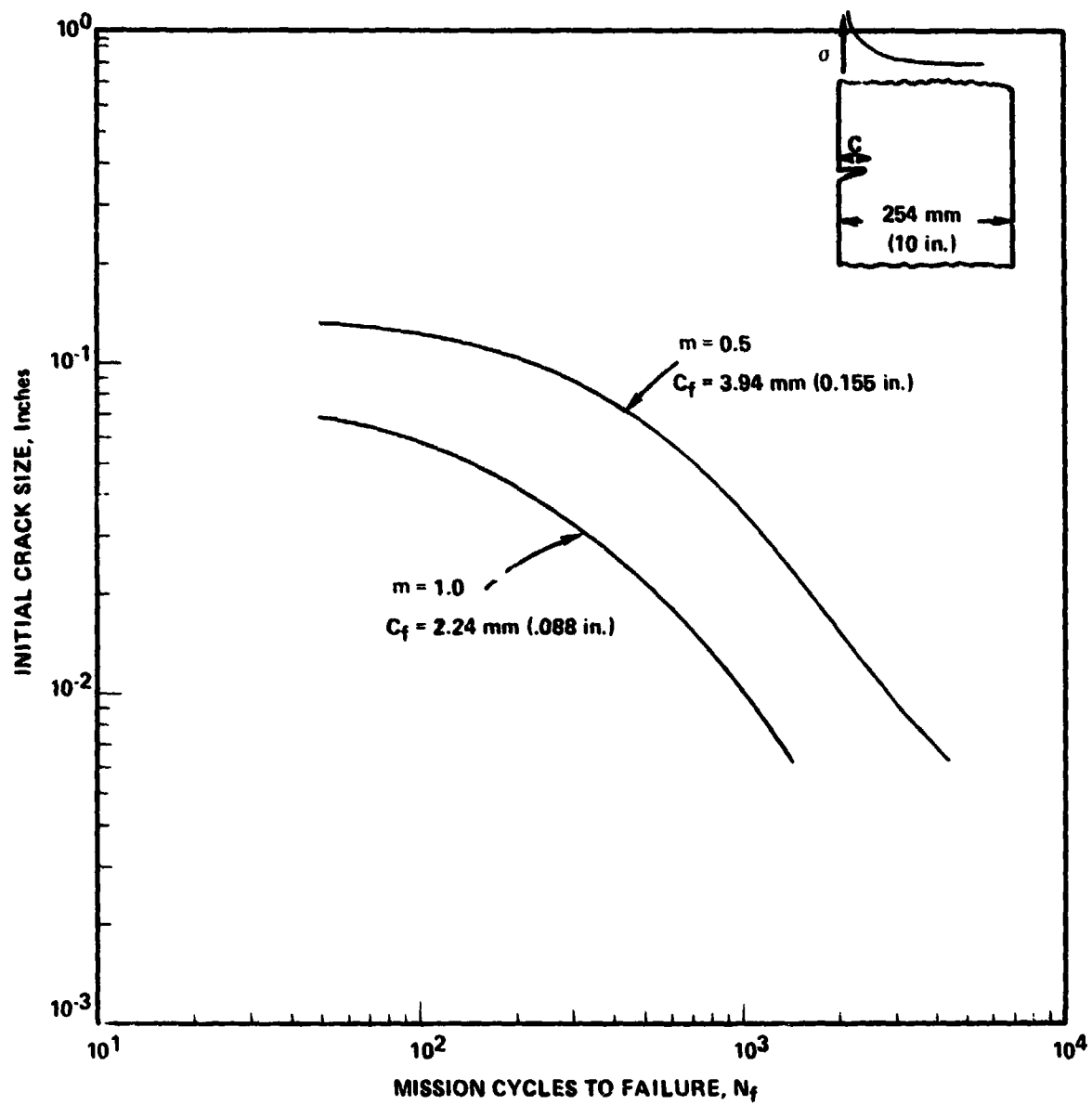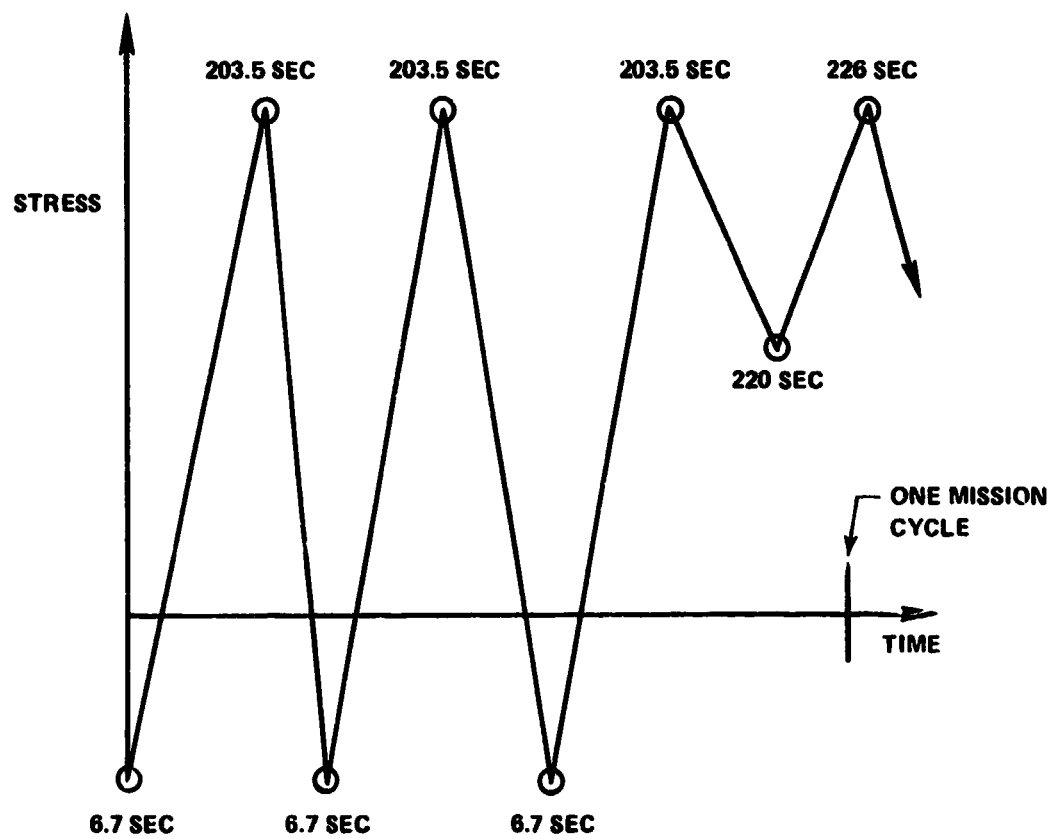   the Crack Growth Analyses. Times Shown Refer
                  to Analyses Times in Previous Figures and in
                  the Text.

The value of m was assumed to be both 0.5 and 1.0, and complete mission analyses were made for both assumptions. The assumption of 0.5 corresponded to an equal weighting of the maximum level and range in stress intensity ($\overline{K}$ = $[K_{max} \Delta K]^{1/2}$), and the assumption of 1.0 related to the case where $\overline{K}$ = ΔK. Furthermore, the value of unity was consistent with the assumption that the compressive stresses (at the time of 6.7 seconds) completely vanished due to creep since only ranges were involved. In such a case, equilibrium considerations might demand a stress redistribution; but, in any event, the assumption of m = 1.0 should approach a lower limit on the crack growth analysis. Finally, in both cases, full calculation of R (R changed as a function of crack length due to the stress gradients) was made such that negative stresses were assumed to be fully effective in accelerating the propagation rate.

Another consideration must be mentioned. Note that the same stress distribution was assumed to be active as the crack grows. However, further note that these stresses are mainly thermal stresses which should be relieved as the crack grows. As with most of the other assumptions, maintaining the same stress gradients should make the analysis conservative (the crack propagation rate should be over estimated).

The results of these analyses are shown in Figure 5.3-13 in the form of initial crack size versus mission life. Recall that the factory test experience was that a crack length of 3.8 mm (0.15 inch) or greater was found after 1000 mission cycles. In the case of m = 0.5, the critical length (based on $\overline{K}$ = K_c) was 3.94 mm (0.155 inch) while in the case of m being unity the critical length was predicted to be 2.23 mm (0.088 inch). The final predicted crack length was this small apparently because the stress distribution was not reduced as the thermal load path was cut by crack growth. Note that none of the blades failed during testing.

To predict the crack propagation life after completion of the initiation process, it is necessary to assume an initial crack size. Since René 80 is a cast alloy, it has coarse grains with 0.25 mm (0.01 inch) being a reasonable grain size. Consequently, assuming that the initial crack size is the same as one grain diameter, the results in Figure 5.3-13 predict that the number of mission cycles to reach a length of 3.8 mm is 1000 cycles for m = 1.0 (actually failure would occur first) and 2650 cycles for m = 0.5. Since the blades are removed after 1000 cycles, it appears that neither of these two approaches are accurate in that they over predict the number of cycles. Since the assumptions that are made in the analyses are conservative, it is likely that the crack growth rate curve is inappropriate; it is probable that the environment interacts with the substrate once the crack initiates causing faster growth than that which is predicted by an isothermal curve.

6.0 DISCUSSION OF RESULTS

6.1 ANALYTICAL RESULTS

By any standard of evaluation, the different analytical tools used in this investigation all performed excellently. The three-dimensional analyses produced results in quantitative agreement with the blade history. That is, the maximum stress/strain ranges were predicted for areas where actual cracking occurred. Even the elastic analysis gave this agreement. The degreee of qualitative agreement must be inferred through correlation with the hysteresis loop test results and two-dimensional analysis. Based on this, it would appear that excellent qualitative agreement could be attained, provided that the material properties (stress/strain, creep, etc.) are known accurately. The major discrepancy between the testing results and the analytical predictions for this very severe thermomechanical cycle is due to the creep properties. Test results showed a much faster stress relaxation than had been analytically predicted. This suggests that the primary creep representation used was not accurate. This representation, at the present time, is based on static creep testing. This is one obvious area for future investigation and improvement.

6.2 TMF EXPERIMENTS

Because of small strains used in the TMF experiment, it was necessary to exercise extreme care in the control of the thermal component of strain measured in the TMF tests. This precipitated the development of an intricate computer-based system as J.T. Berling's MBRC Company. This system showed excellent possibilities for evaluating actual TMF conditions, and yielded excellent comparisons with the analytical predictions once the accelerated creep at $1100°$ C was recognized. This type of system appeared to be necessary for the generic class of high-temperature, nickel-base superalloys, which exhibit small inelastic strain ranges and wide temperature variations in application.

6.3 SHORTCUT METHODS

This research investigated a number of different shortcut techniques, each with a different level of complexity. These were:

1. Use an elastic three-dimensional analysis to predict the mission cycle strain-temperature-time profile. Then program this strain-temperature-time profile on a laboratory specimen.

2. Use an elastic three-dimensional analysis to predict the mission cycle strain-temperature-time profile. Use this as boundary conditions for simpler two-dimensional or three-dimensional nonlinear analyses.

3. Use a nonlinear three-dimensional analysis to predict the first cycle strain-temperature-time profile. Use this to program a laboratory specimen or to provide boundary conditions for simpler nonlinear analyses.

All of the above shortcut methods appear useful, particularly when the economics of the problem, as discussed in the next section, are considered.

Method 1 can only be used when the problem area in question is uniaxial, such as the squealer tip; otherwise, multiaxial test specimens would need to be designed. This method requires the smallest amount of time and cost for analysis but the total amounts could be greater than for Method 2 or the 3-D analysis portion of Method 3. This is because the thermomechanical hysteresis loop testing requires significant amounts of time and money. It does provide an excellent check and feedback loop, particularly if the hysteresis loop tests could be carried out to failure.

Method 2 is potentially the most economical of the three methods, both in terms of time and cost. Just as with Method 1, in situations where the shakedown strain range is not appreciably different from the elastic strain range, this would provide acceptable answers for designing, since factors of safety are always applied to life predictions. This method, while lacking the checks and feedback of the testing, is not restricted to uniaxial conditions.

Method 3 is the last step short of a ful'y stabilized analysi . It would be used when a larger difference between shakedown and elastic strain ranges is anticipated or when there is insufficient data to accurately model the cyclic inelastic material properties.

6.4 ANALYSIS ECONOMICS

Any evaluation of this research and its usefulness must take into account the economics of the time and cost involved. The manpower, computer cost, and problem time span are all much more than required by the in-situ one-dimensional and two-dimensional design methods. This must be balanced by the better quality of information obtained and the need for that quality of information. All of the above factors can be improved, particularly with in-house computer programs.

6.5 LIFE PREDICTION RESULTS

The life analysis demonstrated that without exception, assumptions could be made such that all approaches could predict crack initiation by the end of the factory test (see Table 6.5-1). However, such a statement cannot be misinterpreted as meaning that the life analysis predictions were good from the point of view of understanding the cause of initiation. In most cases the reason for the goodness of prediction could be traced to a misinterpretation of the cause of the damage. This is particularly true of the methods which

Table 6.5-1. Summary of the Life Analysis Methods.

	Method	Minimum Mission Life Predicted (Cycles)	Maximum Mission Life Predicted (Cycles)	Comment
1.	Time and Life Fraction Rule	8.7	1000	Depends on Assumed Stress Relaxation
2.	Frequency Modified Approaches	500	$>10^4$	Depends on the Method and Plastic Strain Range
3.	Strain Range Partitioning	30	$>10^4$	Depends on Assumption of Ductility Modification
4.	Mean (Maximum) Stress Methods	67	$>10^3$	Depends on Isothermal Data Set That is Used
5.	Crack Propagation Analysis (Co=0.25 mm)	1000	2650	Depends on Assumed Dependence of Mean Stress

Experience: (1) Blades had cracks of length 3.8 mm or greater after 1000 factory cycles

(2) One thermal mechanical test specimen had coating cracks after 135 cycles.

105

relied on inelastic strain to predict damage. Note that the stress analyses and the TMF results both showed little to no inelastic strain range (with 0.03% being the maximum that could be obtained from either source). Reviewed again, any of the actual data analyses of Section 5.3-1 suggested that such a small inelastic range would result in a prediction of at least 1100 mission cycles for crack initiation in the blade (account made for the three burst-and-chop cycles per mission cycle). Better agreement with experience was achieved through the assumption of ductility normalization and the use of the detrimental effect of high temperature pre-exposure on the subsequent ductility.

Conversely, methods that used total strain range and the maximum temperature fared better in life prediction. These methods were based on isothermal data which had substantially more inelastic strain range at the same total strain range of 0.33% than was predicted by analysis of the blade or was measured by the TMF experiments. Accordingly, the question of what constituted damage was not properly interpreted by the total strain-based methods. Finally, no method could predict the early crack initiation that was required by the most conservative propagation analysis.

A strong clue to the cause of the premature blade cracking was found in the fluorescent penetrant analysis of the one long-running TMF experiment (that was shown in Figure 5.2-9). Though the specimen showed no indication of crack initiation by a compliance technique, the coating was filled with many cracks. This suggested that ultimately, the most probable cause of the extent of cracking found in the factory tests [3.8 mm (0.15 inch) or greater] involved initial coating cracking at the lower temperature where the coating was brittle, followed by environmentally accelerated crack propagation in the substrate. With this scenario, crack initiation was due to the fatigue of the coating and not due to the fatigue of the substrate as assumed by the crack initiation methods when utilizing high temperature isothermal data.

Finally, it is noted that all of the above statements are based directly or indirectly on the results of the stress analyses, wherein the amount of creep is underestimated. Given that more creep occurs than was predicted, it might be possible that more creep ratcheting might occur, somehow causing a larger loop width. However, the above coating cracking/environmental argument appears more reasonable. In any case, a better understanding of high-temperature thin-section creep is required, as well as, more generally, a better understanding of constitutive equations.

6.6 CRACK PROPAGATION RESULTS

In this case it was shown that the most conservative analysis that could be made resulted in a crack propagation lifetime of 1000 factory cycles. The analysis was based on the result of a 650° C (1200° F) crack growth curve derived from one experiment. However, unless the curve was highly erroneous, the results suggested that a good propagation analysis could not be achieved since all of the assumptions used in establishing the 1000-cycle prediction were conservative. The analysis strongly suggested that more crack propagation data be generated, preferably involving a TMF cycle which included the maximum temperature of 1100° C (2000° F).

106

7.0 CONCLUSIONS

The following conclusions were generated by the results of this program:

- The objective of the program was met. The utility of advanced structural-analysis techniques and advanced life-prediction techniques in the assessment of hot-section components was demonstrated.

- Three-dimensional transient heat-transfer analysis is both technically and economically feasible.

- Three-dimensional elastic stress analysis is both technically and economically feasible.

- Three-dimensional nonlinear stress analysis is technically feasible but its use will be 'imited by the economics.

- There are shortcuts to the nonlinear stress analysis which are economically feasible with little loss in predictive accuracy.

- The continuing improvement in computer costs and the use of in-house computer facilities versus commercial facilities would benefit the economics.

- Further improvements in interactive graphics would prove beneficial in both time and cost.

- For structural problems where the predominant loading is thermal, a good approximation of the strain range can be obtained from elr; ic analysis results even though inelastic conditions (creep auu plasticity) exist. It should be noted, however, that absolute strain values (ϵ_{max}, ϵ_{min}) could differ significantly between elastic and inelastic analysis.

- Cyclic test results imposing a strain/temporal cycle typical of an HPT blade-tip region indicate that at high temperatures [>980° C (1800° F)] relaxation occurs significantly faster than predicted by analysis for René 80. Reasonable hysteresis loop stabilization was evidenced subsequent to the initial cycle from test results, whereas analysis would predict 16 cycles to be required before comparable stabilization occurred. Both the creep damage model and creep material properties data must be investigated to determine the source of the discrepancy.

- Inelastic analysis results show that for high-pressure-turbine blade-tip regions plasticity occurs only during the initial cycle. Subsequent to this a tradeoff between creep strain and plastic strain occurs. Additionally ratcheting of the stress-strain curve is observed with movement in the negative strain and positive stress directions. Peak tensile stresses (crack opening) occur during the cool-down portion of the cycle.

- A very accurate computer-controlled thermomechanical test capability is demonstrated. It is now possible to contemplate testing over larger temperatu·e ranges and strain rates than has been possible in the past.

- None of the crack-initiation analysis scheme was reliable for this application. As demonstrated by numerous investigators, it was shown that total-strain-based approaches appeared to work best when used in conjunction with the maximum temperature of a fully thermal mechanical cycle. Even in this case, though correlation was achieved, understanding was lacking. Methods based on inelastic strain appeared undesirable in this case due to the need to predict (or measure) inelastic strains on the order of 0.01%. Prediction based on this level of inelastic strain range were inaccurate unless additional assumption were made.

- The crack-propagation analysis appeared to be reasonable using relatively low temperature [650° C (1200° F)] crack-growth data since the maximum tensile stresses occurred at the lowest temperature of the cycle [340° C (650° F)]. The rest of the analysis was totally conservative; and yet, the minimum life that could be predicted was equal to the total number of factory cycles (1000 cycles). Thus, better understanding of crack propagation in TMF is needed.

- The most probable cause of damage appeared to be related to coating cracking and subsequent environmentally assisted crack growth. The coating cracking would be thought to occur at the lower temperature of the TMF cycle, where it is brittle. Methods for predicting coating cracking are needed.

LIST OF ABBREVIATIONS, ACRONYMS, AND SYMBOLS

ANSYS   –   Engineering Analysis System Program

CYANIDE   –   Cyclic Analysis of Inelastic Deformation

FM   –   Frequency Modified

MASS   –   Mechanical Analysis of Space Structures

N_i –   Cycles to Crack Initiation

SRP   –   Strain Range Partitioning

STP   –   Surface Temperature Program

T_3 –   Compressor Discharge Temperature

T_4 –   Turbine Inlet Temperature

THTD   –   Transient Heat-Transfer - Version D

TMF   –   Thermal Mechanical Fatigue

ν –   Frequency

REFERENCES

1. CF6-6/TF39 Stage 1 HPT Blade Tip Crack Evaluation, General Electric Company - Aircraft Engine Group, Design Record Book Number 2, April 1977.

2. G.R. Halford, J.F. Saltsman, and M.H. Hirschberg, Ductility Normalized-Strainrange Partitioning Life Relations for Creep-Fatigue Life Predictions, NASA TN-73737, 1977.

3. J.F. Saltsman and G.R. Halford, "Application of MPC Creep-Fatigue Data for 2-1/4 Cr-1Mo Steel," ASME-MPC Symposium on Creep-Fatigue Interaction, 1976, pp 283-298.

4. G.R. Halford and A.J. Natchigall, Strainrange Partitioning Behavior of the Nickel-Base Superalloys, René 80 and IN 100, NASA TN 7828, 1978.

5. G.R. Halford, M.H. Hirschberg, and S.S. Manson, "Temperature Effects on the Strainrange Partitioning Approach for Creep Fatigue Analysis," Fatigue at Elevated Temperatures, ASTM STSP 520, ASTM, 1973, pp 658-669.

6. S.S. Manson and G.R. Halford, "Treatment of Multiaxial Creep-Fatigue by Strainrange Partitioning," 1976 ASME-MPC Symposium on Creep-Fatigue Interaction, December 1976, pp 299-322.

7. S.S. Manson, "The Challenge to Unify Treatment of High Temperature Fatigue - A Partisan Proposal Based on Strainrange Partitioning," Fatigue at Elevated Temperatures, ASTM STP 520, ASTM, 1973, pp 744-782.

8. G.R. Halford and S.S. Manson, "Life Prediction of Thermal-Mechanical Fatigue Using Strainrange Partitioning," Thermal Fatigue of Materials and Components, ASTM 612, D.A. Spera and D.F. Mowbray, Eds., ASTM, pp 239-254.

9. L.F. Coffin, Jr., A.E. Carden, S.S. Manson, L.K, Severud, and W.L. Greenstreet, "Time-Dependent Fatigue of Structural Alloys - A General Assessment (1975)," ORNL Report 5073, Oak Ridge National Laborator- January 1977.

10. L.F. Coffin, Jr., "Fatigue at High Temperature," Fatigue at Elevated Temperatures, ASTM STP 520, ASTM, 1973, pp 5-34.

11. L.F. Coffin, Jr., "A Note on Low-Cycle Fatigue Laws," Report No. 70-C-309, General Electric Co., Schenectady, NY, September 1970.

12. B.N. Leis, "An Energy-Based Fatigue and Creep-Fatigue Damage Parameter," Trans. ASME, Journal of Pressure Vessel Technology, Vol. 99, Series J, No. 4, November 1977.

13. W.J. Ostergren, "Correlation of Hold Time Effects in Elevated Temperature Low Cycle Fatigue Using a Frequency Modified Damage Function," 1976 ASME-MPC Symposium on Creep-Fatigue Interaction, December 1976, pp 179-202.

14. K.N. Smith, P. Watson, and T.H. Topper, "A Stress-Strain Function for the Fatigue of Metals," Journal of Materials, Vol. 5, No. 4, December 1970, pp 767-776

15. C.E. Jaske, "Thermal-Mechanical, Low-Cycle Fatigue of AISI 1010 Steel," Thermal Fatigue of Materials and Components, ASTM STP 612, D.A. Spera and D.F. Mowbray (Editors), ASTM, 1976, pp 170-198.

16. T.S. Cook, "Cyclic Stress-Strain Behavior of Inconel IN718," presented at ASTM Meeting at Bal Harbor, November 1980, to appear in an ASTM STP.

17. E.L. Robinson, "Effect of Temperature Variation on the Creep Strength of Steels," Trans. ASME, Vol. 60, 1938, pp 253-259.

18. S.S. Manson and G. Halford, "A Method of Estimating High Temperature Low-Cycle Fatigue Behavior of Materials," Thermal and High-Strain Fatigue, The Metals and Metallurgy Trust, 1967, pp 154-170.

19. S. Taira, "Lifetimes of Structures Subjected to Varying Load and Temperatures," Creep in Structures, N.J. Hoff, Ed., Academic Press, New York, 1962.

20. S.S. Manson, G.R. Halford, and D.A. Spera, "The Role of Creep in High Temperature Low-Cycle Fatigue," Advanced in Creep Design, the A.E. Johnson Memorial Volume, A.I. Smith and A.M. Nicolson, Eds., Applied Science Publishers Ltd., London, 1975, pp 229-249.

21. D.A. Spera, "A Linear Creep Damage Theory for Thermal Fatigue of Materials," Ph.D. Thesis, The University of Wisconsin, 1968.

22. J.H. Laflen, "Integrated Creep Rupture Damge in High Cycle Fatigue: A Method of Predicting Goodman Diagram at Elevated Temperatures," M.S. Thesis, University of Cincinnati, 1972.

23. S.S. Manson, "Fatigue: A Complex Subject - Some Simple Approximations," Exp. Mech., Vol. 5, No. 7, 1965, pp 193-226.

24. J.R. Ellis, M.T. Jackob, C.E. Jaske, and D.A. Utah, "Elevated-Temperature Fatigue and Creep-Fatigue Properties of Annealed 2-1/4 CR-1Mo Steel," Structural Materials for Service at Elevated Temperatures in Nuclear Power Generation, MPC-1, ASME, New York, 1975, pp 213-246.

25. J. LeMaitre, J.L. Chaboche and Y. Munakata, "Method of Metal Characterization for Creep and Low Cycle Fatigue Predictions in Structures," Proc. Symposium Mechanical Behavior of Materials, Kyoto, Japan, August 1973, pp 239-249.

26. M. Kaufman, "Examination of the Influence of Coatings on Thin Superalloy
     Sections," NASA CR-121115, August 1972.

27. S.D. `ntolovich, P. Domas, J.L. Strudel, "Low Cycle Fatigue of René
     80 as Affected by Prior Exposure," Met. Trans, Vol. 104, Dec. 1979,
     pp 1859-1868.

28. D.A. Woodford, "Environmental Damage of a Cast Nickel-Base Superalloy,"
     General Electric Company, Schenectady, New York, Report No. 80 CRD 160,
     July 1980.

29. J.H. Laflen, "Mission Crack Growth Analysis: The MISKRA III Computer
     Program," General Electric Company - Aircraft Engine Group, R73AEG403,
     September 1973.

30. H.F. Bueckner, "Weight Functions for the Notched Bar," General Electric
     Company, 69LS45, May 1969.

31. K. Walker, "The Effect of Stress Ratio During Crack Propagation and
     Fatigue for 2024-T3 and 7075-T6 Aluminum," ASTM STP 462, 1970, pp 1-14.